

## Radio and Millimeter Continuum Surveys and their Astrophysical Implications

Gianfranco De Zotti · Marcella Massardi ·  
Mattia Negrello · Jasper Wall

Received: date / Accepted: date

**Abstract** We review the statistical properties of the main populations of radio sources, as emerging from radio and millimeter sky surveys. Recent determinations of local luminosity functions are presented and compared with earlier estimates still in widespread use. A number of unresolved issues are discussed. These include: the (possibly luminosity-dependent) decline of source space densities at high redshifts; the possible dichotomies between evolutionary properties of low- versus high-luminosity and of flat- versus steep-spectrum AGN-powered radio sources; and the nature of sources accounting for the upturn of source counts at sub-mJy levels. It is shown that straightforward extrapolations of evolutionary models, accounting for both the far-IR counts and redshift distributions of star-forming galaxies, match the radio source counts at flux-density levels of tens of  $\mu$ Jy remarkably well. We consider the statistical properties of rare but physically very interesting classes of sources, such as GHz Peak Spectrum and ADAF/ADIOS sources, and radio afterglows of  $\gamma$ -ray bursts. We also discuss the exploitation of large-area radio surveys to investigate large scale structure through studies of clustering and the Integrated Sachs-Wolfe effect. Finally we briefly describe the potential of the new and forthcoming generations of radio telescopes. A compendium of source counts at different frequencies is given in an appendix.

**Keywords** Radio continuum: galaxies · Galaxies: active · Galaxies: starburst · Galaxies: statistics · Quasars: general

---

G. De Zotti and Marcella Massardi  
INAF - Osservatorio Astronomico di Padova, Vicolo dell'Osservatorio 5, I-35122 Padova, Italy  
and SISSA/ISAS, Via Beirut 2-4, I-34014 Trieste, Italy  
Tel.: +39-049-8293444, Fax: +39-049-8759840  
E-mail: gianfranco.dezotti,marcella.massardi@oapd.inaf.it

Mattia Negrello  
Department of Physics and Astronomy, Open University, Walton Hall, Milton Keynes MK7  
6AA, United Kingdom  
E-mail: m.negrello@open.ac.uk

Jasper V. Wall  
Department of Physics and Astrophysics, University of British Columbia, Vancouver, Canada  
V6T 1Z1  
E-mail: jvw@astro.ubc.ca

## 1 Introduction

For several decades, extragalactic radio surveys remained the most powerful tool to probe the distant universe. Even ‘shallow’ radio surveys, those of limited radio sensitivity, reach sources with redshifts predominantly above 0.5. Since the 1960s, the most effective method for finding high- $z$  galaxies has been the optical identification of radio sources, a situation persisting until the mid-1990s, when the arrival of the new generation of 8-10 m class optical/infrared telescopes, the refurbishment of the Hubble Space Telescope, the Lyman-break technique (Steidel et al. 1996) and the Sloan Digital Sky Survey (York et al. 2000) produced an explosion of data on high-redshift galaxies.

This is not a historical account (see Sullivan III 2009); but listing the revolutions in astrophysics and cosmology wrought by radio surveys serves to set out concepts and terminology. On the astrophysics side we note the following:

1. **Active Galactic Nuclei (AGNs)** The discovery of radio galaxies (Bolton et al. 1949; Ryle et al. 1950) whose apparently prodigious energy release (Burbidge 1959) suggested Compton catastrophe, calling the cosmological interpretation of redshifts into question.
2. **Synchrotron emission** The identification of synchrotron emission (Ginzburg 1951; Shklovskii 1952) as the dominant continuum process producing the apparent power-law spectra of radio sources.
3. **Quasars** The discovery of quasars, starting with 3C 273 (Hazard et al. 1963; Schmidt 1963), leading to the picture of the collapsed supermassive nucleus (Hoyle & Fowler 1963), and hence to the now-accepted view of the powerful Active Galactic Nucleus (AGN) – massive black-hole - accretion disk systems (Lynden-Bell 1969) powering double-lobed (Jennison & Das Gupta 1953) radio sources via ‘twin-exhaust’ relativistic beams (Blandford & Rees 1974; Scheuer 1974).
4. **Relativistic beaming** The discovery of superluminal motions of quasar radio components (Cohen et al. 1971), this non-anisotropic emission (anticipated by Rees 1967) resolving the Compton non-catastrophe (Woltjer 1966) and leading to the development of unified models of radio sources: quasars and radio galaxies are one and the same, with orientation of the axis to the viewer’s line of sight determining classification via observational appearance (Antonucci & Miller 1985; Barthel 1989; Urry & Padovani 1995).

On the cosmology side we note the following:

1. **Scale of the observable Universe** An irrefutable argument by Ryle & Scheuer (1955) placed the bulk of ‘radio stars’ beyond 50 Mpc, and it was quickly realized when arcmin positional accuracy became available (Smith 1952) that the majority of the host galaxies were beyond the reach of the optical telescopes of the epoch. Minkowski (1960) measured a redshift of 0.46 for 3C 295, the redshift record for a galaxy for 10 years. Astronomers had discovered a set of objects substantially ‘beyond’ the recognized Universe. By 1965 the redshift record was 2.0 for the quasar 3C 9 (Schmidt 1965). Only after the turn of the century did the redshift record become routinely set by objects discovered in surveys other than at radio wavelengths (e.g. Stern 2000).
2. **History of the Universe** Early radio surveys generated a passionate and personal debate, the Steady-State vs Big-Bang controversy. It was rooted in the simplest statistics to be derived from any survey: the *integral* source counts, the

number of objects per unit sky area above given intensities or flux densities. As discussed by Ryle & Scheuer (1955), the source count from the 2C radio survey (Shakeshaft et al. 1955) showed a cumulative (integral) slope of  $\sim -3$ , far steeper than that expected from the Steady-State prediction, any reasonable Friedman model, or from a static Euclidean universe. For each of these, the initial slope at the highest flux densities is  $-3/2$ . (Euclidean case: the number of sources,  $N$ , is proportional to the volume, i.e. to  $r^3$  for a sphere; the flux density is  $\propto r^{-2}$ , so that  $N \propto S^{-3/2}$ .) Bondi & Gold (1948) together with Hoyle (1948) were uncompromising proponents of the new Steady-State theory. Ryle et al. interpreted the 2C apparent excess of faint sources in terms of the radio sources having far greater space density at earlier epochs of the Universe. Confusion, the blending of weak sources to produce a continuum of strong sources, was then shown to have disastrous effects on the early Cambridge source counts. From an independent survey in the South, Mills et al. (1958) found an initial slope of  $-1.65$  after corrections for instrumental effects, significantly lower than that found for 2C. Scheuer (1957) developed the P(D) technique, circumventing confusion and showing that the interferometer results of 2C were consistent with the findings of Mills et al. But the damage had been done: cosmologists, led by Hoyle, believed that radio astronomers did not know how to interpret their data.

In 1965 the ‘source-count controversy’ became irrelevant in one sense. Penzias & Wilson (1965) found what was immediately interpreted (Dicke et al. 1965) as the relic radiation from a hot dense phase of the Universe. The Big Bang was confirmed.

Ryle was right all the time. Integral source-count slopes of  $-1.8$  or even as shallow as  $-1.5$  were nowhere near what the known redshifts plus Steady State cosmology – or even any standard Friedman cosmology – predicted. These all come out at  $-1.2$  or  $-1.3$ , shallower than the asymptotic  $-1.5$  as sources of infinite flux density are not observed, and nobody has ever claimed the initial source count slope at any frequency to be as flat as this. The discovery of the fossil radiation (see Peebles et al. 2009) may indeed have shown that a Big Bang took place; but the source counts demonstrated further that *objects in the Universe evolve either individually or as a population* – a concept not fully accepted by the astronomy community until both galaxy sizes and star-formation rates were shown to change with epoch.

Source counts from radio and mm surveys – with errors and biases now understood – are currently recognized as essential data in delineating the different radio-source populations and in defining the cosmology of AGNs. These counts are dominated down to milli-Jansky (mJy) levels by the canonical radio sources, believed to be powered by supermassive black-holes (e.g. Begelman et al. 1984) in AGNs. At fainter flux-density levels, a flattening of slope in the Euclidean normalized *differential* counts (i.e. counts of sources with flux density  $S$ , within  $dS$ , multiplied by  $S^{2.5}$ , see §2) was found (Windhorst et al. 1984; Fomalont et al. 1984; Condon & Mitchell 1984), interpreted at the time as the appearance of a new population whose radio emission is, to some still-debated extent, associated with star-forming galaxies.

Radio-source spectra are usually described as power laws ( $S_\nu \propto \nu^{-\alpha}$ )<sup>1</sup>; the early low-frequency meter-wavelength (e.g. 178 MHz) surveys found radio sources with spectra almost exclusively of steep power-law form, with  $\alpha \sim 0.8$ . Later surveys at cm-

---

<sup>1</sup> We note that this negative sign convention for  $\alpha$  is not universal; however the convention has been adopted for the K-corrections of optical quasars and for the extrapolation from optical to X-rays ( $\alpha_{ox}$ ).

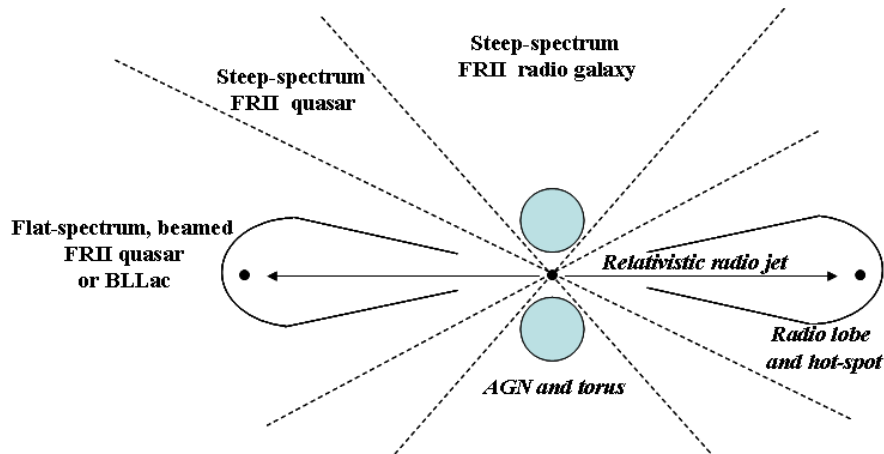


**Fig. 1** Unified scheme for high radio-power Fanaroff-Riley (1974; FR II) sources (following Jackson & Wall 1999).

wavelengths (higher frequencies, e.g. 5 GHz) found objects of diverse spectral types, some with spectra rising to the high frequencies, some with steep low-frequency portions flattening and rising to the high frequencies, and yet others with a hump in the radio regime, or indeed two or more humps. In general, anything which was not ‘steep-spectrum’ in form was called ‘flat-spectrum’, an inaccurate nomenclature: very few truly flat-spectrum sources have been found and even then the flatness persists over only a limited frequency range. Nevertheless AGN-powered radio sources are traditionally classified in two main categories: steep- ( $\alpha > 0.5$ ) and flat-spectrum ( $\alpha < 0.5$ ). Broadly speaking, to radio telescopes the steep-spectrum objects showed extended double-lobed structures, while the flat-spectrum objects were point sources, unresolved until the Very-Long-Baseline Interferometry (VLBI) technique provided sub-arc-second mapping. The compact nature of flat-spectrum sources led to the conventional interpretation of synchrotron self-absorption at frequencies below the bump(s), implying brightness temperatures of  $\sim 10^{11}$  K for the estimated magnetic field strengths.

From a physical point of view, it is appropriate to consider the integrated spectra as composites, built of the combination of different *components* of radio sources. *Unified models* provide a framework for such a discussion.

In the widely accepted ‘unification’ scheme (Scheuer & Readhead 1979; Orr & Browne 1982; Scheuer 1987; Barthel 1989) the appearance of sources, including this steep-spectrum/flat-spectrum dichotomy, depends primarily on their their axis orientation relative to the observer. This paradigm stems from the discovery of relativistic jets (Cohen et al. 1971; Moffet et al. 1972) giving rise to strongly anisotropic emission. In the radio regime (Fig. 1), a line-of-sight close to the source jet-axis offers a view of the compact, Doppler-boosted, flat-spectrum base of the approaching jet. Doppler-boosted low-radio-power (Fanaroff & Riley 1974, type I (FRI; edge-dimmed)) sources are associated with BL Lac objects, characterized by optically-featureless continua, while the powerful type II (FR II; edge-brightened) sources are seen as flat-spectrum radio quasars (FSRQs). The view down the axis offers unobstructed sight of the black-hole – accretion disk nucleus at wavelengths from soft X-rays to UV to IR, and this accretion-disk radiation may outshine the starlight of the galaxy by 5 magnitudes. The source

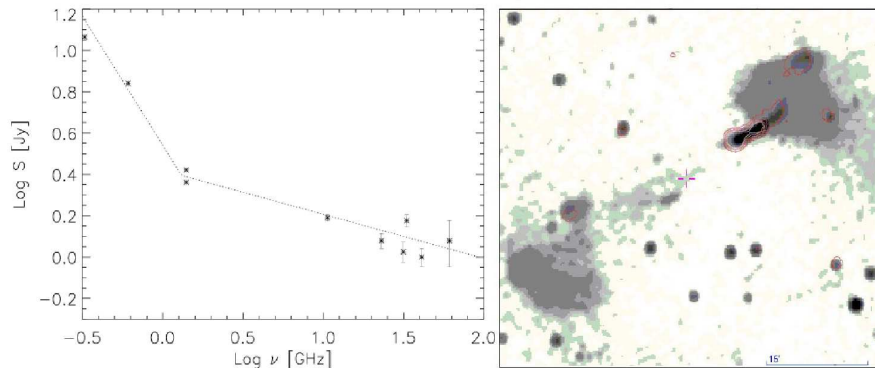


**Fig. 2** Spectral behaviour in the millimeter band of the radio galaxy NGC6251 (left panel) and (right panel) 11-GHz isophotes overlaid on the 0.3 GHz map (Mack et al. 1997). The low-frequency spectrum is due to the steep-spectrum outer lobes while at higher frequencies the flatter-spectrum core-jet system dominates.

appears stellar, either as a FSRQ or a BL Lac object. FSRQs and BL Lacs are collectively referred to as *blazars*. In the case of a side-on view, the observed low-frequency emission is dominated by the extended, optically-thin, steep-spectrum components, the radio lobes; and the optical counterpart generally appears as an elliptical galaxy. A dusty torus (Antonucci & Miller 1985) hides the black-hole – accretion-disk system from our sight (Fig. 1). At intermediate angles between the line-of-sight and the jet axis, angles at which we can see into the torus but the alignment is not good enough to see the Doppler-boosted jet bases, the object appears as a ‘steep-spectrum quasar’.

In general, then, each source has both a compact, flat-spectrum core and extended steep-spectrum lobes (Fig. 2). This already implies that a simple power-law representation of the integrated radio spectrum can only apply to a limited frequency range. The reality is even more complex (Wall 1994). External absorption or, more frequently, self-absorption (synchrotron and free-free) can produce spectra rising with frequency at the low-frequency optically-thick regime, while at high frequencies the synchrotron emission becomes optically thin, power law, and energy losses of relativistic electrons (“electron ageing”, Kellermann 1966) translate into a spectral steepening.

Two classes of ultra-steep-spectrum ( $\alpha > 1.3$ ) sources have been discovered. One is associated with galaxy clusters; the objects are of relatively low luminosity and generally are not associated with any host galaxy. They are diffuse and of several types, including cluster ‘radio halos’, ‘radio relics’ and ‘mini-halos’, and each type appears to involve reactivation of the hot intra-cluster medium by shocks or cooling flows, the observed form depending on the cluster evolutionary state (Feretti 2008). These ‘radio ghosts’ will not be discussed further here. The second class of ultra-steep-spectrum source is very radio-luminous and these are mostly identified with very-high-redshift radio galaxies. The high redshifts tempt the suggestion that the steep spectral index is due to the effect of redshift moving the steepest part of the spectrum (where electron ageing effects are strong) into the observed frequency range. However, Klamer et al. (2006) demonstrated that this is not the dominant mechanism, and that high-redshift radio galaxies, discovered by the steep-spectrum technique, have intrinsically power-law spectra. The selection of ultra-steep-spectrum sources is a very effective, but not the only (Jarvis et al. 2009), way to find *high redshift radio galaxies* (see Miley & De Breuck

2008, for a comprehensive review), including the one holding the current record, TN J0924-2201 at  $z = 5.19$  ( $\alpha_{0.365}^{1.4} \simeq 1.6$ ; van Breugel et al. 1999). The highest-redshift radio-loud *quasar* known to date, the  $z = 6.12$  QSO J1427+3312 (McGreer et al. 2006), also has a steep radio spectrum ( $\alpha_{1.4}^{8.4} = 1.1$ ) although it was not discovered through this characteristic.

In very compact regions, synchrotron self-absorption can occur up to very high radio frequencies, giving rise to sources with spectral peaks in the GHz range. At high radio luminosities this category comprises the GHz Peaked Spectrum (GPS) sources (O’Dea 1998) some of which peak at tens of GHz (High Frequency Peakers; Edge et al. 1998; Dallacasa et al. 2000, 2002; Tinti et al. 2005). At low luminosities, high-frequency spectral peaks, again due to strong synchrotron self-absorption, may be indicative of radiatively inefficient accretion, thought to correspond to late phases of the AGN evolution, with luminosities below a few percent of the Eddington limit (advection-dominated accretion flows (ADAF, Quataert & Narayan 1999) or adiabatic inflow-outflow scenarios (ADIOS, Blandford & Begelman 1999, 2004)).

As the ‘flat’ spectra are actually the superposition of emitting regions peaking over a broad frequency range (Kellermann & Pauliny-Toth 1969; Cotton et al. 1980), whose emission is strongly amplified and blue-shifted by relativistic beaming effects, a power-law description is a particularly bad approximation. The spectral shapes are found to be complicated, and generally show single or multiple humps. Many of these show flux-density variations, attributed to the birth and expansion of new components and shocks forming in relativistic flows in parsec-scale regions. The variations may be on times scales from hours to months or even years, and substantial resources have been devoted to monitoring these variable sources, led by groups at Michigan (USA) and Metsahövi (Finland) (e.g. Aller et al. 2003; Valtonen et al. 2008). The latter reference shows how global (multi-wavelength and multi-telescope) these monitoring programmes have become; moreover the quasi-periodicity for the object in question, OJ 287, indicates that it is probably a binary black-hole system. With regard to flux variations, we also note the ‘Intra-Day Variables’ (IDVs), blazars whose flux densities vary wildly on time scales from minutes to days: these are flat-spectrum objects with extremely small components that show inter-stellar scintillation (ISS) via the turbulent, ionized inter-stellar medium (ISM) of our Galaxy (e.g. Lovell et al. 2007). Detailed discussion of all these variable objects is beyond the scope of this review.

The discovery of Compact Steep Spectrum sources (CSS; Kapahi 1981; Peacock & Wall 1982; O’Dea 1998) originally appeared to be an exception to the conventional wisdom that steep and flat spectra are associated with extended and compact sources respectively. CSS sources are unresolved or barely resolved by standard interferometric observations (arcsec resolution), and the integrated spectra show peaks at  $< 0.5$  GHz, above which the spectral indices (on average,  $\alpha \sim 0.75$ ) are typical of extended radio sources. There is compelling evidence that these objects, as well as GPS and associated types of object (HFPs and CSOs – Compact Symmetric Objects) are *young radio galaxies*, as summarized concisely by Snellen (2008).

It follows from the above that the conventional two-population approach (flat- and steep-spectrum) assuming power-law spectra is particularly defective at high radio frequencies, where several different factors (emergence of compact cores of powerful extended sources, steepening by electron energy losses, transition from the optically-thick to the optically-thin synchrotron regime of very compact emitting regions, etc.) combine to produce complex spectra (see Fig. 3). Nevertheless, for many practical

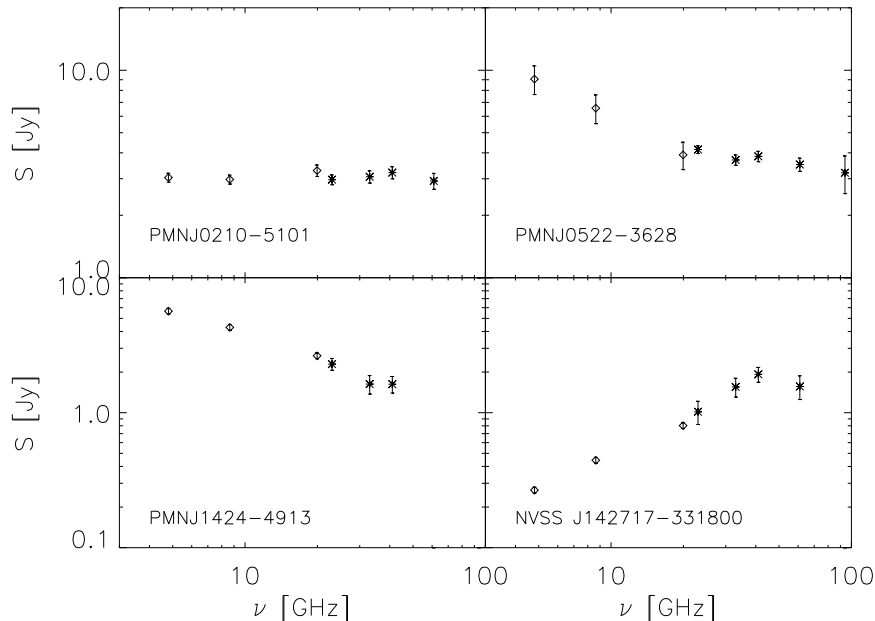


**Fig. 3** Examples of radio-source spectra at mm wavelengths: a flat-spectrum source (*top left panel*); a steep-spectrum source (*bottom left panel*); a source whose spectrum flattens at  $\nu \sim 10$  GHz (*top right panel*); a High Frequency Peaker (HFP) source (*bottom right panel*). Data from the NEWPS Catalogue (López-Cañiegos et al. 2007, *asterisks*) and from the AT20G Survey (*diamonds*, Massardi et al. 2008a).

applications the conventional approach remains useful in describing the bulk population properties of AGN-powered radio sources.

The radio emission of star-forming galaxies is mostly optically-thin synchrotron from relativistic electrons interacting with the galactic magnetic field, but with significant free-free contributions from the ionized interstellar medium (Condon 1992; Bressan et al. 2002; Clemens et al. 2008). At mm wavelengths, however, the radio emission is swamped by (thermal) dust emission, whose spectrum rises steeply with increasing frequency. The well-known tight correlation between radio and far-IR emission of star-forming galaxies (Helou et al. 1985; Gavazzi et al. 1986; Condon et al. 1991) vastly increases the body of data relevant to characterize, or at least constrain the evolutionary properties of this population. However, to date few attempts have been made to build comprehensive models encompassing both radio and far-IR/sub-mm data (but see Gruppioni et al. 2003).

In this paper we first review the observed radio to mm-wave source counts (§ 2), the data on the local luminosity function of different radio source populations (§ 3), and the source spectral properties (§ 4). Next (§ 5) we look at evolutionary models for the classical radio sources as well as for individual populations, such as GPS sources, ADAF/ADIOS sources, and (§ 6) star-forming galaxies and  $\gamma$ -ray afterglows at radio wavelengths. We deal briefly with the Radio Background (§ 7) and the Sunyaev-Zeldovich effect on cluster and galaxy scales (§ 8). Section 9 contains a summary of the

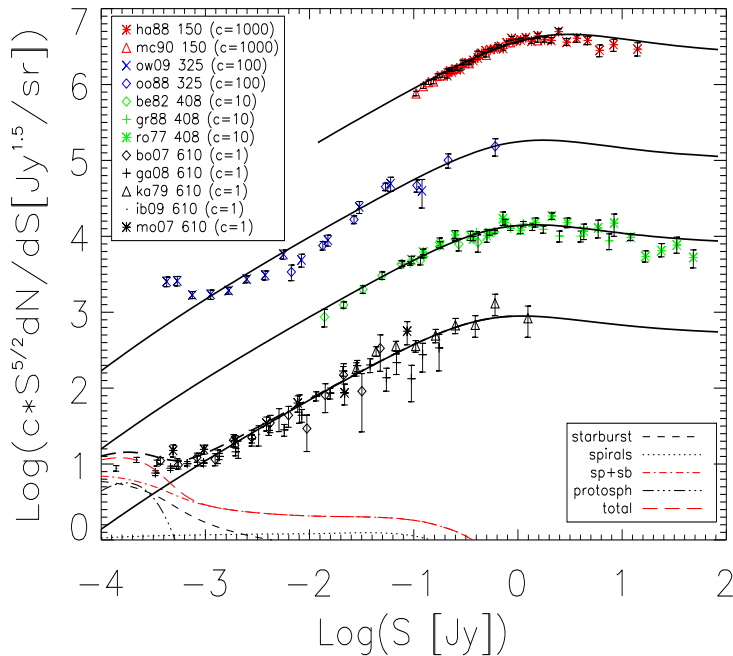


**Fig. 4** Differential source counts at 150, 325, 408, 610 MHz normalized to  $cS_\nu^{-2.5}$ , with  $c = 1000, 100, 10, 1$  respectively. Reference codes are spelt out in the notes to Tables 1, 3, and 4. The lines are fits yielded by an updated evolution model (Massardi et al., in preparation).

information on large scale structure stemming from large-area radio surveys. Finally, in § 10 we summarize perspectives for the future, and § 11 contains some conclusions.

Unless otherwise noted, we adopt a flat  $\Lambda$ CDM cosmology with  $\Omega_\Lambda = 0.7$  and  $H_0 = 70 \text{ km s}^{-1} \text{ Mpc}^{-1}$ .

## 2 Observed source counts

### 2.1 From surveys to counts

The counts of sources demand cosmic evolution, but by themselves provide limited information on this evolution. Since even bright radio sources are frequently optically faint to invisible, the traditional way to characterize the evolutionary properties relies heavily on source counts from blind surveys, with limited and incomplete cross-wavelength identification and redshift information. However, as discovered in the 2C survey, getting from a sky survey to a source count is difficult, and modern instrumentation, while generally avoiding the confusion issue which bedevilled 2C, does not remove the difficulties.

It is surface brightness, or rather differential surface brightness above a background (CMB, Galactic radiation, ground radiation), which is measured in radio/mm surveys.



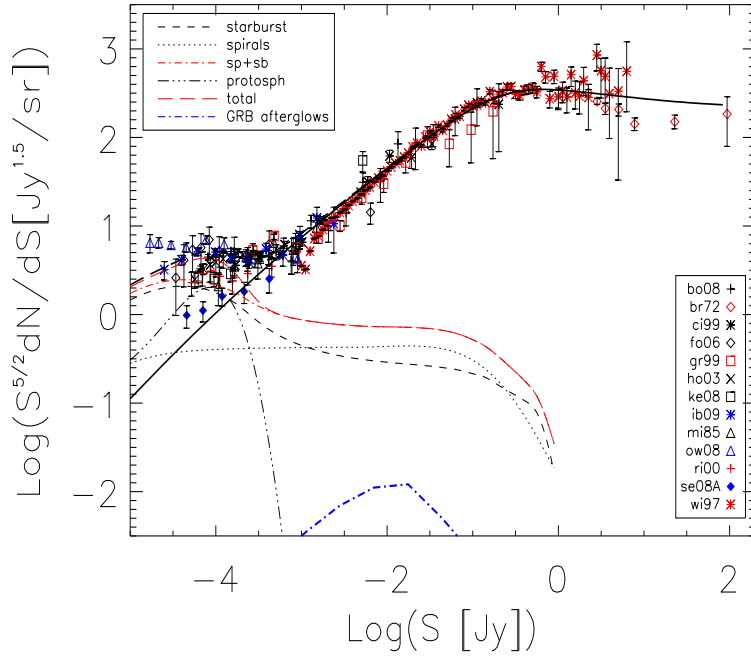


**Fig. 5** Normalized differential source counts at 1.4 GHz. Note that the filled diamonds show the counts of AGNs only, while all the other symbols refer to total counts. Reference codes are spelt out in the note to Table 5. A straightforward extrapolation of evolutionary models fitting the far-IR to mm counts of populations of star-forming (normal late type (spirals or sp), starburst (sb), and proto-spheroidal) galaxies, exploiting the well established far-IR/radio correlation, naturally accounts for the observed counts below  $\sim 30 \mu\text{Jy}$  (see §6). At higher flux densities the counts are dominated by radio-loud AGNs: the thick solid line shows the fit of the same model as in Fig. 4. The dot-dashed line shows the counts of  $\gamma$ -ray burst (GRB) afterglows predicted by the Ciardi & Loeb (2000) model.

Discrete sources stand out from this background by virtue of apparent high differential *surface brightness*,  $\Delta T_b$ . The simple relations linking  $\Delta T_b$  to point-source flux density (via the Rayleigh-Jeans approximation and the radiometer equation incorporating telescope and receiver parameters) appear in basic radio astronomy texts, e.g Burke & Graham-Smith (1997).

Surveys are complete only to a given limit in  $\Delta T_b$ , translating to *Jy per beam area*<sup>2</sup>. For point sources, this limit is clearly defined. For extended sources, the total flux density

$$S_\nu = \int_{\Omega} B_\nu(\theta, \phi) d\Omega, \quad (1)$$

i.e. the incremental brightness  $B$  must be integrated over the extent of the source to find the total flux density. If a source is extended and its brightness temperature is constant across the beam response, then given the Rayleigh-Jeans approximation  $B = 2k_B T_b / \lambda^2$

<sup>2</sup> 1 Jy (Jansky) =  $10^{-26} \text{ W Hz}^{-1} \text{ m}^{-2}$  or  $10^{-23} \text{ erg cm}^{-2} \text{ s}^{-1} \text{ Hz}^{-1}$

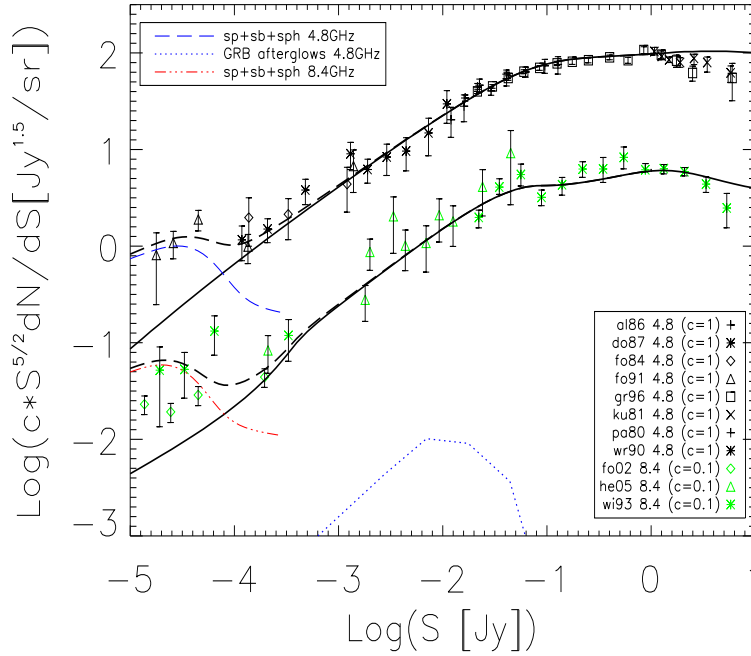


**Fig. 6** Differential source counts at 4.8 and 8.4 GHz normalized to  $c \times S_\nu^{-2.5}$ , with  $c = 1$  and 0.1, respectively. Reference codes are spelt out in the notes to Tables 6 and 7. In the upper inset sp, sb, and sph stand for spiral, starburst and proto-spheroidal galaxies, respectively. The fit to the 4.8 GHz counts is from the same model as in Figs. 4 and 5, while at 8.4 GHz we show the fit yielded by the De Zotti et al. (2005) model, tailored for data above 5 GHz. The dotted line shows the counts of GRB afterglows at 3 GHz predicted by the Ciardi & Loeb (2000) model.

( $k_B$  is the Boltzmann constant,  $\lambda$  is wavelength), for a survey sensitivity limit of  $S_{\text{lim}}$  per beam, we have from eq. (1)

$$T_{b,\text{min}} = \frac{\lambda^2 S_{\text{lim}}}{2k_B \int d\Omega}. \quad (2)$$

The integral is the beam solid angle; for a circular Gaussian beam with full width at half maximum of FWHM arcsec, this may be approximated as  $2.66 \cdot 10^{-11}$  FWHM<sup>2</sup> sterad. Two iconic sky surveys at 1.4 GHz with the NRAO Very Large Array illustrate the brightness limit issue. For the FIRST survey (Becker et al. 1995) with FWHM = 5 arcsec and  $S_{\text{min}} = 1$  mJy, eq. (2) gives  $T_{\text{min}} \approx 24$  K, while for the NVSS survey (Condon et al. 1998) with a 45 arcsec beam and  $S_{\text{min}} = 3$  mJy,  $T_{\text{min}} \approx 0.9$  K. There are significant selection effects which arise as a consequence, most notably the lack of sensitivity in FIRST to the majority of spiral galaxies, near and far, as well as to low surface brightness features such as ghost or relic radiation. The redeeming features of its higher resolution are emphasized below.

It is a major undertaking to proceed from a list of deflections in Jy per beam, either apparently unresolved, or resolved as regions of emission, to a complete catalogue of radio/mm sources. In the first place, there is the surface brightness limitation described above; in the compromises of survey design it is critical to decide just what population(s) of sources will be incompletely represented. There is the issue of overlap: for instance Centaurus A, NGC 5128, the nearest canonical radio galaxy, extends over 9 degrees of the southern sky; there are many discrete distant sources catalogued within the area covered by Cen A. There is also the double nature of radio-galaxy emission: this requires that components found as individual detections be ‘matched up’ or assembled to find the true flux density of single sources, cores as well as double lobes. Moreover many sources show extended regions of lower surface brightness which are poorly aligned. If source scale is large enough, pencil-beam or filled aperture telescopes are better at finding and mapping these than are aperture-synthesis interferometers. The issue of ‘missing flux’ is notorious for interferometers, because of their limited response to the longer wavelengths of the spatial Fourier transform of the brightness distribution.

The difficulties have been brought to sharp focus by the excellent decision to carry out the two major VLA surveys, FIRST (Becker et al. 1995) and NVSS (Condon et al. 1998), both at 1.4 GHz but differing in resolution by a factor of 9. From these highly complementary surveys, the reality of how different resolutions affect raw source lists may be seen immediately (Blake & Wall 2002b). FIRST and NVSS are far more than the sum of the parts. The low resolution of NVSS gains the spiral galaxies and much other low-surface-brightness detail not seen in FIRST. The relatively high resolution of FIRST can be used to sort out the blends and overlaps in NVSS, and it enables direct cross-waveband identifications, a shortcoming of the lower NVSS resolution. Used together they can provide samples complete on many criteria; but significant effort in examining many individual emission features is still required.

With regard to surveys using interferometers, the noise level in an interferometric image is given by:

$$\sigma_{\text{image}} = \frac{\sqrt{2}k_B T_{\text{sys}}}{A\eta_e\eta_q} \sqrt{\frac{1}{t N_{\text{base}}\Delta\nu}}. \quad (3)$$

where  $T_{\text{sys}}$  is the system temperature,  $A$  is the antenna surface area,  $\eta_e$  is the aperture efficiency, the ratio of effective collecting area to surface area,  $\eta_q$  is the sampling efficiency depending on digitization levels and sampling rate,  $t$  is the integration time,  $N_{\text{base}} = N(N-1)/2$  is the number of baselines,  $N$  is the number of antennas, and  $\Delta\nu$  is the bandwidth. ( $\eta_e$  is generally 0.3 to 0.8, and  $\eta_q$  0.7 to 0.9.) The integration time per pointing needed to reach a detection limit of say  $S_{\text{lim}} = 5\sigma_{\text{image}}$  can be straightforwardly obtained from eq. (3). The number of pointings necessary to cover a sky solid angle  $\Omega_s$  with a telescope field of view FOV is<sup>3</sup>

$$n_p = \Omega_s/\text{FOV}. \quad (4)$$

If the integral counts of sources scale as  $S^{-\beta}$ , the number of sources detected in a given area scales as  $t^{\beta/2}$ . For a given flux density, the number of detections is proportional

---

<sup>3</sup> This assumes uniform response over the field-of-view. The inevitable non-uniformity across the FOV implies an additional factor of  $\sim 2$  for uniform sky coverage. The data from separate pointings are combined by squaring the relative response to weight the data by the square of the signal-to-noise ratio (SNR). If the beam is approximated by a Gaussian, then this process effectively halves the beam size; see Condon et al. (1998).

to the surveyed area, i.e. to  $t$ . Thus, to maximize the number of detections in a given observing time it is necessary to go deeper if  $\beta > 2$  and to survey a larger area if  $\beta < 2$ . The ‘narrow and deep’ vs. ‘wide and shallow’ argument for maximizing source yield always resolves, at radio frequencies, in favour of the latter, because  $\beta > 2$ , implying a differential count slope of less than  $-3$ , has never been observed at any flux-density level. On the other hand, very steep counts are observed at millimeter and sub-millimeter wavelengths (Austermann et al. 2009; Coppin et al. 2006).

Compilation of complete and reliable catalogues, complete samples, almost invariably involves data at other frequencies. Source-component assembly for example is an iterative process which may require cross-waveband identification of the host object, galaxy, quasar, etc. The identification process leads on to the construction of complete samples, complete at both the survey frequency and at some other wavelength, i.e. in optical/IR identifications. Such samples are rare and require great observational effort. One of the best known of these, the ‘3CRR’ sample (Laing et al. 1983) is a revised version of the revised 3C catalogue (Bennett 1962) from the original 3C survey of Edge et al. (1959). (The sample is also the most extreme sample of high-power radio AGN, and its contents are far from typical of the radio-mm survey population.) The process will become easier with large-area optical surveys such as SDSS (York et al. 2000) and with the advent of synoptic telescopes such as LSST.

Given complete samples, then, we can compile source counts. (It should be noted that these are frequently constructed by approximations from raw deflection lists, to circumvent the labour discussed above. *Caveat emptor*.<sup>4</sup>) Today the task of checking for systematic effects from approximations or statistical procedures is made easier because the counts from different survey samples – except for the very deepest ones – overlap at various flux-density levels. The counts are usually presented in ‘relative differential’ form, the differential counts  $dN/dS$  giving the number of sources per unit area with flux density  $S$  within  $dS$ , subsequently and conveniently normalized to the ‘Euclidean’ form, i.e. multiplied by  $cS^{2.5}$ , with  $c$  being a suitably chosen constant. (A uniform source distribution in a static Euclidean universe yields  $dN/dS \propto S^{-2.5}$  as described earlier). A summary of the available source counts at different frequencies is given in Tables 1–10 (see also Figs. 5–7).

In the case of surveys covering small areas, the field-to-field variations arising from the source clustering (sampling variance) further adds to the uncertainties. The fractional variance of the counts is (Peebles 1980):

$$\left\langle \frac{n - \langle n \rangle}{\langle n \rangle} \right\rangle^2 = \frac{1}{\langle n \rangle} + \sigma_v^2 \quad (5)$$

with

$$\sigma_v^2 = \frac{1}{\Omega^2} \int \int w(\theta) d\Omega_1 d\Omega_2 \quad (6)$$

where  $\theta$  is the angle between the solid angle elements  $d\Omega_1$  and  $d\Omega_2$ , and the integrals are over the solid angle covered by the survey.

---

<sup>4</sup> The buyer should also beware of confusing as complete samples (a) lists of sources in which large volumes of data are assembled from different surveys and different completeness algorithms (e.g. PKSCat90, Wright & Otrupcek 1990), and (b) spectral samples, in which flux-density measurements at different frequencies are assembled to obtain the integrated spectra of samples of sources not necessarily selected by survey completeness (e.g. Pauliny-Toth et al. 1966; Kellermann et al. 1969).

The angular correlation function of NVSS and FIRST sources (see § 9) is consistent with a power-law shape (Blake & Wall 2002a,b; Overzier et al. 2003):

$$w(\theta) \simeq 10^{-3}(\theta/\text{deg})^{-0.8}, \quad (7)$$

for angular separations up to at least  $4^\circ$ . Inserting eq. (7) in eq. (6) we get

$$\sigma^2 = 2.36 \times 10^{-3}(\Omega/\text{deg}^2)^{-0.4}. \quad (8)$$

The errors given in Tables 1–7 include this contribution for surveys over areas  $\leq 25 \text{ deg}^2$ .

Differences between source counts for independent fields are in general far larger than these errors imply (Condon 2007). There is little doubt that different calibrations, beam corrections and resolution corrections are the dominant if not exclusive culprits. Further advances in calibration procedures and characterization of the structures of faint sources will be required before sampling variance comes to dominate the errors in faint counts of radio sources.

## 2.2 Low frequency surveys

Low-frequency surveys have a long and illustrious (but initially chequered) history, as we have mentioned. The most extensive ones, both in terms of area (see also § 9) and of depth, are those at  $\sim 1 \text{ GHz}$  and at  $\sim 5 \text{ GHz}$ . The NRAO VLA Sky Survey (NVSS; Condon et al. 1998) covers the sky north of  $\delta = -40^\circ$  (82% of the celestial sphere) at 1.4 GHz, down to  $\sim 2.5 \text{ mJy}$ . It has resolution of 45 arcsec FWHM and the raw catalogue contains  $1.8 \times 10^6$  entries. It is complemented by the Sydney University Molonglo Sky Survey (SUMSS; Mauch et al. 2003) at 0.843 GHz. The survey was completed in 2007 with the Molonglo Galactic Plane Survey (MGPS; Murphy et al. 2007), and now covers the whole sky south of declination  $-30^\circ$ .

The VLA 1.4-GHz FIRST survey (for Faint Images of the Radio Sky at Twenty-cm; Becker et al. 1995) is the high-resolution (5 arcsec FWHM) counterpart of NVSS, and has yielded accurate ( $< 1 \text{ arcsec rms}$ ) radio positions of faint compact sources. The new catalog, released in July 2008 (format errors corrected in October 2008), covers  $\sim 8444 \text{ deg}^2$  in the North Galactic cap and  $611 \text{ deg}^2$  in the south Galactic cap, for a total of  $9055 \text{ deg}^2$  yielding a list of  $\sim 816,000$  objects. Northern and Southern areas were both chosen to coincide approximately with the area covered by the SDSS. The typical flux density detection threshold of point sources is of about  $1 \text{ mJy/beam}$ , decreasing to  $0.75 \text{ mJy/beam}$  in the southern Galactic cap equatorial stripe.

Almost full-sky coverage was also achieved at  $\sim 5 \text{ GHz}$  – albeit to a much higher flux-density level – by the combination of the Northern Green Bank GB6 survey with the Southern Parkes-MIT-NRAO (PMN) survey. The GB6 catalog (Gregory et al. 1996) covers the range  $0^\circ \leq \delta \leq 75^\circ$  down to  $\sim 18 \text{ mJy/beam}$ , the FWHM major and minor diameters are of  $3'.6$  and  $3'.4$ , respectively. The flux-density limit of the PMN catalog (Griffith & Wright 1993) is typically  $\sim 30 \text{ mJy/beam}$  but varies with declination, which spans the range from  $-87.5^\circ$  to  $+10^\circ$ ; the FWHM is of  $\simeq 4'.2$ .

Other large-area, low-frequency surveys:

- the VLA Low-Frequency Sky Survey (VLSS; Cohen et al. 2007) is a 74-MHz continuum survey covering the entire sky North of  $\delta = -30^\circ$  to a typical point-source detection limit of  $0.7 \text{ Jy}$ ;

- the Cambridge 6C survey at 151 MHz (Hales et al. 1993, and references therein) covers most of the extragalactic sky above  $\delta = 30^\circ$ , but generally away from the Galactic plane, with  $4.2' \times 4.2' \csc \delta$  resolution. The 7C survey (Hales et al. 2007), at the same frequency, covers a similar region of the sky with higher resolution ( $70'' \times 70'' \csc(\delta)$ ). A somewhat lower-resolution survey has been carried out in the low-declination strip  $9h < RA < 16h$ ,  $20^\circ < \delta < 35^\circ$  (Waldram et al. 1996).
- The 8C survey (Rees 1990; Hales et al. 1995) covers the polar cap above  $\delta = 60^\circ$  at 38 MHz with a typical limiting flux density of about 1 Jy/beam.
- The Westerbork Northern Sky Survey (WENSS; Rengelink et al. 1997; de Bruyn et al. 2000) covers the 3.14 sr north of  $\delta = +30^\circ$  at 326 MHz with  $54'' \times 54'' \csc(\delta)$  resolution in total intensity and linear polarization, to a flux-density limit of approximately 18 mJy/beam.

For more complete references to low-frequency radio surveys, see Tables 1–7.

### 2.3 Deep surveys and sub-mJy counts

The deepest surveys cover small areas of sky on the scales of the primary beams of synthesis telescopes; they are carried out with such telescopes in single long exposures, or in nested overlapping sets of such exposures. Because source counts are steep, only small survey areas are required to obtain large enough samples of faint sources to be statistically significant.

From such surveys, the deepest counts at 1.4 to 8.4 GHz show an inflection point at  $\lesssim 1$  mJy (Mitchell & Condon 1985; Windhorst et al. 1985; Hopkins et al. 1998; Richards 2000; Bondi et al. 2003; Ciliegi et al. 2003; Hopkins et al. 2003; Seymour et al. 2004; Huynh et al. 2005; Prandoni et al. 2006; Fomalont et al. 2006; Simpson et al. 2006; Bondi et al. 2007; Ivison et al. 2007; Bondi et al. 2008; Owen & Morrison 2008). The point of inflection was originally interpreted as signalling the emergence of a new source population (e.g. Condon 1984a, 1989). Windhorst et al. (1985) suggested that the majority of sub-mJy radio sources are faint blue galaxies, presumably undergoing significant star formation (SF), and Danese et al. (1987) successfully modeled the sub-mJy excess counts with evolving starburst galaxies, a model that also described the IRAS 60  $\mu\text{m}$  counts.

More recent data and analyses have confirmed that starburst galaxies are indeed a major component of the sub-mJy 1.4 GHz source counts, perhaps dominating below 0.3–0.1 mJy (Benn et al. 1993; Rowan-Robinson et al. 1993; Hopkins et al. 1998, 2000; Seymour et al. 2004, 2008; Muxlow et al. 2005; Moss et al. 2007; Padovani et al. 2009). However, spectroscopic results by Gruppioni et al. (1999b) suggested that early-type galaxies were the dominant population at sub-mJy levels. Further, it was recently suggested (and modeled) that the flattening of the source counts may be caused by radio-quiet AGN (radio-quiet quasars and type 2 AGN), rather than star forming galaxies (Simpson et al. 2006). Distinct counts for high and low-luminosity radio galaxies show that low-luminosity FRI-type galaxies probably make a substantial contribution to the counts at 1 mJy and somewhat below (Gendre & Wall 2008). Based on a combination of optical and radio morphology as an identifier for AGN and SF galaxies, Fomalont et al. (2006) suggested that at most 40% of the sub-mJy radio sources are AGNs, while Padovani et al. (2007b) indicated that this fraction may be 60–80%. Huynh et al. (2008) found that the host galaxy colors and radio-to-optical ratios indicate that low-luminosity (or “radio-quiet”) AGN make up a significant proportion

of the sub-mJy radio population. Smolčić et al. (2008), using a newly developed rest-frame-colour based classification in conjunction with the VLA-COSMOS 1.4 GHz observations, concluded that the radio population in the flux-density range of  $\sim 50 \mu\text{Jy}$  to 0.7 mJy is a mixture of 30–40% of star forming galaxies and 50–60% of AGN galaxies, with a minor contribution ( $\sim 10\%$ ) of QSOs.

The origin of these discrepancies can be traced to three main reasons (see also § 3). First, the identification fraction of radio sources with optical counterparts, which is generally taken to be representative of the full radio population, spans a wide range (20% to 90%) in literature depending on the depth of both the available radio and optical data. Second, it is important to make a distinction between the presence of an AGN in the optical counterpart of a radio source, and its contribution to the radio emission (Seymour et al. 2008). Non-radio AGN indicators like optical/IR colours, emission lines, mid-IR SEDs, X-ray emission, etc. are not well correlated with the radio emission of the AGNs and therefore are not necessarily valid diagnostics of radio emission powered by accretion onto a supermassive black hole (Muxlow et al. 2005). Third, there are uncertainties in specifying survey level: deep surveys normally cover but one primary beam area, heavily non-uniform in sensitivity. A survey claimed complete at some specified flux density in the central region alone is in fact heavily biased to sources of 5 to 10 times this flux density; the survey as a result is biased to the higher-flux-density population, namely AGNs.

Seymour et al. (2008) used four diagnostics (radio morphology, radio spectral index, radio/near-IR and mid-IR/radio flux-density ratios) to single out, in a statistical sense, radio emission powered by AGN activity. They were able to calculate the source counts separately for AGNs and star-forming galaxies. The latter were found to dominate below  $\simeq 0.1$  mJy at 1.4 GHz, while AGNs still make up around one quarter of the counts at  $\sim 50 \mu\text{Jy}$ .

Bondi et al. (2008) pointed to evidence of a decline of the 1.4 GHz counts below  $\sim 0.1$  mJy. It is possible that a new upturn may be seen at  $\lesssim 1 \mu\text{Jy}$ , due to the emergence of normal star-forming galaxies (Windhorst et al. 1999; Hopkins et al. 2000).

Essentially all surveys and catalogues are carried out and compiled without reference to polarization (the NVSS being an important exception): linear polarization is generally less than a few percent, and certainly at mJy levels, below the uncertainties in flux densities due to calibration, noise and confusion. An average of circular polarizations is generally used. (Subsequent to surveys, thousands of measurements of polarization on individual sources have been carried out at different frequencies, with the rotation measures thus derived used to map the details of the Galactic magnetic field – see e.g. Brown et al. (2007)). The DRAO 1.4-GHz survey of the ELAIS N1 field (Taylor et al. 2007) was carried out expressly to examine polarization statistics. The data at the faintest flux densities, 0.5 to 1.0 mJy, show a trend of increasing polarization fraction with decreasing flux density, previously noted by Mesa et al. (2002) and Tucci et al. (2004), at variance with current models of population mix and evolution.

## 2.4 High frequency surveys and counts

High-frequency surveys up into the mm-wavelength regime vitally complement their low-frequency counterparts. The early cm-wavelength surveys (Parkes 2.7 GHz, NRAO 5 GHz) in the late 1960s and 1970s found that flat-spectrum sources – or at least sources whose integrated spectra were dominated by components showing synchrotron

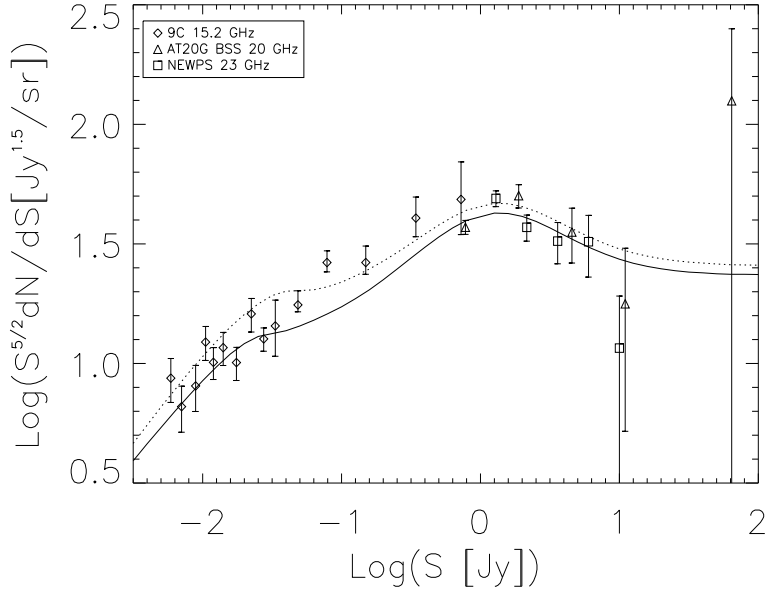


**Fig. 7** Differential source counts normalized to  $S_\nu^{-2.5}$  for the 15 GHz 9C survey (Waldram et al. 2003, 2009), for the 20 GHz ATCA Bright Source Sample (Massardi et al. 2008a), and for the WMAP 23 GHz survey (Massardi et al. 2009). The model by De Zotti et al. (2005) is also shown for comparison (solid line: 20 GHz, dotted: 15 GHz).

self-absorption – constitute 50% or more of all sources in high flux-density samples. Modelling space density to examine evolution demands determination of the extent and nature of this emergent population, most members of which are blazars.

High-frequency surveys are very time-consuming. For telescopes with diffraction-limited fields of view the number of pointings necessary to cover a given area scales as  $\nu^2$ . For a given receiver noise and bandwidth, the time per pointing to reach the flux level  $S$  scales as  $S^{-2}$  so that, for a typical optically-thin synchrotron spectrum ( $S \propto \nu^{-0.7}$ ), the survey time scales as  $\nu^{3.4}$ . However usable bandwidth is roughly proportional to frequency, so that the scaling becomes  $\sim \nu^{2.4}$ ; but a 20 GHz survey still takes more than  $\sim 25$  times longer than a 5 GHz survey to cover the same area to the same flux-density limit.

High-frequency surveys have an additional aspect of uncertainty: variability. The self-absorbed components are frequently unstable, young and rapidly evolving. Variability by itself would not be an issue except for the fact that it leads to serious biases. This is primarily because a survey will always select objects in a high state at the expense of those in a low state, and the steep source count at high flux densities exacerbates this situation. A second issue concerns the spectra. Sources are predominantly detected ‘high’; to return after the survey for flux-density measurements at other frequencies guarantees (statistically) that these new measurements will relate to a lower state. Non-contemporaneous spectral measurements – if above the survey frequency – will be biased in the sense of yielding spectra apparently steeper than at the survey



epoch. The bias can have serious consequences for e.g. K-corrections in space-density studies, as described below.

Cosmic Microwave Background (CMB) studies, boosted by the on-going NASA WMAP mission and by the forthcoming ESA Planck mission, require an accurate characterization of the high-frequency properties of foreground radio sources both in total intensity and in polarization. Radio sources are the dominant contaminant of small-scale CMB anisotropies at mm wavelengths. This can be seen by recalling that the mean contribution of unresolved sources with flux  $S_i$  to the antenna temperature  $T_A$  measured within a solid angle  $\Omega$  is:

$$T_A = \frac{\sum_i S_i \lambda^2}{2k_B \Omega} = \frac{\sum_i S_i \ell^2 \lambda^2}{8k_B \pi^2}, \quad (9)$$

where  $k_B$  is the Boltzmann constant,  $\lambda$  is the observing wavelength, and we have taken into account that for high multipoles ( $\ell \gg 1$ ),  $\Omega \simeq (2\pi/\ell)^2$ . If sources are randomly distributed on the sky, the variance of  $T_A$  is equal to the mean, and their contribution to the power spectrum of temperature fluctuations grows as  $\ell^2$  while the power spectra of the CMB and of Galactic diffuse emissions decline at large  $\ell$ 's (small angular scales). Therefore, Poisson fluctuations due to extragalactic sources are the dominant contaminant of CMB maps on scales  $\lesssim 30'$ , i.e.  $\ell \gtrsim 400$  (De Zotti et al. 1999; Toffolatti et al. 1999).

The diversity and complexity of radio-source spectra, particularly for sources detected at the higher frequencies, make extrapolations from low frequencies, where extensive surveys exist, unreliable for the purpose of establishing CMB contamination. Removing this uncertainty was the primary motivation of the Ryle-Telescope 9C surveys at 15.2 GHz (Taylor et al. 2001; Waldram et al. 2003). These were specifically designed for source subtraction from CMB maps produced by the Very Small Array (VSA) at 34 GHz. The surveys have covered an area of  $\simeq 520 \text{ deg}^2$  to a  $\simeq 25 \text{ mJy}$  completeness limit. Waldram et al. (2009) reported on a series of deeper regions, amounting to an area of  $115 \text{ deg}^2$  complete to approximately 10 mJy, and of  $29 \text{ deg}^2$  complete to approximately 5.5 mJy. The counts over the full range 5.5 mJy – 1 Jy are well described by a simple power-law:

$$\frac{dN}{dS} \simeq 51 \left( \frac{S}{\text{Jy}} \right)^{-2.15} \text{ Jy}^{-1} \text{ sr}^{-1}. \quad (10)$$

A 20-GHz survey of the full Southern sky to a limit of  $\simeq 50 \text{ mJy}$  has been carried out by exploiting the Australia Telescope Compact Array (ATCA) fast-scanning capabilities ( $15^\circ \text{ min}^{-1}$  in declination along the meridian) and the 8-GHz bandwidth of an analogue correlator. The correlator was originally developed for the Taiwanese CMB experiment AMiBA (Lo et al. 2001) but has been applied to three of the 6 22 m dishes of the ATCA. A pilot survey (Ricci et al. 2004; Sadler et al. 2006) at 18.5 GHz was carried out in 2002 and 2003. It detected 173 sources in the declination range  $-60^\circ$  to  $-70^\circ$  down to 100 mJy. The full survey was begun in 2004 and was completed in 2008. More than 5800 sources brighter than 45 mJy were detected below declination  $\delta = 0^\circ$ . An analysis of a complete flux-limited sub-sample ( $S_{20\text{GHz}} > 0.50 \text{ Jy}$ ) comprising 320 extragalactic radio sources was presented by Massardi et al. (2008a).

Shallow (completeness levels  $\gtrsim 1 \text{ Jy}$ ) all-sky surveys at 23, 33, 41, 61, and 94 GHz have been carried out by the Wilkinson Microwave Anisotropy Probe (WMAP). Analyses of WMAP 5-year data have yielded from 388 (Wright et al. 2009) to 516

(Massardi et al. 2009) detections. Of the latter, 457 are identified with previously-catalogued extragalactic sources, 27 with Galactic sources; 32 do not have counterparts in lower frequency all sky surveys and may therefore be just high peaks of the highly non-Gaussian fluctuation field.

Counts at  $\sim 30$  GHz have been estimated from DASI data over the range 0.1 to 10 Jy (Kovac et al. 2002), from CBI maps in the range 5–50 mJy (Mason et al. 2003), and down to 1 mJy from the SZA blind cluster survey (Muchovej et al. 2009, in prep.).

Clary et al. (2005) used 33-GHz observations of sources detected at 15 GHz to extrapolate the 9C counts in the range  $20 \text{ mJy} \leq S_{33} \leq 114 \text{ mJy}$ . Mason et al. (2009) carried out Green Bank Telescope (GBT) and Owens Valley Radio Observatory (OVRO) 31-GHz observations of 3165 NVSS sources; 15% of them were detected. Under the assumption that the  $S_{31\text{GHz}}/S_{1.4\text{GHz}}$  flux ratio distribution is independent of the 1.4 GHz flux density over the range of interest, they derived the maximum likelihood 1.4 to 31 GHz spectral index distribution, taking into account 31-GHz upper limits, and exploited it to estimate the 31-GHz source counts at mJy levels:  $N(> S) = (16.7 \pm 0.4) \text{ deg}^{-2} (S/1 \text{ mJy})^{-0.80 \pm 0.01}$  ( $0.5 \text{ mJy} < S < 10 \text{ mJy}$ ). The derived counts were found to be 15% lower than predicted by the De Zotti et al. (2005) model.

Preliminary indications of a spectral steepening of flat-spectrum sources above  $\sim 20$  GHz, beyond the expectations of the blazar sequence model (Fossati et al. 1998; Ghisellini et al. 1998) have been reported. Waldram et al. (2007) used the spectral-index distributions over the range 1.4–43 GHz based on ‘simultaneous’ multifrequency follow-up observations (Bolton et al. 2004) of a sample of extragalactic sources from the 9C survey at 15 GHz to make empirical estimates of the source counts at 22, 30, 43, 70, and 90 GHz by extrapolating the power-law representation of the 15-GHz counts [eq. (10)]. Sadler et al. (2008) carried out simultaneous 20- and 95-GHz flux densities measurements for a sample of AT20G sources. The inferred spectral-index distribution was used to extrapolate the AT20G counts to 95 GHz. The extrapolated counts are lower than those predicted by the De Zotti et al. (2005) model, and (except at the brightest flux densities) also lower than the extrapolation by Holdaway et al. (1994) of the 5-GHz counts. On the other hand, they are within the range of the Waldram et al. (2007) estimates in the limited flux density range where both data sets are valid, although the slopes are significantly different. Both Waldram et al. (2007) and Sadler et al. (2008) assume that the spectral index distribution is independent of flux density. This can only be true for a limited flux density interval, since the mixture of steep-, flat-, and inverted-spectrum sources varies with flux density. In fact, the median 20–95 GHz spectrum ( $\alpha = 0.39$ ) found by Sadler et al. (2008) is much flatter than that ( $\alpha = 0.89$ ) measured at 15–43 GHz by Waldram et al. (2007) for a fainter sample.

Of course, extrapolations from low frequencies can hardly deal with the full complexity of source spectral and variability properties, and may miss sources with anomalously inverted spectra falling below the threshold of the low-frequency selection. They are therefore no substitute for direct blind high-frequency surveys. On the other hand, the recent high frequency surveys (9C, AT20G, WMAP) did not produce “surprises”, such as a population of sources not present in samples selected at lower frequencies. The analysis of WMAP 5-yr data by Massardi et al. (2009) has shown that the counts at bright flux densities are consistent with a constant spectral index up to 61 GHz, although at that frequency there is a marginal indication of a spectral steepening. The WMAP counts at 94 GHz are highly uncertain because of the limited number of de-

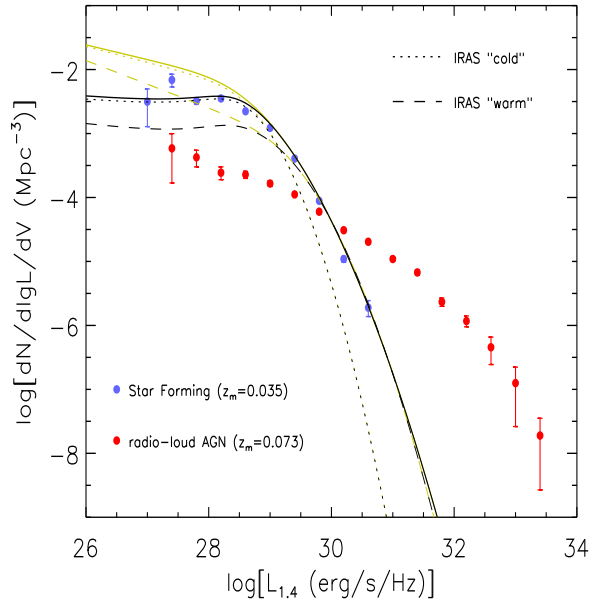


**Fig. 8** Local luminosity functions at 1.4 GHz of radio AGNs (red dots) and of star-forming galaxies (blue dots), as estimated by Mauch & Sadler (2007). The lines show extrapolations to 1.4 GHz of the  $60\mu\text{m}$  local luminosity functions of “warm” (usually interpreted as starburst; dashed) and “cold” (normal late type; dotted) IRAS galaxies by Takeuchi et al. (2003); the solid lines are the sum of the two contributions. The yellow lines refer to the linear radio/far-IR relationship of eq. (14), while the black lines are based on that of eq. (15), which deviates from linearity at low luminosities.

tections and the lack of a reliable flux calibration. However, taken at face value, the WMAP 94-GHz counts are below the predictions by the De Zotti et al. (2005) model by  $\simeq 30\%$ . This indication is confirmed by recent measurements of the QUaD collaboration (Friedman & QUaD Collaboration 2009) who suggest that the model counts should be rescaled by a factor of 0.7 and of 0.6 at 100 and 150 GHz, respectively.

An indication in the opposite direction, albeit with very poor statistics, comes from the MAMBO 1.2-mm (250 GHz) blank-field imaging survey of  $\sim 0.75 \text{ deg}^2$  by Voss et al. (2006). This survey has uncovered 3 flat-spectrum radio sources brighter than 10 mJy, corresponding to an areal density several times higher than expected from extrapolations of low-frequency counts without spectral steepening.

A 43-GHz survey of  $\sim 0.5 \text{ deg}^2$ , carried out with  $\sim 1600$  snapshot observations with the VLA in D-configuration, found only one certain source down to 10 mJy (Wall et al., in preparation). A statistical analysis of the survey data yielded a source-count law in good agreement with predictions of Waldram et al. (2007) and Sadler et al. (2008). There is no strong indication of a previously unrecognized population intruding at this level.

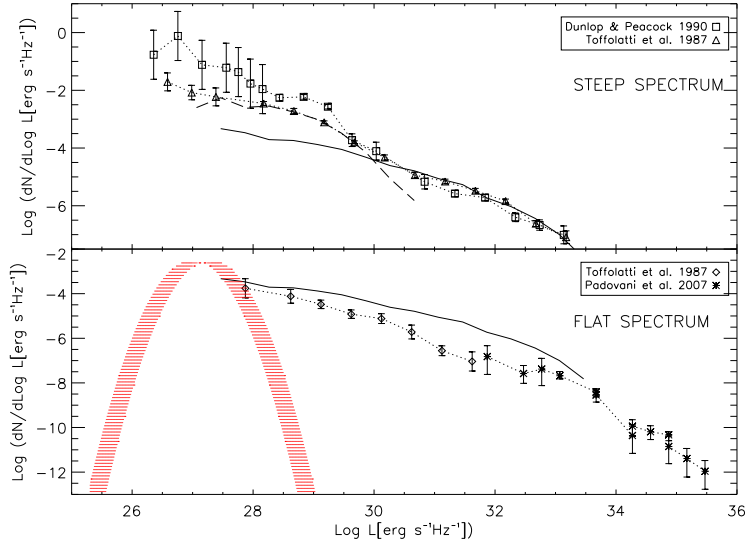


**Fig. 9** Contributions of steep- (upper panel) and flat/inverted-spectrum (lower panel) sources to the local luminosity functions at 1.4 GHz. In both panels the solid line shows Mauch & Sadler’s (2007) estimate of the *total* (i.e., flat/inverted- plus steep-spectrum) local radio luminosity function of AGNs. In the upper panel, the dashed line shows Mauch & Sadler’s (2007) estimate of the local luminosity function of starburst galaxies (mostly steep-spectrum), that dominate for  $\log L(\text{erg s}^{-1} \text{Hz}^{-1}) < 30$ ; the estimates by Toffolatti et al. (1987) and Dunlop & Peacock (1990) of the local luminosity functions of steep-spectrum sources include both starburst galaxies and AGNs. The Toffolatti’s local luminosity function of flat-spectrum sources (lower panel) joins smoothly with the estimated local luminosity function of BL Lac objects obtained by Padovani et al. (2007). The cross-hatched area shows the range spanned by the estimates by Pierpaoli & Perna (2004) of the local luminosity functions of ADADF sources.

### 3 Local luminosity functions

The local luminosity function (LLF) describes the local space density of sources as a function of luminosity: it constitutes an important boundary condition for evolutionary models. Its determination is complicated by several factors discussed e.g. by Toffolatti et al. (1987). Ideally we would like to have a large, complete radio-selected sample of sources, all with redshift measurements, all at low enough redshifts for evolutionary effects to be insignificant, yet distant enough for the redshifts to be accurate distant estimators. The sources should be distributed over large enough volumes for clustering effects to average away.

In practice, however, the well-known fact that the redshift distribution of complete samples of radio sources peaks at  $z \sim 1$  for all flux-density levels down to  $\sim 10$  mJy, implies that local sources are swamped by the much more numerous distant ones. Singling them out by means of complete redshift measurements is therefore impractical, and we must confine ourselves to those brighter than some optical magnitude limit, i.e. we must deal with both radio and optical selection. If the magnitude limit for redshift measurements is too shallow, we lose the contribution of optically-faint galaxies. To some extent this bias may be corrected using bivariate (optical/radio) luminosity functions

(Felten 1976; Auriemma et al. 1977). Alternatively, radio surveys of optically-selected samples can be used.

Spectacular progress has been recently achieved combining large-area spectroscopic surveys (Las Campanas, SDSS, 2dF and 6dF) with the NVSS and FIRST surveys (Machalski & Godlowski 2000; Magliocchetti et al. 2002; Sadler et al. 2002; Best et al. 2005; Mauch & Sadler 2007). A more local sample has been used by Condon et al. (2002).

If full redshift information is available for a flux-limited radio-selected sample containing too few local sources for a meaningful LLF to be directly derived, the LLF can be estimated from the luminosity distribution of the sample, for any chosen evolution function (Wall et al. 1980). The results are, by definition, model dependent, although the evolution function may be tightly constrained by source counts and other data.

The key to this process is disentangling the star-forming galaxies from the AGNs. Radio AGNs dominate above  $S_{1.4\text{GHz}} \simeq 10 \text{ mJy}$ ; at lower flux densities an increasing fraction of nearby galaxies whose radio emission is fuelled by active star formation appears. Optical spectra can be used to identify the dominant process responsible for the radio emission of each source. Star-forming galaxies have spectra typical of HII regions with strong narrow emission lines of  $\text{H}\alpha$  and  $\text{H}\beta$ , while AGNs may have a variety of spectra, including pure absorption lines (like spectra of giant elliptical galaxies), LINER or conventional type 1 or type 2 AGN spectra. Optical AGN spectra, however, do not necessarily imply that the radio emission is of nuclear origin. In fact, there is a body of evidence that the star-formation and nuclear activities are tightly connected, but the radio and optical emissions of AGNs are largely uncorrelated – about 90% of AGNs are radio-quiet. An important diagnostic tool to distinguish between galaxies whose radio emission is due to star formation and those harbouring a radio-loud AGN is the very-well-established, remarkably tight and nearly linear correlation between FIR and radio continuum emission from star-forming galaxies (Helou et al. 1985; Gavazzi et al. 1986; Condon et al. 1991). A frequently-used criterion (Condon et al. 2002) is that galaxies with radio to far-IR flux ratio more than three times higher than the mean for star-forming galaxies are classified as AGN-powered. Mauch & Sadler (2007) found disagreement between spectroscopic classification and the radio/FIR diagnostic at the  $\sim 10\%$  level; a similar reliability was estimated for their classification based on optical spectroscopy. Objects with composite AGN + starburst radio emission are probably a primary source of classification ambiguity. This suggests that the classification uncertainties may contribute significantly to the overall errors on the local luminosity function of each population. Nevertheless, rather accurate estimates of the separate 1.4-GHz local luminosity functions of AGNs and starburst galaxies are now available (see Fig. 8).

With the star-formers disentangled from the radio AGNs, a further dichotomy in the local luminosity function evaluation is required. Evolutionary models for radio AGNs generally split the total radio AGN local luminosity function into the contributions of the steep- and flat-spectrum sources. As discussed in §4, this is a rather crude, but frequently unavoidable, simplification. (Obviously, also the radio spectra of star-forming galaxies must be known for evolution models, but the problem is simpler because in most cases the spectra are “steep”, with mean  $\alpha \sim 0.7$  and a relatively narrow dispersion.)

The 1.4-GHz selection emphasizes steep-spectrum sources, but the flat-spectrum sources may be important in some luminosity ranges. The estimates of separated local luminosity functions for the two populations go back to Wall et al. (1981), Peacock

(1985), Toffolatti et al. (1987), Subrahmanya & Harnett (1987), with little progress thereafter. Rigby et al. (2008) estimated that the density of steep-spectrum sources with  $\log L(1.4 \text{ GHz})/\text{erg s}^{-1} \text{ Hz}^{-1} > 32$  is  $\simeq (3.0 \pm 1.2) \times 10^{-7} \text{ Mpc}^{-3}$ .

Moderate to low-luminosity flat- or inverted-spectrum sources are mostly classified as BL Lac objects. Very weak, inverted-spectrum radio sources in the centers of otherwise quiescent ellipticals may correspond to late phases of AGN evolution (ADAF or ADIOS sources, see § 5.5.2). The observational information on this latter population is very limited. Pierpaoli & Perna (2004) assumed that their space density equals that of elliptical galaxies brighter than  $L_*$ , and adopted a log-normal luminosity function with mean  $\log L(2.7 \text{ GHz})/\text{erg s}^{-1} \text{ Hz}^{-1}$  in the range 27–28, and dispersion  $\sigma = 0.25$ . As illustrated by Fig. 9, the data on the local luminosity function of flat/inverted-spectrum sources already constrain the space density of these sources.

As for BL Lacs, a serious hindrance in the determination of the luminosity function is their essentially featureless spectrum, complicating (or defeating) redshift determination. However, several lines of evidence suggest that their luminosity function evolves weakly if at all (Padovani et al. 2007a), so that the useful volume for computing the local luminosity function extends up to substantial redshifts. The estimate by Padovani et al. (2007a) compares well with the LLF of flat-spectrum sources obtained by Toffolatti et al. (1987). On the contrary, high luminosity flat-spectrum sources are very rare locally and evolve strongly, so that a model independent estimate of the local luminosity function is essentially impossible.

#### 4 Source spectra and evolution

This discussion of radio spectra is far from exhaustive: it sets out to serve two purposes. One is related to the K-corrections, the correction for spectral form which must be used to derive luminosities at rest-frame frequencies. Getting these corrections right is essential in determining space density. The second issue concerns relating source counts at different frequencies, and in particular modelling the poorly-determined high-frequency counts from the well-defined low-frequency counts. This limited discussion thus ignores some aspects of radio spectral measurements which are critical to the astrophysics of radio AGNs, such as variability and monitoring, mentioned briefly in the Introduction.

We have noted that spectra of radio sources are frequently represented as simple power-laws,  $S \propto \nu^{-\alpha}$ , with the spectral index,  $\alpha \sim 0.8$  for steep-spectrum sources and  $\sim 0$  for the flat-spectrum ones. However, all radio galaxies deviate from this simple behaviour. Various physical mechanisms contribute to shaping the emission spectrum. At low rest-frame frequencies spectra generally show a sharp decline with decreasing frequency, attributed to synchrotron self-absorption; a low energy cut-off to the spectrum of relativistic electrons may also have a role (Leahy et al. 1989). The decline is mostly observed at rest frequencies of tens of MHz, but the absorption turnover frequency can be orders of magnitude higher, as in GPS and ADAF/ADIOS sources.

In the optically-thin regime, the spectral index of synchrotron emission, the dominant radiation mechanism encountered in classical radio astronomy, reflects the index of the energy distribution of relativistic electrons. This distribution is steepened at high energies by synchrotron losses as the source radiates, and by inverse Compton losses on either the synchrotron photons themselves or on photons of the external environment (Krolik & Chen 1991). Inverse Compton losses off the cosmic microwave background

(CMB) increase dramatically with redshift since the radiation energy density grows as  $(1+z)^4$ . As a consequence, a decline with increasing redshift of the frequency at which the spectral steepening occurs can be expected.

While inverse Compton losses are most important to sources with weak magnetic fields, powerful sources may possess more intense magnetic fields enhancing the synchrotron emission. The faster electron energy losses yield a more pronounced steepening, correlated with radio power ( $P$ ). Disentangling the effects of radio power and redshift is difficult because in flux-limited samples the more powerful sources are preferentially found at higher redshifts. A further complication arises because a convex spectral shape means that redshifting produces an apparent systematic steepening of the spectrum between two fixed observed frequencies as redshift increases. Since the redshift information is frequently missing, K-corrections cannot be applied and a  $P$ - $\alpha$  correlation may arise from any combination of these three causes.

This is the situation for the correlation reported by Laing & Peacock (1980). Employing (a large proportion of) redshift estimates for a sample drawn from the 38 MHz 8C survey, Lacy et al. (1993) showed that the high-frequency (2 GHz) spectral index correlated more closely with redshift than with luminosity. While at first sight this may suggest the dominant importance of inverse Compton losses on high-frequency spectra, Lacy et al. (1993) pointed out that the correlation between spectral index and redshift weakens when the radio K-correction is applied. This means that such correlation may be induced, at least in part, by the spectral curvature due to self absorption at the very low selection frequency. In fact, magnetic fields in the very luminous Lacy et al. sources should be strong enough for synchrotron losses to dominate inverse Compton losses. Blundell et al. (1999), studying a number of complete samples of radio sources selected at frequencies close to 151 MHz, with a coverage of the  $P$ - $z$  plane (see § 5) substantially improved over previous studies, concluded that:

1. The rest-frame spectral index at low frequency depends on the source luminosity ( $P$ - $\alpha$  correlation), but also on physical size ( $D$ - $\alpha$  correlation) in the sense that sources with larger physical sizes  $D$  have steeper spectra.
2. The rest-frame spectral index at high frequency (GHz) depends on the source redshift.

Simple expressions for the average rest-frame spectra of FRI and FRII radio galaxies as a function of radio power and Fanaroff–Riley type (Fanaroff & Riley 1974) were derived by Jackson & Wall (2001).

With regard to the second issue, relating source counts at different frequencies, relevant aspects are to what extent a power-law approximation of the source spectra may be viable, i.e. to what extent low-frequency self-absorption, electron ageing effects at high frequencies etc. can be neglected; up to what frequencies do blazars have “flat” spectra; are source spectra correlated with other parameters (luminosity, redshift) and, if so, how can these correlations be described?

In this regard we have noted that surveys at frequencies of 5 GHz and higher are dominated (at least at the higher flux densities) by ‘flat-spectrum’ sources. The spectra of these sources are generally not power-laws, but have complex and individual behaviour, showing spectral bumps, flattenings or inversions (i.e. flux increasing with increasing frequency), frequently bending to steeper power-laws at higher frequencies. Examples are shown in Fig. 3. The complex behaviour results from the superposition of the peaked (self-absorption) spectra of up to several components. These components are generally beamed relativistically with the object-axis close to the line of sight; they

are the parts of jet-base components racing towards the observer at highly relativistic speeds.

The dominant populations of flat-spectrum sources are BL Lac objects and flat-spectrum radio quasars (FSRQs), collectively referred to as “blazars”. Their spectral energy distributions (i.e. the distributions of  $\nu L_\nu$ ) show two broad peaks. The low-energy one, extending from the radio to the UV and sometimes also to X-rays, is attributed to synchrotron emission from a relativistic jet, while the high-energy one, in the  $\gamma$ -ray range, is interpreted as an inverse-Compton component arising from up-scattering of either the synchrotron photons themselves (synchrotron self-Compton process, SSC, e.g. Maraschi et al. 1992; Bloom & Marscher 1993) or photons produced by the accretion disc near the central black-hole and/or scattered/reprocessed in the broad-line region (Blandford 1993; Sikora et al. 1994).

Gear et al. (1994) investigated the radio to sub-millimeter spectra of a random sample of very luminous BL Lacs and radio-loud violently variable quasars. They found generally flat or slowly rising 5–37 GHz spectra (median  $\alpha_5^{37} \simeq 0$  for both populations), and declining 150–375 GHz spectra, with a statistically significant difference between BL Lacs and quasars, the former having flatter spectra (median  $\alpha_{150}^{375} \simeq 0.43$ ) than the latter (median  $\alpha_{150}^{375} \simeq 0.73$ ).

Indication of strong spectral curvature was reported by Jarvis & Rawlings (2000) for a quasi-complete sample drawn from the 2.7 GHz Parkes half-Jansky flat-spectrum sample (Drinkwater et al. 1997). It should be noted however that the data used to construct the radio spectra are heterogeneous, and the bias which this introduces is very serious (Wall et al. 2005). An extrapolation of this spectral behaviour to frequencies above 20 GHz would be in conflict with WMAP finding of a median spectral index  $\alpha \simeq 0$  (Bennett et al. 2003).

Fossati et al. (1998) found evidence for an anticorrelation between the frequency of the synchrotron peak  $\nu_p$  and the blazar luminosity, and proposed a scenario, dubbed “the blazar sequence”, for a unified physical understanding of the vast range of blazar properties. The scenario was further extended by Ghisellini et al. (1998). The idea is that blazars indeed constitute a spectral sequence, the source power being the fundamental parameter. The more luminous sources are “redder”, i.e. have both the synchrotron and the inverse Compton components peaking at lower frequencies than the lower-luminosity “blue” blazars. If so, the sub-mm steepening could be a property of only the brightest sources. The validity of the scenario has been questioned, however (e.g., Giommi et al. 1999; Padovani et al. 2003; Caccianiga & Marchã 2004; Antón & Browne 2005; Nieppola et al. 2006; Landt et al. 2006; Padovani 2007; Nieppola et al. 2008).

On the whole, the spectral curvature question is still subject to dispute. Substantial progress is expected from the forthcoming surveys by the Planck mission (The Planck Collaboration 2006), covering the range 30–857 GHz, that will provide the first complete samples allowing unbiased studies of the high frequency behaviour.

## 5 Evolutionary models: radio AGNs

By 1966 the counts produced from the Cambridge 3C and 4C surveys at 178 MHz (Gower 1966) had already defined the characteristic shape confirmed and refined by later surveys: in the Euclidean normalized presentation, a ‘Euclidean’ portion at the brightest flux densities, followed at lower flux densities by a ‘bump’ (dubbed ‘bulge’ by



Wall 1994), and then a roll-off toward the faint intensities. The ‘bump’ is the signature of strong cosmic evolution, implying that the universe must have evolved from a state of ‘violent activity’ in the past to a more quiescent phase at the present epoch, in contradiction to the steady state model as pointed out by Ryle & Clarke (1961). It is also in complete contradiction to uniformly-populated Friedman models (e.g. Wall et al. 1980). A further implication of strong evolution, also noted by Ryle & Clarke (1961), is that it swamps the effect on the source counts of different cosmological models, frustrating the original hopes that the counts could inform on the geometry of the universe. The evolution is indeed spectacular, yielding co-moving source densities at  $z \sim 1-2$  a factor of  $\gtrsim 10^3$  higher than those of local sources of similarly high luminosities (Longair 1966). As stressed by Condon (1989), this means that the fraction of nearby radio sources is low even at large flux densities; the median redshifts of radio sources in complete samples with limits ranging from mJy to Jy are close to 0.8.

Two reference evolutionary scenarios for radio sources (not to be interpreted literally) were used in the 1960s to interpret the counts; they remain popular today. In the *luminosity evolution* scenario, the comoving density of sources is constant but luminosities vary with cosmic epoch, while in the *density evolution* scenario the comoving density of sources of any luminosity varies. A density *and* luminosity evolution of the luminosity function at the frequency  $\nu$  can be described as:

$$\rho(L, z; \nu) = f_d(z)\rho(L/f_l(z), z = 0; \nu), \quad (11)$$

where  $f_d(z)$  and  $f_l(z)$  are the functions describing the density and the luminosity evolution, respectively.

In his pioneering investigation, Longair (1966) showed that either  $f_d(z) = (1+z)^m$  or  $f_l(z) = (1+z)^{m'}$  would fit his data, provided that only sources with high radio luminosity ( $\log(L_{178\text{MHz}}) \gtrsim 33.5$  in the case of luminosity evolution or  $\log(L_{178\text{MHz}}) \gtrsim 34.9$  in the case of density evolution; luminosities in  $\text{erg s}^{-1} \text{Hz}^{-1}$ ) evolve. This is called power-law evolution in which the function is a power of the expansion factor of the Universe. (To be precise, Longair quoted evolution functions proportional to  $t^n$  in an Einstein–de Sitter universe, where the cosmic time  $t$  is proportional to  $(1+z)^{-3/2}$ ). The power-law evolution diverges at high redshifts, and must be truncated. The problem is avoided in the exponential evolution model proposed both by Doroshkevich et al. (1970) and by Rowan-Robinson (1970),  $f_d(z) = \exp(k\tau(z))$  or  $f_l(z) = \exp(k'\tau(z))$ , where  $\tau$  is the lookback time in units of the Hubble time  $H_0^{-1}$ , and  $k^{-1}$  or  $k'^{-1}$  are the evolutionary timescales in the same units.

A further step in exploring radio-AGN evolution was taken by Schmidt (1968) and Rowan-Robinson (1968): the development of the  $V_{\text{max}}$  or ‘luminosity – volume’ test. The test avoids mentioning source counts, at the time still lingering under a cloud of suspicion. It requires a complete sample, and it requires that if two or more limits to this completeness are in play, they all be considered. For example Schmidt (1968) applied the test to the quasars of the 3CR catalogue, a sample defined by the radio flux-density survey limit and by the optical magnitude limit of the original Palomar Observatory Sky Survey. The test is simple: take each object and “push” it out in increasing redshift until it becomes faint enough to encounter one of the two limits, radio or optical. (The process requires that the optical and radio spectra be known so as to define K-corrections in each band.) Stop “pushing” at the *first* limit encountered; this defines  $z_{\text{max}}$  and hence  $V_{\text{max}}$ , the maximum co-moving volume in which the object could be found. Calculate the co-moving  $V$  for the object, the volume defined by the object’s redshift, and then

form the ratio  $V/V_{\max}$ . Do this for all objects in the sample. It is easy to show that if they are uniformly distributed in space, the values should be uniformly distributed between 0 and 1.0, i.e.  $\langle V/V_{\max} \rangle = 0.5 \pm 1/\sqrt{12N}$  where  $N$  is the number of objects in the sample. The statistic is a maximum-likelihood estimator and is unbiased. It remains in widespread use and has undergone many refinements, e.g the  $C^-$  method of Lynden-Bell (1971), the application to combined samples (Avni & Bahcall 1980),  $V_{\max}$  methods to extract an evolution function (Choloniewski 1987, and references therein), methods to estimate the luminosity function directly (Felten 1976; Eales 1993), and the banded  $V/V_{\max}$  method (Dunlop & Peacock 1990). There is a vast literature; Willmer (1997) is a good starting point.

Schmidt (1968) found strong evolution for the 3CR quasars, in accord with the evolution derived by e.g. Longair (1966). Longair & Scheuer (1970) showed how very closely the test was related to the source-count test and emphasized that the two methods were far from independent. However,  $V/V_{\max}$  is versatile, simple in concept, model-free, and comes with a statistical pedigree, in contrast to source counts, the trial and error process of guessing suitable evolution functions, and the frequently less-than-transparent statistical methods used to compare these with source-count and redshift data.

However, the evolution functions mentioned above may carry physical significance. For example a physical interpretation was offered by Cavaliere et al. (1985) who pointed out that models for gravitational energy release near collapsed massive objects yield  $dL/dt = -A(t)L^{1+p}$ . If  $A = \text{constant}$  and  $p = 0$  we get the exponential luminosity evolution function with timescale  $k^{-1} = A^{-1}$ . If  $A(t) \propto t^{-1}$  we get a power-law evolution. It must be stressed that these evolutionary laws apply to *source populations*, not to *individual sources*: the evolutionary timescales,  $k^{-1}$ , are found to be of order of a few to several Gyrs, while the lifetimes of bright radio AGN phases are at least one and probably two orders of magnitude shorter (Bird et al. 2008). Grueff & Vigotti (1977) made an early attempt to build a model explicitly constrained by astrophysical factors. They linked the radio-source formation to that of parent galaxies and assumed radio-emitting lifetimes inversely proportional to radio luminosities.

Most evolution models have ignored the distributions of spectral indices around the mean values (which may be luminosity dependent) for both steep- and flat-spectrum sources (but see Condon 1984a). If such distributions can be approximated as Gaussians with dispersion  $\sigma$ , and the differential counts have a power-law shape,  $n(S) = kS^{-\beta}$ , the mean spectral index  $\bar{\alpha}$  of sources with given value of  $S$  shifts with frequency (Kellermann 1964; Condon 1984a; Danese & de Zotti 1984):

$$\bar{\alpha} = \bar{\alpha}_0 + \sigma^2(1 - \beta) \ln(\nu/\nu_0), \quad (12)$$

and the amplitude of the counts scales with frequency as  $k = k_0(\nu/\nu_0)^q$ , with:

$$q = \bar{\alpha}_0(1 - \beta) + 0.5\sigma^2(1 - \beta)^2 \ln(\nu/\nu_0). \quad (13)$$

The dispersion of the mean spectral indices thus counteracts the effect on counts of the high-frequency steepening (§4). The effect is amplified by the increase with frequency of the variability amplitude (Impey & Neugebauer 1988; Ciaramella et al. 2004). We note however that (a) power-law approximations for source counts hold over very limited flux-density ranges only; and (b) a Gaussian approximation for spectral-index distributions holds only for low-frequency surveys. By 1.4 GHz, spectral-index distributions have pronounced tails towards flat spectra and by 5 GHz, the spectral-index

distribution is almost the sum of two Gaussians with peaks at  $\sim 0.8$  (steep-spectrum sources) and  $\sim 0.0$  (flat-spectrum sources). Clearly, the above equations can be used to calculate  $\bar{\alpha}$  and  $q$  for each population.

### 5.1 Low versus high luminosities

Extensive discussions can be found in the literature on whether or not the cosmological evolution is a property of powerful radio sources only. The origin of the discussion is Longair (1966)'s classic study. He adopted a luminosity function extending over about 8 decades in luminosity and with a shape not far from a power-law, so that density and luminosity evolution were essentially equivalent over the flux density range covered by the counts available at the time. Under these assumptions, the relative narrowness of the evolution bump in normalized counts (width less than 2 orders of magnitude) compared to the breadth of the luminosity function (8 orders of magnitude) could be accounted for if *only the brightest sources evolve strongly*. It was a fundamental discovery of Longair (1966)'s investigation that 'differential evolution' was therefore essential: if all sources evolved equally, there are far too many faint sources, i.e. the model bump is far too broad.

As more data accumulated, the evolutionary models were refined. Robertson (1978, 1980) and Wall et al. (1980) factorized the evolving luminosity function as  $\rho(L, z) = F(L, z)\rho_0(L)$ , where  $F(L, z)$  is the evolution function, able to represent density or luminosity evolution, or a combination of both. Models assuming a luminosity-independent evolution function were found to produce unsatisfactory results, while (following the qualitative description of the previous paragraph) good fits of the data were obtained only by assuming a far stronger  $F(L, z)$  for more luminous sources. Danese et al. (1987) proposed a luminosity-dependent luminosity evolution model in which the luminosity evolution timescale increases with decreasing luminosity and exceeds  $H_0^{-1}$ , so that sources evolve weakly (if at all), below some critical luminosity  $L_s \sim 10^{31} \text{ erg s}^{-1} \text{ Hz}^{-1}$ . This is in keeping with the indications that a variety of physical processes can sustain a steady low-level fueling of the central engine for times longer than the Hubble time (Cavaliere et al. 1985). The Danese et al. (1987) model was exploited by Toffolatti et al. (1998) to carry out remarkably successful predictions of radio source contributions to small scale anisotropies measured by Cosmic Microwave Background experiments.

The differential evolution is suggestive of two populations. Pushing the high/low luminosity dichotomy to the extreme, some investigators explicitly considered two populations, one of non-evolving low-luminosity sources, and the other of high-luminosity, strongly evolving sources. Wall (1980) identified the two populations with FR I and FR II radio galaxies. The border between FR I and FR II is, approximately, at  $L_{1.4\text{GHz}} \sim 10^{32} \text{ erg s}^{-1} \text{ Hz}^{-1}$ , although the division appears to be dependent on both radio power and optical luminosity of the host galaxy (cf. Ledlow & Owen 1996). Jackson & Wall (1999) extended the scheme to flat-spectrum sources, assuming that BL Lac objects and flat-spectrum radio quasars are the beamed counterparts of FR I and FR II objects respectively, as discussed in § 5.4.

Before the advent of 2dF and SDSS sky surveys, the space distribution of low-luminosity radio AGN was a matter of speculation. For example, Laing et al. (1983) showed that the low-luminosity radio galaxies of 3CRR [ $\log(L_{178\text{MHz}}/\text{erg s}^{-1} \text{ Hz}^{-1}) < 34$ ] gave values of  $\langle V/V_{\text{max}} \rangle \approx 0.50$ , suggesting little or no evolution. This view

was supported by Clewley & Jarvis (2004) who found that the comoving space density of sources fainter than  $L_{1.4\text{GHz}} \sim 4 \cdot 10^{32} \text{ erg s}^{-1} \text{ Hz}^{-1}$  remains approximately constant with increasing redshift up to  $z \simeq 0.5$ . However, numbers were small and uncertainties undoubtedly permitted some mild evolution. On the basis of discovering two distant FRI galaxies in the Hubble Deep Field, Snellen & Best (2001) proposed that FRI galaxies showed significant evolution. With recourse to the 2dF sample of galaxy redshifts, Sadler et al. (2007) quantified this: they found substantial cosmological evolution over the redshift range  $0 < z < 0.7$  of radio galaxies with  $10^{31} < L_{1.4\text{GHz}} < 10^{32} \text{ erg s}^{-1} \text{ Hz}^{-1}$ , i.e. in the luminosity range of FRI sources. They also found indications that the most powerful radio galaxies in their sample (with  $L_{1.4\text{GHz}} > 10^{33} \text{ erg s}^{-1} \text{ Hz}^{-1}$ ) undergo more rapid evolution over the same redshift range. The latter findings are consistent with those by Willott et al. (2001), who used emission-line strength rather than morphology (FRI/FR II) to discriminate between radio-source populations. The critical radio luminosity dividing sources with weak/absent emission lines (the less radio-luminous population of FRI and FR II), and the more radio-luminous population of strong-line FR II radio galaxies and quasars, is approximately  $L_{1.4\text{GHz}} \sim 6 \cdot 10^{32} \text{ erg s}^{-1} \text{ Hz}^{-1}$ . Both populations show evidence for evolution, but the comoving density of the more powerful sources rises far more dramatically than that of the low-luminosity population.

It must be noted, however, that a luminosity-dependent evolution function,  $F(L, z)$ , does not necessarily imply a luminosity-dependent luminosity evolution. For example, in the case of a luminosity function  $\rho \propto L^{-\gamma}$  a uniform power-law evolution,  $L(z) = L(0)(1+z)^{\alpha}$ , yields  $\rho[L(z)] = \rho[L(0)](1+z)^{\alpha\gamma}$ ; the evolution function depends on the slope of the luminosity function. If the luminosity function levels off below some ‘bending’ luminosity  $L_b$ , a luminosity-independent luminosity evolution translates into a constant comoving space density at low luminosities, with strong variations with epoch confined to the steep portion of the luminosity function. As shown by Condon (1984b), it is then possible to fit a wide range of radio data with a model assuming that all sources evolve equally.

Finally, we note that the debate on the evolution of low luminosity radio AGNs has been somewhat muddled for some time by the poor knowledge of their local luminosity function. As discussed in § 3, it is now clear that the faint portion of the radio luminosity function is dominated by starburst galaxies, while the luminosity function of radio AGNs flattens below  $\log L(1.4 \text{ GHz})/\text{erg s}^{-1} \text{ Hz}^{-1} \simeq 31$ .

## 5.2 Steep- versus flat-spectrum sources

The width of the bump in the Euclidean normalized counts increases with increasing frequency. The bump of the steep-spectrum population dominating the low-frequency counts shifts to fainter flux densities and gradually fades as survey frequency increases. But as survey frequency increases the evolution bump of flat-spectrum sources becomes steadily more prominent, combining with the steep-spectrum bump to produce an increasingly broad overall maximum, a broader range of flux densities over which the count slope is close to Euclidean (Kellermann & Wall 1987). This initially misled investigators to consider different space distributions and evolutionary laws for steep- and flat-spectrum sources, with less evolution for the latter. Demonstrating the lack of independence of  $V/V_{\text{max}}$  and source-count results, similar indications of little evolution for flat-spectrum objects came from this direction. Schmidt (1968) found a

slight indication in the 3CR sample of quasars that  $\langle V/V_{\max} \rangle$  appeared to be less for the flatter-spectrum objects. When substantial flat-spectrum quasar samples became available from cm-wavelength surveys, it was found that  $\langle V/V_{\max} \rangle \simeq 0.5$ , consistent with a uniform distribution (Schmidt 1976; Masson & Wall 1977). This is in contrast to  $\langle V/V_{\max} \rangle \simeq 0.7$  for steep-spectrum quasars, indicative of a strong increase of their space density with  $z$ .

Peacock & Gull (1981) stressed that the data available at the time poorly constrained the luminosity function over most areas of the luminosity-redshift plane (see also Wall et al. 1981), and pointed out that within the regions where the luminosity function was reasonably well defined, steep- and flat-spectrum sources behave similarly: both spectral types undergo differential evolution, the strength of evolution increasing with luminosity. The analysis by Condon (1984a) confirmed that the two spectral classes may indeed evolve similarly within the constraints of the data. This position received further support from comparative analysis of evolution of AGNs in the radio, optical and X-ray bands by Danese et al. (1985), who noted that the apparently weaker evolution of flat-spectrum sources might be related to relativistic beaming effects that boost the apparent radio luminosity. In particular, BL Lac objects are probably associated with low-luminosity steep-spectrum radio sources which also show weak evolution. More extensive data and further analyses (Danese et al. 1987; Dunlop & Peacock 1990) reconciled the epoch-dependent spatial distributions of the two populations, showing that they were essentially identical. This finding produced a necessary consistency for the success of the unified scheme for radio-loud AGNs; it is clearly not possible for side-on and end-on versions of the same populations to have different space distributions. ‘Unified evolutionary schemes’, in which flat-spectrum quasars and BL-Lac objects are ‘beamed’ versions of FR I and FR II sources, were presented by Urry & Padovani (1995) and Jackson & Wall (1999) and are discussed in § 5.4.

Some of the apparent discrepancy between these analyses can perhaps be resolved noting that, while  $\langle V/V_{\max} \rangle > 0.5$  means an increase with redshift of the source density,  $\langle V/V_{\max} \rangle \simeq 0.5$  does not necessarily mean no evolution. Evolution increasing the source density up to  $z \sim 2$  and decreasing it afterwards may yield  $\langle V/V_{\max} \rangle \simeq 0.5$  for quasars visible up to high  $z$ ; at high- $z$  the visibility of flat/inverted-spectrum quasars is enhanced compared to the steep-spectrum ones by the more favourable K-correction. This may be part of the explanation; but probably the majority of the explanation for disparate  $\langle V/V_{\max} \rangle$  results arises from selecting the steep-spectrum samples from their initial steep portion of source count, while selecting the flat-spectrum sources from an effectively fainter (and flatter) portion of the source count.

### 5.3 High- $z$ evolution

At some epoch, radio galaxies and quasars have to be born; some epoch after recombination has to have assembled galaxies suitable to harbour both massive black hole cores and fuel systems for these to produce collimated twin-beam radio AGNs. We have described how easily we can trace the very strong increase of the co-moving number density of powerful radio sources between redshift  $\simeq 0$  and 2. How hard is it to find the more distant epoch at which this relatively high co-moving density falls to signify the epoch of AGN birth?

This is an important issue. The radio activity is associated with processes driving the growth of supermassive black holes (SMBHs) in galactic nuclei, which in turn is

tied to galaxy formation and evolution. The radio activity may also drive feedback processes that have a key role in the evolution of black holes and their host galaxies (Granato et al. 2004; Best et al. 2006; Bower et al. 2006; Croton et al. 2006). Powerful radio galaxies and quasars trace the most massive SMBHs (Dunlop et al. 2003; McLure et al. 2004) which are hosted by the most massive galaxies (Ferrarese & Ford 2005). Radio survey data are unaffected by dust extinction and may thus provide crucial tests of the optical/IR results on galaxy formation.

One of the achievements of the outstanding Dunlop & Peacock (1990) free-form evolution analysis was to provide evidence for a decline (or high redshift “cut-off”) in the number density of sources with both steep and flat spectra at redshifts beyond 2.5 to 3.0. However their samples were incomplete in redshift information, and the results were dependent on the accuracy of photometric redshifts ascribed to sources of the optically-faintest host galaxies.

Tracing the redshift cutoff is still under investigation. Shaver et al. (1996) reported evidence of a strong decrease of the space density of flat-spectrum radio-loud quasars (FSRQs) for  $z > 3$ . Jarvis & Rawlings (2000) disputed this, pointing out that the apparently curved nature of many of the radio spectra involved, and in particular a spectral steepening to the high frequencies, might reduce or remove the significance of an apparent redshift cutoff. Ignoring such steepening leads to the prediction of more high- $z$  sources than are actually seen, and this could be misinterpreted as evidence for a decline of the space density. They concluded that the comoving volume covered by the available samples is too small to make definitive statements about any redshift cutoff for the most luminous flat-spectrum sources, although both a constant comoving density and a decline as abrupt as those envisaged by Shaver et al. (1996) were found to be marginally inconsistent with the data. Using a larger sample with a more rigorous analysis, Wall et al. (2005) found evidence, significant at  $> 4\sigma$ , of a diminution in space density of flat-spectrum quasars at  $z > 3$ , consistent with the redshift-cutoff forms of both optically-selected (Schmidt et al. 1995; Fan et al. 2004) and X-ray selected (Hasinger et al. 2005; Silverman et al. 2005) quasars. Wall et al. drew attention to a major source of bias in the Jarvis et al. sample, the non-contemporaneous nature of the radio flux-density measurements. It is certain that this introduces too much apparent high-frequency curvature and decline into the radio spectra. The effect of the bias was demonstrated by Wall et al., using both contemporaneous and non-contemporaneous spectral data.

Using three samples selected at low frequencies, Jarvis et al. (2001) found that the space density of the most radio-luminous *steep-spectrum* radio sources is consistent with being constant between  $z \simeq 2.5$  and  $z \simeq 4.5$  and excluded a decline as steep as suggested by Shaver et al. (1996, 1999). This conclusion was confirmed by Cruz et al. (2007). However, the samples remain small and incomplete in redshift information and as for Dunlop & Peacock (1990), the faintest host galaxies require redshift estimation from a  $K-z$  plot. It is much harder to track any redshift diminution for steep-spectrum radio galaxies than for FSRQ and the statistical uncertainties are inevitably greater; showing that the steep-spectrum samples are consistent with a uniform distribution does not disprove the redshift cutoff found by Wall et al. (2005) for FSRQ.

These apparently contradictory results may again be accounted for by luminosity-dependent evolution. Hook et al. (1998) reported indications that the high- $z$  decline of the space density of flat-spectrum quasars is more pronounced and starts at lower redshifts for less powerful sources. These indications were confirmed by subsequent studies that did not distinguish between flat- and steep-spectrum sources (Waddington et al.

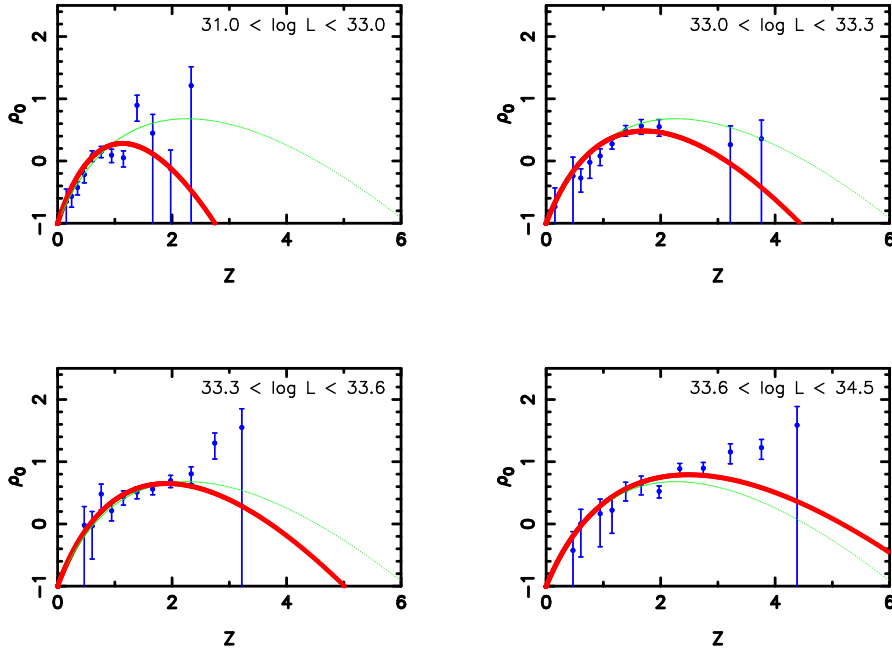


**Fig. 10** Relative space density of flat-spectrum radio quasars from the Parkes Quarter-Jansky sample, as derived from a Maximum-Likelihood analysis similar to that of Wall et al. (2008). The sample and Single-Object Survey (SOS) technique used were described by Wall et al. (2005). The peak of FSRQ activity is a monotonic function of 2.7-GHz monochromatic radio luminosity ( $L$  in units of  $\text{ergs s}^{-1} \text{Hz}^{-1}$ ) in the pseudo-downsizing sense, i.e. lower luminosities have the peak of their activity at lower redshifts. The green curve in each diagram represents the global solution for the entire sample. This ‘down-sizing’ is similar to that found for quasars selected at X-ray wavelengths (Hasinger et al. 2005) and for submm galaxies (SMG) from JCMT surveys (Wall, Pope & Scott 2008).

2001; Vigotti et al. 2003; Cirasuolo et al. 2005, 2006). The luminosity dependence of the high- $z$  decline is qualitatively similar to the *downsizing* observed for galaxies and optically and X-ray selected quasars (Cowie et al. 1996; Barger et al. 2005; Pérez-González et al. 2008). A new analysis in progress by Wall et al. (2009 in preparation) uses a Bayesian modelling process similar to that described by Wall et al. (2008), and this pseudo-downsizing effect is very clear for FSRQ, as shown in Fig. 10.

There remains further need for complete redshift information on faint samples of steep-spectrum radio sources to clarify their high-redshift evolution. An important step in this direction has been the Combined EIS-NVSS Survey Of Radio Sources (CENSORS, Brookes et al. 2008) that included spectroscopic observations of 143 out of a total of 150 sources with  $S_{1.4\text{GHz}} > 3.8 \text{ mJy}$ . Of these, 137 form a complete sample to a flux-density limit of 7.2 mJy. The resulting redshift distribution agrees well with the distribution in Fig. 28 of Condon (1984a) but is not well reproduced by any of the Dunlop & Peacock (1990) models (see, e.g., Fig. 11). These data promise substantial improvement in this field.

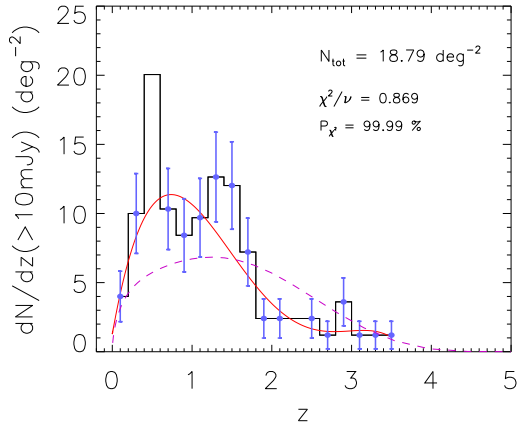


**Fig. 11** Redshift distribution of sources brighter than 10 mJy at 1.4 GHz in the CENSORS sample (Brookes et al. 2008), compared with that predicted by the PLE model by Dunlop & Peacock (1990, dashed line) and with the fit of eq. (26). As the model applies to the AGN population, the two sources classified as starburst galaxies (nos. 95 and 124) were excluded from the histogram. The Kaplan-Meier estimator was used to take into account the lower limits into account.

#### 5.4 Unified evolutionary schemes

Urry & Padovani (1995) carried out a thorough examination of the most widely accepted version of the unification scheme encompassing steep- and flat-spectrum radio sources. This scheme is based on the premise that relativistic beaming of lobe-dominated, steep-spectrum, moderate radio power FR I and high-radio-power FR II radio galaxies gives rise to core dominated, flat-spectrum BL Lac objects and radio loud quasars, respectively, when the line of sight is close to the jet axis (Fig. 1). Urry & Padovani based their analysis on a comparison of luminosity functions for the different objects, and they showed that with reasonable assumptions for the beaming parameters, these were in agreement. (We remind the reader that in the case of beamed emission, the true luminosities are lower than those inferred from the observed fluxes assuming isotropic emission by a factor  $\omega/4\pi$ , where  $\omega$  is the solid angle of the beaming cone(s). For example, in the case of twin beams each with semi-aperture angle of  $7^\circ$ ,  $\omega/4\pi \simeq 0.094$ .)

More recent analyses (Liu & Zhang 2007; Cara & Lister 2008), using observations of the jet kinematics and the apparent superluminal speeds for a complete sample (Lister 2008), have confirmed the general validity of the scheme and have improved the accuracy in parameter determination. The assumption that the observed luminosity function of FR II galaxies has the same power-law shape as the intrinsic luminosity function of radio-loud quasars was successfully tested using a maximum likelihood method. Padovani & Urry (1992) had originally developed their method of comparing the calculated beamed luminosity functions of flat-spectrum quasars and BL Lac objects with the observed ones before their comprehensive review paper. Now the observed distribution of Lorentz factors of relativistic jets (Hovatta et al. 2008) is found to be



in good agreement with their estimate. The observed distribution of viewing angles also turned out to be consistent with predictions of their unified model. Hovatta et al. (2008) found that the transition from blazars to ordinary radio loud quasars occurs at a viewing angle of  $15^\circ$  to  $20^\circ$ , to be compared with Urry & Padovani (1995)’s estimate of  $14^\circ$ .

Wall & Jackson (1997) and Jackson & Wall (1999) derived an evolutionary model aimed at explaining the behaviour of both the flat- and steep-spectrum populations within a unified scheme. Following Urry & Padovani (1995), they assumed BL Lacs to be the beamed versions of FR I galaxies, and FSRQs to be the beamed versions of FR II galaxies. However the analysis differed from that of Urry & Padovani in deriving model parameters directly from the data rather than by comparing luminosity functions. As a first step, Jackson & Wall derived evolution models separately for FR I and FR II radio galaxies, using data (counts and redshifts) *solely from low-frequency surveys* in order to avoid beamed objects and to establish space-density behaviour for these parent populations. The evolution models they derived happened to have redshift cutoffs, and for the FR I galaxies the approximation of space density constant with epoch was adopted. These both gave good fits to the low-frequency data, but neither feature is essential to the outcome of the experiment. Together with observed ratios of beamed (core) flux to unbeamed flux, Jackson & Wall then used a Monte Carlo process to orient statistically-large samples of FR I and FR II sources randomly to the line of sight. Using a grid of beaming parameters (range of Lorentz factors, torus opening angles), they then calculated the number of beamed objects (BL Lacs and FSRQs) produced at different flux densities. Identifying these objects with the cm-excess sources found in cm-wavelength surveys, they then closed the loop by using the higher-frequency source counts (primarily at 5 GHz) to find the permissible range of beaming parameters. The process was able to reproduce the exact form of the higher-frequency counts with their broader bump (§ 5.2) as well as torus opening angles and Lorentz factors in reasonable agreement with observations. Liu & Zhang (2007) found that the Lorentz factor distribution is much steeper for low-redshift ( $z < 0.1$ ) low-luminosity sources than for the more powerful, high- $z$  ones, although the uncertainties are large. Therefore the most extreme relativistic jets are rarer in the low- $z$  population. This indicates that the low- and high-redshift groups are likely to be from different parent populations, consistent with the dual-population scheme of Jackson & Wall (1999).

The Jackson & Wall (1999) unification scheme was adopted by Wilman et al. (2008) to reproduce the observed variety of radio-loud AGNs, including radio galaxies, steep- and flat-spectrum quasars, and strongly beamed sources such as BL Lacs and FSRQs. These authors produced a simulation of a sky area of  $20 \times 20 \text{ deg}^2$  out to  $z = 20$ , and down to a flux density of 10 nJy at several frequencies from 151 MHz to 18 GHz. The model comprises 5 source populations with different evolutionary properties: FR I and FR II AGNs, “radio-quiet” AGNs (defined as all X-ray - selected AGNs), and star-forming galaxies in quiescent and star-bursting phases. The simulation includes redshift-dependent size distributions both for radio-loud AGNs and for star-forming galaxies. Clustering is modeled by attributing to each population an effective halo mass and computing the corresponding bias factors,  $b(z)$ . The simulations have been built with the SKA in mind and will serve to inform design of the SKA, design of analysis software and design of observing programmes.

## 5.5 Special classes of sources

### 5.5.1 GHz peaked spectrum (GPS) sources

GPS sources are powerful ( $\log L_{1.4\text{GHz}} \gtrsim 32 \text{ erg s}^{-1} \text{ Hz}^{-1}$ ), compact ( $\lesssim 1 \text{ kpc}$ ) radio sources with convex spectra peaking at GHz frequencies (see O’Dea 1998, for a comprehensive review). They are identified with both galaxies and quasars. It is now widely agreed that GPS sources correspond to the early stages of the evolution of powerful radio sources, when the radio-emitting region grows and expands within the interstellar medium of the host galaxy, before plunging out into the intergalactic medium and becoming an extended radio source (Fanti et al. 1995; Readhead et al. 1996; Begelman 1996; Snellen et al. 2000). Conclusive evidence that these sources are young came from VLBI measurements of propagation velocities. Speeds of up to  $\simeq 0.4c$  were measured, implying dynamical ages  $\sim 10^3$  years (Polatidis et al. 1999; Taylor et al. 2000; Tschager et al. 2000). The identification and investigation of these sources is therefore a key element in the study of the early evolution of radio-loud AGNs.

The model by De Zotti et al. (2000) implies that extreme GPS quasars, peaking at  $\nu > 20 \text{ GHz}$ , should comprise a substantial fraction of bright radio sources in the WMAP survey at  $\nu \simeq 20 \text{ GHz}$ , while GPS galaxies with similar  $\nu_{\text{peak}}$  should be about 10 times less numerous. For a maximum rest-frame peak frequency  $\nu_{p,i} = 200 \text{ GHz}$ , the model predicts about 10 GPS quasars with  $S_{30\text{GHz}} > 2 \text{ Jy}$  peaking at  $\geq 30 \text{ GHz}$  over the  $10.4 \text{ sr}$  at  $|b| > 10^\circ$ . Although the number of quasars with spectral peaks at  $\geq 30 \text{ GHz}$  in the WMAP survey is consistent with this, when additional data (Trushkin 2003) are taken into account such sources look more like blazars caught during a flare that is optically thick up to high frequencies. Furthermore, Tinti et al. (2005) showed that most (perhaps two thirds) of the quasars in the sample of High Frequency Peaker (HFP, GPS sources peaking above a few GHz) candidates selected by Dallacasa et al. (2000) are likely to be blazars, while all the 10 candidates classified as galaxies are consistent with being truly young sources. This conclusion was strengthened by the VLBA variability and polarization studies of Tornainen et al. (2005), Orienti et al. (2006, 2007), and Orienti & Dallacasa (2008).

An implication of these results is that the samples of confirmed GPS *quasars* are too small to allow meaningful study of their evolutionary properties. The situation is somewhat better for GPS *galaxies*. Tinti & de Zotti (2006) found that the observed redshift and peak frequency distributions of these sources can be satisfactorily accounted for in the framework of the self-similar expansion model proposed by Begelman (1996, 1999). According to this model, the properties of the sources are determined by the interaction of a compact, jet-driven, over-pressured, non-thermal radio lobe with a dense interstellar medium. Fits of the redshift and peak frequency distributions require a decrease of the emitted power and of the peak luminosity with source age or with decreasing peak frequency, consistent with expectations from Begelman’s model, but at variance with the Snellen et al. (2000) model.

### 5.5.2 Late stages of AGN evolution

Late stages of the AGN evolution, characterized by low radiation/accretion efficiency, were brought into sharper focus by the discovery of ubiquitous, moderate-luminosity hard X-ray emission from nearby ellipticals. VLA studies at high radio frequencies (up to  $43 \text{ GHz}$ ) have shown, albeit for a limited sample of objects, that all the observed

compact cores of elliptical and S0 galaxies have spectra rising up to  $\simeq 20\text{--}30$  GHz (di Matteo et al. 1999).

There is growing evidence that essentially all massive ellipticals host super-massive black holes (e.g. Ferrarese & Ford 2005). Yet nuclear activity is not observed at the level expected from Bondi (1952) spherical accretion theory, in the presence of extensive hot gaseous halos, and for the usually-assumed radiative efficiency  $\simeq 10\%$  (di Matteo et al. 1999). However as proposed by Rees et al. (1982), the final stages of accretion in elliptical galaxies may occur via Advection-Dominated Accretion Flows (ADAFs), characterized by a very low radiative efficiency (Fabian & Rees 1995). The ADAF scenario implies strongly self-absorbed thermal cyclo-synchrotron emission due to a near-equipartition magnetic field in the inner parts of the accretion flows, most easily detected at cm to mm wavelengths. However the ADAF scenario is not the only possible explanation of the data, and is not problem-free. *Chandra* X-ray observations of Sgr A at the Galactic Center are suggestive of a considerably lower accretion rate compared to Bondi's prediction (Baganoff et al. 2003), so that the very low ADAF radiative efficiency may not be required.

A stronger argument against a pure ADAF in the Galactic Center is that the emission is strongly polarized at mm/sub-mm wavelengths (Aitken et al. 2000; Agol 2000). Moreover di Matteo et al. (1999) and Di Matteo et al. (2001) found that the high-frequency nuclear radio emission of a number of nearby early-type galaxies is substantially below the prediction of standard ADAF models. The observations are more consistent with the adiabatic inflow-outflow solutions (ADIOS) developed by Blandford & Begelman (1999), whereby the energy liberated by the accretion drives an outflow at the polar region. This outflow carries a considerable fraction of the mass, energy and angular momentum available in the accretion flow, thus suppressing the radio emission from the inner regions. Both the intensity and the peak of the radio emission depend on the mass loss rate.

Tentative estimates of the counts due to these sources and of the associated small-scale fluctuations were presented by Pierpaoli & Perna (2004). As shown in Fig. 9 their model A assumes a local luminosity function (upper boundary of the cross-hatched area) higher than current estimates of the local luminosity function of all flat/inverted spectrum sources. Consistency is obtained only for their minimal model B (lower boundary of the cross-hatched area).

## 6 Evolutionary models: star-forming galaxies

### 6.1 Star-forming, normal and sub-mm galaxies

The radio emission of star-forming galaxies correlates with their star formation rate, as demonstrated by the well-established tight correlation with far-IR emission (Helou et al. 1985; Gavazzi et al. 1986; Condon 1992; Garrett 2002). Yun et al. (2001) found that the overall trend in the range  $L_\nu(60\mu\text{m}) \simeq 10^{30}\text{--}10^{32.5}$  erg s $^{-1}$  Hz $^{-1}$  is indistinguishable from a linear relation:

$$L_{1.4\text{GHz}} = 1.16 \times 10^{-2} L_\nu(60\mu\text{m}). \quad (14)$$

Galaxies with  $L_\nu(60\mu\text{m}) < 10^{30}$  erg s $^{-1}$  Hz $^{-1}$  are found to have radio to far-IR luminosity ratios systematically lower than those given by eq. (14). The apparent deviation from linearity in the radio/far-IR correlation at low luminosities is supported

by a comparison of  $60\ \mu\text{m}$  and 1.4 GHz local luminosity functions (Yun et al. 2001; Best et al. 2005). Simply shifting the  $60\ \mu\text{m}$  luminosity function (Saunders et al. 1990; Takeuchi et al. 2003) along the luminosity axis according to eq. (14) yields a good match to the radio luminosity function (Best et al. 2005; Mauch & Sadler 2007) for  $L_{1.4\text{GHz}} \gtrsim 10^{28}\ \text{erg s}^{-1}\ \text{Hz}^{-1}$ . At yet lower luminosities, however, the extrapolated luminosity function lies increasingly above the observed one. Full agreement is recovered (Fig. 8) by replacing eq. (14) with

$$L_{1.4\text{GHz}} = 1.16 \times 10^{-2} L_b \left[ \left( \frac{L_\nu(60\ \mu\text{m})}{L_b} \right)^{-3.1} + \left( \frac{L_\nu(60\ \mu\text{m})}{L_b} \right)^{-1} \right]^{-1}, \quad (15)$$

in which  $L_b = 8.8 \times 10^{29}\ \text{erg s}^{-1}\ \text{Hz}^{-1}$ .

While a radio/far-IR correlation is expected since young stars are responsible both for dust heating and for the generation, via supernova explosions, of synchrotron emitting relativistic electrons, a clear explanation of its tightness and of its linearity over a large luminosity range is still missing. A decrease of the  $L_{1.4\text{GHz}}/L_\nu(60\ \mu\text{m})$  ratio with *increasing* far-IR luminosity is expected from the increase of the effective dust temperature,  $T_d$ , with luminosity (Blain & Longair 1996). For a galaxy like the Milky Way, the far-IR SED peaks at  $170\ \mu\text{m}$ , whereas for an Ultra Luminous Infrared Galaxy (ULIRG) it peaks at about  $60\ \mu\text{m}$  (Lagache et al. 2005). This factor of 3 increase in temperature for a factor  $\sim 10^3$  increase in luminosity corresponds to  $T_d \propto L_{\text{FIR}}^{1/6}$ . If the radio luminosity is proportional to the global far-IR luminosity, this increase in dust temperature results in a decrease of the  $L_{1.4\text{GHz}}/L_\nu(60\ \mu\text{m})$  ratio by a factor of 2.5–3.

On the other hand, there are different contributions to the global far-IR luminosity. In Luminous and Ultra Luminous Infrared galaxies, the emission is dominated by warmer dust, associated with star-formation, while infrared “cirrus” emission, heated by older stars, becomes increasingly important in galaxies with lower and lower star-formation rates. The latter component may be weakly correlated with radio emission, if at all. Moreover, in very low luminosity galaxies interstellar magnetic fields may be so weak as to let synchrotron emitting electrons escape into intergalactic space or to lose energy primarily via inverse Compton scattering of CMB photons. These processes may over-compensate the effect of decreasing dust temperature<sup>5</sup>.

Anyway, the tight empirical relationship between radio and far-IR luminosities for star-forming galaxies allows us to take advantage of the wealth of data at far-IR/sub-mm wavelengths to derive the radio evolution properties. We expect a different evolution for starburst and normal late-type galaxies as the starburst activity is likely triggered by interactions and mergers that were more frequent in the past, while in normal galaxies the star-formation rate has probably not changed much over their lifetimes. The bulk of the sub-mm counts measured by SCUBA surveys (Scott et al. 2006; Coppin et al. 2006) is due to yet another population, the sub-mm galaxies (SMGs), proto-spheroidal galaxies in the process of forming most of their stars (Granato et al. 2004).

There have been a number of attempts to model the evolution of star-forming galaxies and in particular to account for the apparent intrusion of this population into the source counts at  $S_{1.4\text{GHz}} \leq 1\ \text{mJy}$ ; see e.g. King & Rowan-Robinson (2004). A straightforward extrapolation to radio frequencies of the evolutionary models by Negrello et al. (2007) for the three populations (normal, starburst and sub-mm galaxies), exploiting

<sup>5</sup> We are grateful to J. Condon for enlightening comments on this issue.

eq. (15) and the SEDs of NGC 6946 for normal late-type galaxies and of Arp220 for starburst and proto-spheroidal galaxies, yields the curves shown in Figs. 4–6, nicely reproducing the counts at tens of  $\mu\text{Jy}$  levels. We note however that new observational data, some of which is described in § 2.3, may permit substantial refinement of these models.

The cross-over between synchrotron plus free-free emission prevailing at cm wavelengths, and thermal dust emission, generally occurs at  $\lambda \simeq 2\text{--}3$  mm (in the rest frame), so that at frequencies of tens of GHz there are contributions from both components (see De Zotti et al. 2005).

## 6.2 Radio afterglows of $\gamma$ -ray bursts (GRBs)

The afterglow emission of GRBs can be modelled as synchrotron emission from a decelerating blast wave in an ambient medium, plausibly the interstellar medium of the host galaxy (Waxman 1997; Wijers & Galama 1999; Mészáros 1999). The radio flux above the self-absorption break at  $\lesssim 5$  GHz, is proportional to  $\nu^{1/3}$  up to a peak frequency that decreases with time. This implies that surveys at different frequencies probe different phases of the expansion of the blast wave. Owing to their high brightnesses, GRB afterglows may be detected out to exceedingly high redshifts and are therefore important tracers of (a) the early star formation in the Universe, and of (b) the absorption properties of the intergalactic medium across the reionization phase. Estimates of the counts of GRB afterglows have been made by Ciardi & Loeb (2000), who found that at a fixed time-lag after the GRB in the observer’s frame, there is only a mild change in the observed flux density at radio wavelengths with increasing redshift. This stems in part from the fact that afterglows are brighter at earlier times and that a given observed time refers to an intrinsic time in the source frame that is earlier as the source redshift increases. According to Ciardi & Loeb (2000) estimates, a large area survey at  $\simeq 1$  cm to a flux limit  $\simeq 1$  mJy should discover some GRBs (see also Seaton & Partridge 2001; De Zotti et al. 2005). Predictions of Ciardi & Loeb’s models at 1.4 and 3 GHz are shown in Figs. 5 and 6.

## 7 The radio background

The radio background provides a key constraint on the counts of sources too faint to be individually detected. At frequencies below 1 GHz, the extragalactic radio background is swamped by the much more intense Galactic emission, primarily the synchrotron emission from diffused and integrated supernova remnants. Estimates at meter wavelengths made over 40 years ago (Bridle 1967) using the  $T$ – $T$  plot method (Turtle et al. 1962) yielded an antenna temperature of the extragalactic background at 178 MHz of  $T_{\text{bkg}} = 30 \pm 7$  K, about one third of the minimum total sky brightness at that frequency. Subtraction of the Galactic emission assuming that it scales as  $\csc |b|$ , ( $b$  = Galactic latitude) is very inaccurate, as (i) Galactic emission towards the Galactic poles is not removed, and (ii) there are major features such as the North Galactic Spur which follow no such law. In fact the morphology is complex; see for example the superb map at 408 MHz by Haslam et al. (1982).

An independent estimate of the background intensity was obtained by Clark et al. (1970), exploiting the low-frequency measurements obtained with the Radio Astron-

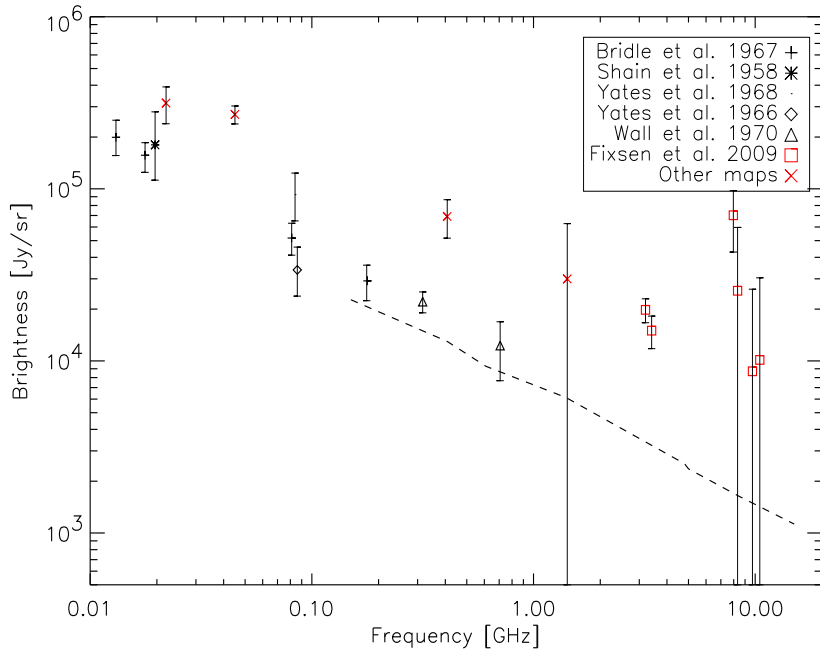


**Fig. 12** Estimates of the extragalactic radio background at different frequencies. The black symbols refer to estimates exploiting the methods mentioned in the first two paragraphs of § 7, while the red symbols refer to estimates by Fixsen et al. (2009) either using ARCADE 2 data (squares) or re-analyzing published data from large area surveys (×). The dashed line shows the extragalactic background spectrum yielded by the models fitting the counts in Figs. 4–7.

omy Explorer (RAE-1) satellite. While the  $T$ - $T$  plot method exploits the isotropy of the background and its different spectral index to separate it from Galactic emission, low-frequency measurements exploit the strong attenuation of the extragalactic radiation below 1 MHz due to free-absorption by electrons in the interstellar medium. Measurements at these frequencies can therefore be used to single out the Galactic-disk component. Extrapolating to higher frequencies and subtracting from measurements of the total flux Clark et al. were able to obtain an estimate of the extragalactic background intensity. Obviously the method works best in regions of low Galactic emission, such as the ‘north halo minimum’ region ( $l \sim 150^\circ$ ,  $b \sim 50^\circ$ ). Once again the isotropic component was identified to be about one-third the minimum total brightness observed at 100 MHz. The spectral index appeared to be similar to the average spectral index observed for extra-galactic sources, suggesting that the isotropic component does represent the extragalactic background rather than an isotropic halo of the Galaxy.

Gervasi et al. (2008) calculated the brightness of the isotropic background anticipated from unresolved extragalactic source, using modern compilations of source counts and fitting smooth functions to these counts. Their results range from  $T_b = 38600$  K at 151 MHz to 0.41 K at 8.44 GHz; over this range the  $T_b$  – frequency law is close to a power law.

Interest in the radio background was recently revived by the results of the second-generation balloon-borne experiment ARCADE-2 (Absolute Radiometer for Cosmol-

ogy, Astrophysics, and Diffuse Emission). After subtracting a model for the Galactic emission and the CMB, Fixsen et al. (2009) found excess radiation at 3 GHz about 5 times brighter than the estimated contribution from extragalactic radio sources, as calculated by Gervasi et al. and in the present work (see Fig. 12). From a re-analysis of several large-area surveys at lower frequencies to separate the Galactic and extragalactic components, Fixsen et al. (2009) obtained an extragalactic background power-law spectrum of  $T = 1.26 \pm 0.09 \text{ K} (\nu/\nu_0)^{-2.60 \pm 0.04}$ , with  $\nu_0 = 1 \text{ GHz}$  from 22 MHz to 10 GHz, in addition to a CMB temperature of  $2.725 \pm 0.001 \text{ K}$ . These results are compared to earlier estimates in Fig. 12, where we show the background brightness,  $I_\nu$ , in Jy/sr, as a function of frequency.  $I_\nu$  is related to the antenna temperature,  $T_a$ , by

$$T_a = \frac{c^2 I_\nu}{2k_B \nu^2} \simeq 3.25 \times 10^{-5} \left( \frac{\nu}{\text{GHz}} \right)^{-2} \frac{I_\nu}{\text{Jy/sr}}. \quad (16)$$

where the numerical coefficient holds for  $T_a$  in K, and  $1 \text{ Jy} = 10^{-23} \text{ erg cm}^{-2} \text{ s}^{-1} \text{ Hz}^{-1}$ . As shown by the figure, the ARCADE results are inconsistent with earlier measurements. We note that the antenna temperature at 81.5 MHz implied by the power-law fit of Fixsen et al. (2009), 854 K, exceeds the minimum *total* sky brightness temperature of 680 K measured by Bridle (1967).

## 8 Sunyaev-Zeldovich effects

The Sunyaev & Zeldovich (SZ) effect (Sunyaev & Zeldovich 1972) arises from the inverse Compton scatter of CMB photons against hot electrons. For a comprehensive background review see Birkinshaw (1999). The CMB intensity change is given by

$$\Delta I_\nu = 2 \frac{(kT_{\text{CMB}})^3}{(hc)^2} y g(x) \quad (17)$$

where  $T_{\text{CMB}} = 2.725 \pm 0.002 \text{ K}$  (Mather et al. 1999) is the CMB temperature and  $x = h\nu/kT_{\text{CMB}}$ .

The spectral form of this ‘‘thermal effect’’ is described by the function

$$g(x) = x^4 e^x [x \cdot \coth(x/2) - 4]/(e^x - 1)^2, \quad (18)$$

which is negative (positive) at values of  $x$  smaller (larger) than  $x_0 = 3.83$ , corresponding to a critical frequency  $\nu_0 = 217 \text{ GHz}$ .

The Comptonization parameter is

$$y = \int \frac{kT_e}{m_e c^2} n_e \sigma_T dl, \quad (19)$$

where  $m_e$ ,  $n_e$  and  $T_e$  are the electron mass, density and temperature respectively,  $\sigma_T$  is the Thomson cross section, and the integral is over a line of sight through the plasma.

With respect to the incident radiation field, the change of the CMB intensity across a galaxy or a cluster can be viewed as a net flux emanating from the plasma cloud, given by the integral of intensity change over the solid angle subtended by the cloud

$$\Delta F_\nu = \int \Delta I_\nu d\Omega \propto Y \equiv \int y d\Omega. \quad (20)$$

In the case of hot gas trapped in the potential well due to an object of total mass  $M$ , the parameter  $Y$  in eq. (20), called integrated Y-flux, is proportional to the gas-mass-weighted electron temperature  $\langle T_e \rangle$  and to the gas mass  $M_g = f_g M$ :

$$Y \propto f_g \langle T_e \rangle M . \quad (21)$$

At frequencies below 217 GHz, the Y-flux is negative and can therefore be distinguished from the positive signals due to the other source populations.

### 8.1 Sunyaev-Zeldovich (SZ) effects in galaxy clusters

The SZ effect from the hot gas responsible for the X-ray emission of rich clusters of galaxies has been detected with high signal-to-noise and even imaged in many tens of objects (Carlstrom et al. 2002; Benson et al. 2004; Jones et al. 2005; Bonamente et al. 2006; Halverson et al. 2009; Staniszewski et al. 2009). Detailed predictions of the counts of SZ effects require several ingredients, generally not well known: the cluster mass function, the gas fraction, the gas temperature and density profiles. All these quantities are evolving with cosmic time in a poorly-understood manner. Therefore, predictions are endowed with substantial uncertainties. Current models generally assume a self-similar evolution of the relationships between the main cluster parameters (mass, gas temperature, gas fraction, X-ray luminosity; Bonamente et al. 2008). Several predictions for the SZ counts are available (e.g. de Luca et al. 1995; Colafrancesco et al. 1997; De Zotti et al. 2005; Chamballu et al. 2008). SZ maps have been constructed, mostly using the output of hydrodynamical cosmological simulations, by Geisbüsch et al. (2005), Pace et al. (2008), Waizmann & Bartelmann (2009), amongst others.

Our understanding of the physics of the intra-cluster plasma is expected to improve drastically thanks to ongoing and forthcoming SZ surveys such as those with the South Pole Telescope (Carlstrom et al. 2009), the Atacama Cosmology Telescope (Kosowsky 2006), APEX-SZ (Dobbs et al. 2006), AMI (Zwart et al. 2008), SZA (Muchovej et al. 2007), OCRA<sub>p</sub> (Lancaster et al. 2007), and the Planck mission (The Planck Collaboration 2006).

### 8.2 Galaxy-scale Sunyaev-Zeldovich effects

The formation and early evolution of massive galaxies is thought to involve the release of large amounts of energy that may be stored in a high-pressure proto-galactic plasma, producing a detectable SZ effect. (Note that the amplitude of the effect is a measure of the pressure of the plasma.) According to the standard scenario (Rees & Ostriker 1977; White & Rees 1978), the collapsing proto-galactic gas is shock-heated to the virial temperature, at least in the case of large halo masses ( $\gtrsim 10^{12} M_\odot$ , Dekel & Birnboim 2006). Further important contributions to the gas thermal energy may be produced by supernova explosions, winds from massive young stars, and mechanical energy released by central super-massive black-holes. The corresponding SZ signals are potentially a direct probe of the processes governing the early phases of galaxy evolution and on the history of the baryon content of galaxies. They have been investigated under a variety of assumptions by many authors (Oh 1999; Natarajan & Sigurdsson 1999; Yamada et al. 1999; Aghanim et al. 2000; Majumdar et al. 2001; Platania et al.



2002; Oh et al. 2003; Lapi et al. 2003; Rosa-González et al. 2004; De Zotti et al. 2004; Chatterjee & Kosowsky 2007; Massardi et al. 2008b; Chatterjee et al. 2008).

Widely different formation modes for present day giant spheroidal galaxies are being discussed in the literature, in the general framework of the standard hierarchical clustering scenario. One mode (Granato et al. 2004; Lapi et al. 2006; Cook et al. 2009) has it that these galaxies generated most of their stars during an early, fast collapse featuring a few violent, gas rich, major mergers; only a minor mass fraction may have been added later by minor mergers. Alternatively, spheroidal galaxies may have acquired most of their stars through a sequence of, mostly dry, mergers (De Lucia & Blaizot 2007; Guo & White 2008).

The second scenario obviously predicts far less conspicuous galaxy-scale SZ signals than the first one. In the framework of the first scenario Massardi et al. (2008b) find that the detection of substantial numbers of galaxy-scale thermal SZ signals is achievable by blind surveys with next generation radio telescope arrays such as EVLA, ALMA and SKA. This population is detectable even with a 10% SKA, and wide-field-of-view options at high frequencies on any of these arrays would greatly increase survey speed. An analysis of confusion effects and contamination by radio and dust emissions shows that the optimal frequency range is 10–35 GHz. Note that the baryon to dark matter mass ratio at virialization is expected to have the cosmic value, i.e. to be about an order of magnitude higher than in present day galaxies. Measurements of the SZ effect will provide a direct test of this as yet unproven assumption, and will constrain the epoch when most of the initial baryons are swept out of the galaxies.

## 9 Wide area surveys and large scale structure

Extragalactic radio sources are well suited to probe the large-scale structure of the Universe: detectable over large cosmological distances, they are unaffected by dust extinction, and can thus provide an unbiased sampling of volumes larger than those usually probed by optical surveys. On the other hand, their 3D space-distribution can be recovered only in the very local Universe ( $z \lesssim 0.1$ ; see Peacock & Nicholson 1991; Magliocchetti et al. 2004) because the majority of radio galaxies detected in the available large-area, yet relatively deep, surveys, carried out at frequencies  $\leq 1.4$  GHz, have very faint optical counterparts, so that redshift measurements are difficult. As a result, only the *angular* (2D) clustering can be measured for the entire radio AGN population. High-frequency surveys have much higher identification rates (Sadler et al. 2006), suggesting that this difficulty may be overcome when such surveys cover sufficient sky and are linked to wide-area redshift surveys.

### 9.1 The angular correlation function and its implications

Just the basic detection of clustering in the 2D distribution of radio sources proved to be extremely difficult (e.g. Webster 1976; Seldner & Peebles 1981; Shaver & Pierre 1989) because at any flux-density limit, the broad luminosity function translates into a broad redshift distribution, strongly diluting the spatial correlations when projected onto the sky. Only with the advent of deep radio surveys covering large areas of the sky, FIRST (Becker et al. 1995), WENSS (Rengelink et al. 1997), NVSS (Condon et al. 1998), and SUMSS (Mauch et al. 2003), did it become possible to detect the angular clustering

of these objects with high statistical significance: see Cress & Kamionkowski (1998) and Magliocchetti et al. (1998, 1999); Blake & Wall (2002a) for FIRST; Blake & Wall (2002b,a) and Overzier et al. (2003) for NVSS; Rengelink (1999) for WENSS; and Blake et al. (2004b). Even then there remained difficulties of interpretation due to spurious correlation at small angular scales caused by the multiple-component nature of extended radio sources (Blake & Wall 2002b); the raw catalogues constructed from these large surveys list *components* of sources rather than single ‘assembled’ sources. Amongst the cited surveys, NVSS is characterized by the most extensive sky coverage and can thus provide the best clustering statistics, despite its somewhat higher completeness limit ( $\sim 3$  mJy vs  $\sim 1$  mJy of FIRST). The two-point angular correlation function  $w(\theta)$ , measured for NVSS sources brighter than 10 mJy, is well described by a power-law of slope  $-0.8$  extending from  $\sim 0.1$  degrees up to scales of almost 10 degrees (Blake & Wall 2002a). A signal of comparable amplitude and shape was detected in the FIRST survey at the same flux density limit, on scales of up to 2-3 degrees (see e.g. Magliocchetti et al. 1998, 1999), while at larger angular separations any positive clustering signal - if present - is hidden by the Poisson noise.

Most of the analyses performed so far with the aim of reproducing the clustering of radio galaxies (see e.g. Blake & Wall 2002b,a; Overzier et al. 2003) assumed a two-point spatial correlation function of the form  $\xi_{\text{rg}}(r) = (r/r_0)^{-\gamma}$ . The power-law shape is in fact preserved when projected onto the sky (Limber 1953), so that the observed behaviour of the angular correlation is well recovered. The correlation length  $r_0$  was found to lie in the range 5–15 Mpc, the large range reflecting the uncertainties in both the redshift distribution of the sources and the time-evolution of clustering. Despite the wide range in measurement of  $r_0$ , the above results suggest that radio galaxies are more strongly clustered than optically-selected galaxies.

A deeper examination of the power-law behaviour of the angular two-point correlation function up to scales of the order of  $\sim 10^\circ$  highlights interesting issues. Within the Cold Dark Matter paradigm of structure formation, the spatial correlation function of matter displays a sharp cut-off near a comoving radius of  $r \sim 100$  Mpc, which at the average redshift for radio sources  $\langle z \rangle \sim 1$ , corresponds to angular separations of only a few ( $\sim 1^\circ - 2^\circ$ ) degrees. This is in clear contrast to the observations of the angular two-point correlation function. The question is how to reconcile the clustering properties of these sources with the standard scenario of structure formation. Some authors have tried to explain the large-scale positive tail of the angular correlation function  $w(\theta)$  as due to a high-density local population of star-forming galaxies (Blake et al. 2004a). Others (Magliocchetti et al. 1999) suggested that the results can be reproduced by a suitable choice of the time-evolution of the bias parameter, i.e. the way radio galaxies trace the underlying mass distribution. The first hypothesis can be discarded on the basis of more recent determinations of the space density of local star-forming galaxies with a 1.4-GHz radio counterpart (e.g. Magliocchetti et al. 2002; Sadler et al. 2002; Mauch & Sadler 2007). Even the second approach, although promising, suffers a number of limitations due to both theoretical modelling and quality of data then available.

Theoretical predictions for the angular two-point correlation function of a given class of objects using Limber (1953) equation

$$w(\theta) = \int dz \mathcal{N}^2(z) \int d(\delta z) \xi[r(\delta z, \theta), z] \bigg/ \left[ \int dz \mathcal{N}(z) \right]^2 \quad (22)$$

require two basic ingredients: their redshift distribution,  $\mathcal{N}(z)$ , i.e. the number of objects brighter than the flux limit of the survey as a function of redshift, and the value of the bias factor as a function of redshift,  $b(z)$ . In equation (22),  $r(\delta z, \theta)$  represents the *comoving* spatial distance between two objects located at redshifts  $z$  and  $z + \delta z$  and separated by an angle  $\theta$  on the sky. For a flat universe and in the small-angle approximation (still reasonably accurate for scales of interest here,  $0.3^\circ \lesssim \theta \lesssim 10^\circ$ )

$$r^2 = \left(\frac{c}{H_0}\right)^2 \left[ \left(\frac{\delta z}{E(z)}\right)^2 + (d_C(z)\theta)^2 \right], \quad (23)$$

with

$$E(z) = [\Omega_M(1+z)^3 + \Omega_\Lambda]^{1/2}, \quad d_C(z) = \int_0^z \frac{dz'}{E(z')}. \quad (24)$$

On sufficiently large scales, where the clustering signal is produced by galaxies residing in distinct dark-matter halos and under the assumption of a one-to-one correspondence between sources and their host halos, the spatial two-point correlation function can be written as the product of the correlation function of dark matter,  $\xi_{\text{DM}}$ , times the square of the bias parameter,  $b$  (Matarrese et al. 1997; Moscardini et al. 1998):

$$\xi(r, z) = b^2(M_{\text{eff}}, z)\xi_{\text{DM}}(r, z). \quad (25)$$

Here,  $M_{\text{eff}}$  is the effective mass of the dark matter haloes in which the sources reside and  $b$  is derived in the extended Press & Schechter (1974) formalism according to the prescriptions of Sheth & Tormen (1999).

Negrello et al. (2006) adopted the  $\mathcal{N}(z)$  from Dunlop & Peacock (1990)'s pure luminosity evolution model. If the effective mass of the dark matter haloes in which the sources reside does not depend on cosmic time, as found for optically-selected quasars (Porciani et al. 2004; Croom et al. 2004), the predicted angular correlation function badly fails to reproduce the observed one. This is because contributions to  $w(\theta)$  on a given angular scale come from both local, relatively close pairs of sources and from high-redshift, more distant ones. But for  $z \gtrsim 1$  angular scales  $\theta \gtrsim 2^\circ$  correspond to linear scales where the correlation function is negative. Since the contribution of distant objects is overwhelming, we expect negative values of  $w(\theta)$ , while observations give us positive values.

The only way out appears to be a damping down of the contribution to  $w(\theta)$  of high- $z$  sources, and this can only be achieved through  $b(z)$ . Negrello et al. (2006) found that the  $w(\theta)$  data can be reproduced by assuming an epoch-dependent effective mass proportional to the mass scale at which the matter-density fluctuations collapse to form bound structures. Such mass decreases with increasing redshift, thus abating the negative high- $z$  contributions to  $w(\theta)$ . This assumption may be justified – locally, AGN-powered radio galaxies are found mainly in very dense environments such as groups or clusters of galaxies, and the characteristic mass of virialized systems indeed decreases with increasing redshift. The best fit to the data was obtained for a high value of the local effective mass,  $M_{\text{eff}}(z=0) \simeq 10^{15} M_\odot/h$ . However the CENSORS data (Brookes et al. 2008) have shown that the redshift distribution peaks at lower redshifts than predicted by Dunlop & Peacock (1990) PLE model (Fig. 11). Using a smooth description of the CENSORS redshift distribution

$$\mathcal{N}(z) = 1.29 + 32.37z - 32.89z^2 + 11.13z^3 - 1.25z^4, \quad (26)$$

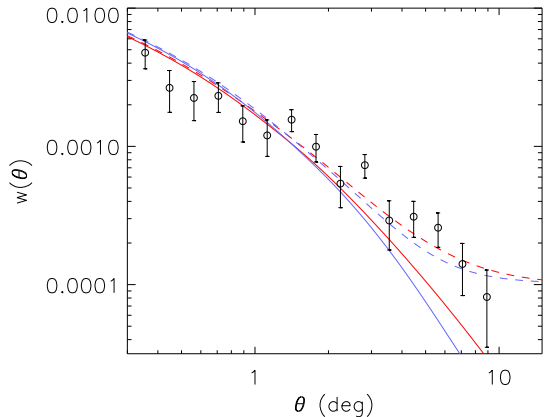


**Fig. 13** Two-point angular correlation function of NVSS sources with  $S_{1.4\text{GHz}} \geq 10 \text{ mJy}$  as measured by Blake & Wall (2002b) compared with the model by Negrello et al. (2006, red curves) and with the updated model (blue curves) fitting the redshift distribution by Brookes et al. (2008). The dashed curves include the contribution of a constant offset  $\epsilon = 0.0001$  to  $w(\theta)$  in order to account for the effect of possible spurious density gradients in the survey.

the best fit is obtained with a somewhat lower value for the local effective mass,  $M_{\text{eff}}(z=0) \simeq 10^{14.5} M_{\odot}/h$  (Fig. 13).

## 9.2 Integrated Sachs–Wolfe (ISW) effect

The ISW effect describes the influence of the evolution of the gravitational potential in time-variable, linear, metric perturbations on CMB photons that traverse them. When the CMB photons enter an overdensity they are gravitationally blue-shifted, and they are red-shifted when they emerge. In an Einstein-de Sitter universe the density contrast grows as the linear scale, so that the gravitational potential associated with the mass fluctuation is independent of time. Hence the red- and the blue-shift exactly compensate each other and the net effect is zero. However, a non-zero effect arises if the gravitational potential decays, as in the case of an open universe when the effect of the space curvature is important, or when the dynamics of the universe are dominated by dark energy.

As first pointed out by Crittenden & Turok (1996), a promising way of probing the ISW effect is through correlating fluctuations in the Cosmic Microwave Background (CMB) with large-scale structure. Since the timescale for the decay of the potential is of the order of the present-day Hubble time, the effect is largely canceled on small scales, because photons travel through multiple density peaks and troughs. This is why surveys covering large areas of the sky and probing the large scale distribution up to  $z \sim 1$  are necessary.

A high quality all-sky CMB temperature map has been provided by the WMAP satellite (Bennett et al. 2003; Hinshaw et al. 2007; Hinshaw & Naeye 2008). A particularly well-suited probe of the large-scale structure is the NVSS survey, and indeed this

has been extensively exploited to look for the ISW signal (Boughn & Crittenden 2004, 2005; Pietrobon et al. 2006; McEwen et al. 2007, 2008; Ho et al. 2008; Giannantonio et al. 2008; Raccanelli et al. 2008).

The comparison of the correlations inferred from the data with model predictions requires once again the redshift distribution and the bias parameter as a function of redshift. All analyses carried out so far have used redshift distributions inconsistent with the CENSORS results. The product of the latter redshift distribution with the redshift-dependent bias factor best fitting the observed  $w(\theta)$  (see the previous subsection), whose integral determines the amplitude of the ISW effect, peaks at redshifts where the contribution to the ISW signal in a  $\Lambda$ CDM cosmology also peaks, namely  $z \simeq 0.4$ . This means that the NVSS sample is very well suited to test the effects of dark energy on the growth of structure. The predicted cross-correlation power spectrum between the surface density fluctuations of NVSS sources and the CMB fluctuations expected for the ‘‘concordance’’  $\Lambda$ CDM cosmology turns out to be in good agreement with the empirical determination using the CMB map obtained from WMAP data. This conclusion is at odds with that of Ho et al. (2008) who found that the WMAP 3-year model predicts an ISW amplitude about  $2\sigma$  below their estimate. Hence we suggest that the amplitude of the ISW cross-correlation does not support the case for new gravitational physics on cosmological scales (Afshordi et al. 2008) or for a large local primordial non-Gaussianity (Afshordi & Tolley 2008).

## 10 The future

There are prospects for dramatic steps forward in radio and millimeter-wave astronomy within the decade, thanks to a new generation of large to gigantic interferometers as well as refurbishment of old interferometers. Interferometric observations gain over single-dish observations not just through resolution but through improved sensitivity, because correlation of the signals from the antennas can distinguish signal from noise and background. Long integrations become possible without the limitation of systematic errors. However, observing with interferometers requires careful set-up of the antenna array (and its parameters in software) to image sources correctly by measuring their flux densities on the appropriate angular scales. There is also the dreaded problem of ‘missing flux’ from (lack of) low-order harmonics in the spatial transform, corresponding to structure on the larger scales (§ 2). In addition, the amount of post-processing required is large in comparison to single-dish measurements, to correct for the many instrumental and atmospheric issues, to convert the Fourier components into brightness images of radio sources, and (because of incomplete sampling in the Fourier plane) to apply algorithms to maximize image fidelity and dynamic range. Interferometers offer an additional advantage: on the increasingly noise-polluted surface of our planet, the processing can excise radio-frequency interference (RFI), which, even at the remote sites of future large arrays, would otherwise seriously compromise observations.

The small beam size at millimeter wavelengths makes large-area deep surveys extremely difficult because of the time penalty. New scanning techniques will need to be developed to perform such surveys. The next generation of interferometers, thanks to larger collecting areas, broader bandwidths and faster scanning capabilities are expected to produce deeper surveys of large sky regions, both in total intensity and in polarization. Receiver advances have resulted in huge bandwidths ( $\geq 10$  per cent) and very low equivalent noise temperatures over these bandwidths. To realize these gains in

sensitivity with interferometers requires development in correlator speed and in processing power. Moreover instead of single-pixel feeds, the development of focal plane arrays (FPAs, or phased-array feeds) looks to realize the long-standing dream of making near-full use of the information brought to the focal plane (e.g. APERTIF, Verheijen et al. 2008). There are further implications for correlator- and processor-power requirements.

The focus of current effort in the radio-astronomy community is towards the realization of the Square Kilometer Array (SKA), the largest and most sensitive radio telescope ever. The SKA stands to be one of the iconic scientific instruments of the 21st century. It will consist of an array of thousands of dishes, each 10–15 m in diameter, as well as a complementary aperture array – a large number of small, fixed antenna elements plus receiver chains arranged in a regular or random pattern on the ground. Between these two technologies, a frequency range of 100 MHz to 25 GHz will be covered. The collecting area will add up to approximately one million square meters, with baselines ranging from  $\sim 15$  m to more than 3000 km. The SKA will require super-fast data transport networks (of order the current total internet capacity) and computing power far beyond current capabilities. Indeed the concept is only feasible if Moore’s Law (the packing density of processing elements approximately doubling every two years) continues to hold; and this in itself requires revolutions in processor technologies. Site-testing has narrowed the choice to remote regions either in Western Australia or in South Africa. The telescope is expected to be fully operational after 2020, but a 10% SKA may be operating as early as 2015. Many different technological solutions will be selected and integrated into the final instrument: they will represent the results of developing the so-called SKA pathfinders (ASKAP, MeerKAT, ATA, LOFAR, e-MERLIN, EVLA; [www-page descriptions are readily available for each](#)).

These pathfinders carry the shorter-term excitement; they themselves represent leaps forward in observational capability. Most of them will be operational by 2015. They will realize dramatic improvements in survey speed and sensitivity; ASKAP for example, is expected to produce a survey similar to the NVSS (Condon et al. 1998) in sky coverage, but bettering it by a factor of 50 in sensitivity and of 5 in angular resolution (Johnston et al. 2008). These new tools will allow us to distinguish the star-forming population from the AGN population at low flux-density levels and to investigate source populations at extreme redshifts.

The SKA itself will impact every area of astronomy and cosmology, from detection and mapping of planetary systems, study of individual stars, star clusters, pulsars, the structure of our Galaxy in both baryons and in magnetic field, through to normal galaxies, AGNs, proto-galaxies, and large-scale structure of the Universe. The compelling science (e.g. Carilli & Rawlings 2004, and updates on the SKA website) to be realized makes irresistible reading.

LOFAR (Rottgering et al. 2006), will open up the frequency window at the low end of the radio spectrum, below 240 MHz. LOFAR will survey the sky to unprecedented depths at low frequencies and will therefore be sensitive to the relatively rare radio sources that have very steep spectra, extreme luminosities and redshifts (§ 1). A unique area of investigation will be the search for redshifted 21cm line emission from the epoch of reionisation.

At the other end of the radio band, the Atacama Large Millimeter Array (ALMA) is eagerly anticipated by the mm continuum and molecular-line community. Being built on a high (5000m), dry plain in the Atacama desert, northern Chile, it is an international project, a giant array of 50 12-m submillimetre quality antennas, with baselines of several kilometres. An additional compact array (ACA) of 12 7-m and 4 12-

m antennas is also foreseen. ALMA will be equipped with mm and sub-mm receivers covering ultimately all the atmospheric windows at 5000m altitude in ten spectral bands, from 31 to 950 GHz. The array will be operational by 2012 with a subset of the high-priority receivers. The steep rise of the dust emission spectrum at mm and sub-mm wavelengths implies that the K-correction compensates, at  $z \gtrsim 0.1$ , for the dimming due to increasing distance (Blain & Longair 1993), making the observed mm flux of dusty galaxies of given bolometric luminosity only weakly dependent on redshift up to  $z \simeq 10$ . This makes ALMA the ideal instrument for investigating the origins of galaxies in the early universe, with confusion made negligible by the high spatial resolution. Using far-IR emission lines and CO rotational emission, ALMA will reveal the astrophysics of early phases of galaxy formation and provide the redshift of large numbers of obscured star-forming galaxies up to very large distances. This will enable us to establish the star-forming history of the universe, without the uncertainties caused by dust extinction in optical studies.

Technological advances have resulted in upgrades of existing telescopes that revolutionize performance. For examples:

1. The Australia Telescope Compact Array (ATCA), a 6 22m-dish array, has recently completed the upgrade of 7 mm receivers (working in the frequency range 30-50 GHz), and the increase of the bandwidth from  $2 \times 128$  MHz to 4 GHz (thanks to the new CABB system). These new capabilities together with its fast scan rate ( $15^\circ/\text{min}$  at the meridian) will allow the extension of the Australia Telescope 20 GHz (AT20G) Survey to higher frequencies or to lower flux densities.
2. The Expanded Very Large Array (EVLA) is an upgrade of the sensitivity and frequency coverage of the VLA. When completed, it will use the 27 25m dishes of the VLA with 8-GHz bandwidth per polarization in the frequency bands 18-26.5, 26.5-40, and 40-50 GHz. This is a 10 to 100-fold increase in sensitivity over the standard VLA. First observations will be in 2010; after full commissioning (2013) the (E)VLA is destined to remain at the forefront of radio astronomy for at least a decade.

Finally, several new survey instruments for the Sunyaev-Zeldovich effect have either started operations or will shortly do so (see § 8.1).

## 11 Conclusions

For decades radio surveys have been a leading agent for extragalactic research, as testified by the breakthroughs they triggered, from the discovery of cosmic evolution, to quasars and the first high- $z$  galaxies. They continue at the forefront of astrophysics and cosmology; e.g., via large-scale structure studies they pose challenges for buildup of the cosmic web; and via downsizing and AGN feedback deemed to produce this downsizing, they have come to the fore in modelling galaxy formation and evolution.

But our physical understanding of the origin and evolution of the AGN-powered radio emission is still poor. While physical models for the cosmological evolution of galaxies and radio-quiet quasars have been progressing rapidly in recent years, the main progress on the radio side has been towards a phenomenological description of evolution of various radio AGN types.

Even on the phenomenological side, there are aspects that are not fully understood. The epoch-dependent luminosity functions of galaxies and radio-quiet quasars are now

quite accurately determined up to high redshifts and there are attempts to provide physical explanations for the evidence for earlier formation of the more massive objects. Direct evidence for a substantial decline of the space densities of radio AGNs at  $z \gtrsim 2$  remains somewhat controversial, although modern evolutionary models accounting for the observed counts and redshift distributions do include such a decline.

The origin of these uncertainties remains as it has been for the last 30 years – a lack of concerted effort to obtain complete redshift sets for radio AGN samples. The new redshift surveys (2dF, SDSS) have helped greatly in defining local space densities. But beyond two or three of the brightest samples such as 3CRR, there are *no* samples with complete redshift data. Even samples of 100 to 200 objects would suffice for most purposes, and could be easily obtained with 8- to 10m-class telescopes. Our deficiency in this regard is highlighted by the reliance of most analyses needing complete redshift information on the Dunlop & Peacock (1990) model distributions – even 20 years on. Doubtless the planned new deep optical and infrared wide-field surveys such as PAN-STARRS (Hodapp et al. 2004) and those with the VST and VISTA (Arnaboldi et al. 2007) will help. However there will remain a need for individual pursuit of the faintest members in samples via deep imaging in different optical and IR bands and via fast spectrographs to complete the redshift information in samples of limited size.

Sixty years since their discovery, radio AGNs remain at the forefront of astrophysics and cosmology. Our continued attempts to solve the mysteries which still surround them will doubtless lead to fresh discoveries of impact as great as those which have distinguished the first 60 years.

**Acknowledgements** We are grateful to the referee, Jim Condon, for a very careful reading of the manuscript and for many very useful comments and suggestions. Thanks are due to Benedetta Ciardi for having provided the 1.4 GHz counts of GRB afterglows in tabular form. GDZ and MM acknowledge partial financial support from ASI contracts I/016/07/0 “COFIS” and “Planck LFI Activity of Phase E2”. JVW acknowledges support via Canadian NSERC Discovery Grants.

### Appendix

We present tabulations of the observed source counts, including when relevant, an estimate of the clustering contribution to the errors. The columns ‘norm. cts.’ and ‘+,-’ give, respectively,  $S^{2.5}dN/dS[Jy^{1.5}/sr]$ , and its positive and negative errors. The column ‘sampl. err.’ gives, for surveys covering less than  $25 \text{ deg}^2$  the contribution to such errors due to the sampling variance [eq. (6)]; such contributions are negligible for larger areas.

Table 1: Euclidean normalized differential source counts at 150 MHz.

$\log(S[Jy])$	norm. cts.	+ , -	ref.
-0.978	765.720	47.160, 55.080	mc90
-0.908	957.960	59.400, 68.760	mc90
-0.859	1079.640	66.600, 77.760	mc90
-0.810	1104.120	68.040, 79.560	mc90
-0.772	1301.400	80.280, 75.600	mc90
-0.728	1330.560	82.080, 86.400	mc90
-0.685	1510.920	93.240, 98.280	mc90
-0.677	1305.360	90.720, 88.920	ha88
-0.636	1580.040	97.561, 91.800	mc90
-0.634	1459.440	89.640, 68.040	ha88
-0.596	1584.000	84.960, 50.760	ha88
-0.587	1652.400	128.161, 107.639	mc90
-0.552	1572.120	84.240, 50.401	ha88

*continued on the next page*



Table 1: *continued*

$\log(S[\text{Jy}])$	norm. cts.	+, -	ref.
-0.533	1947.600	135.360, 126.720	mc90
-0.515	1879.920	85.680, 59.400	ha88
-0.471	1922.040	118.080, 32.400	ha88
-0.467	1918.080	133.560, 83.879	mc90
-0.428	2070.720	94.680, 79.560	ha88
-0.391	2548.080	197.641, 129.959	mc90
-0.385	2230.560	101.880, 85.320	ha88
-0.347	2569.679	117.360, 115.560	ha88
-0.309	2768.040	126.720, 123.479	ha88
-0.304	2472.479	172.081, 160.919	mc90
-0.266	2872.800	131.400, 127.800	ha88
-0.228	2937.599	157.321, 109.799	ha88
-0.196	3187.080	171.001, 207.360	mc90
-0.184	3117.600	191.519, 93.240	ha88
-0.141	2981.160	206.639, 153.720	ha88
-0.109	3538.079	216.721, 180.720	ha88
-0.071	3618.000	251.999, 184.679	mc90
-0.060	4046.400	248.400, 176.401	ha88
-0.016	3726.000	230.401, 189.000	ha88
0.027	3866.400	208.800, 194.399	ha88
0.076	4136.401	284.399, 237.602	ha88
0.130	3726.000	259.199, 242.640	ha88
0.190	4388.399	338.401, 251.998	ha88
0.190	3837.600	237.600, 223.201	mc90
0.255	3895.199	331.201, 280.800	ha88
0.321	3808.800	356.400, 274.681	ha88
0.391	4978.800	464.401, 388.799	ha88
0.467	3614.399	424.801, 336.238	ha88
0.565	4068.000	450.001, 457.201	ha88
0.668	3805.201	482.400, 454.321	ha88
0.783	2823.120	502.919, 500.760	ha88
0.919	3349.800	595.799, 613.080	ha88
1.147	2927.520	626.041, 554.399	ha88

Reference codes. ha88: Hales et al. (1988); mc90: McGilchrist et al. (1990).

Table 2: Euclidean normalized differential source counts at 325 MHz.

$\log(S[\text{Jy}])$	norm. cts.	+, -	sampl. err.	ref.
-3.372	25.400	3.700, 3.700	0.044	ow09
-3.270	25.900	3.700, 3.700	0.044	ow09
-3.125	16.900	1.800, 1.800	0.029	ow09
-2.949	17.200	2.400, 2.400	0.030	ow09
-2.776	19.300	2.000, 2.000	0.033	ow09
-2.602	27.300	2.900, 2.900	0.047	ow09
-2.426	30.800	4.200, 4.200	0.053	ow09
-2.250	58.000	7.901, 7.901	0.100	ow09
-2.175	33.935	7.911, 7.911	0.241	oo88
-2.077	48.700	9.400, 9.400	0.084	ow09
-1.873	75.660	9.784, 9.784	0.538	oo88
-1.824	89.000	14.701, 14.701	0.153	ow09
-1.573	166.577	19.838, 19.838	1.185	oo88
-1.523	243.600	43.702, 43.702	0.418	ow09
-1.272	450.850	51.078, 51.078	3.207	oo88

*continued on the next page*

Table 2: *continued*

$\log(S[\text{Jy}])$	norm. cts.	+, -	sampl. err.	ref.
-1.222	495.600	105.103, 105.104	0.851	ow09
-0.971	468.133	86.201, 86.201	3.330	oo88
-0.921	398.100	162.501, 162.502	0.684	ow09
-0.670	1005.126	213.841, 213.841	7.150	oo88
-0.218	1535.170	396.048, 396.048	10.921	oo88

Reference codes. ow09: Owen et al. (2009); oo88: Oort et al. (1988).

Table 3: Euclidean normalized differential source counts at 408 MHz.

$\log(S[\text{Jy}])$	norm. cts.	+, -	sampl. err.	ref.
-1.857	86.625	22.647, 22.647	2.577	be82
-1.673	124.875	11.847, 11.847	3.715	be82
-1.488	200.250	23.275, 23.275	5.957	be82
-1.304	304.875	34.947, 34.947	9.069	be82
-1.120	430.875	46.790, 46.790	12.817	be82
-1.111	437.400	36.010, 36.010	0.835	gr88
-1.034	441.000	27.013, 27.013	0.842	gr88
-1.021	491.908	53.754, 59.034	-	ro77
-0.936	478.125	58.020, 58.020	14.223	be82
-0.910	619.861	59.305, 47.119	-	ro77
-0.903	540.000	19.827, 19.827	1.031	gr88
-0.757	732.600	23.442, 23.442	1.398	gr88
-0.752	835.875	115.215, 115.215	24.865	be82
-0.746	762.302	88.416, 66.481	-	ro77
-0.604	1039.737	149.211, 102.227	-	ro77
-0.602	892.800	27.054, 27.054	1.704	gr88
-0.568	789.750	148.125, 148.125	23.493	be82
-0.456	1014.417	152.595, 132.557	-	ro77
-0.430	925.865	70.137, 49.421	-	ro77
-0.398	1116.000	36.063, 36.063	2.130	gr88
-0.383	833.625	215.184, 215.183	24.798	be82
-0.298	1020.239	204.589, 185.769	-	ro77
-0.271	1117.862	77.449, 85.302	-	ro77
-0.222	1143.000	61.238, 61.239	2.182	gr88
-0.144	1711.456	381.828, 319.545	-	ro77
-0.123	1515.126	155.710, 115.090	-	ro77
-0.071	1278.000	81.036, 81.037	2.440	gr88
0.024	1201.945	172.364, 118.204	-	ro77
0.051	1449.000	118.832, 118.833	2.766	gr88
0.138	1342.800	147.622, 147.623	2.563	gr88
0.167	1515.126	227.471, 190.644	-	ro77
0.243	1234.800	135.021, 135.021	2.357	gr88
0.326	1850.918	189.560, 181.435	-	ro77
0.398	1008.000	165.611, 165.612	1.924	gr88
0.474	1513.772	227.473, 213.932	-	ro77
0.602	1008.000	165.611, 165.612	1.924	gr88
0.632	1171.481	278.653, 264.436	-	ro77
0.769	1291.174	345.812, 339.041	-	ro77
0.875	873.000	205.206, 205.207	1.666	gr88
0.923	1493.462	471.192, 494.210	-	ro77
1.081	969.058	118.882, 90.041	-	ro77
1.223	543.089	101.008, 85.167	-	ro77
1.377	647.889	153.950, 111.570	-	ro77

*continued on the next page*

Table 3: *continued*

$\log(S[\text{Jy}])$	norm. cts.	+, -	sampl. err.	ref.
1.525	768.124	205.943, 169.792	-	ro77

Reference codes. be82: Benn et al. (1982); gr88: Grueff (1988);  
ro77: Robertson (1977).

Table 4: Euclidean normalized differential source counts at 610 MHz.

$\log(S[\text{Jy}])$	norm. cts.	+, -	sampl. err.	ref.
-4.252	4.540	1.034, 1.034	0.805	ib09
-4.056	6.920	0.780, 0.780	0.637	ib09
-3.857	8.790	0.745, 0.745	0.586	ib09
-3.662	11.350	0.875, 0.875	0.646	ib09
-3.480	7.600	0.559, 0.559	0.251	ga08
-3.467	10.330	0.938, 0.938	0.564	ib09
-3.432	11.060	1.103, 1.103	0.593	bo07
-3.334	8.800	0.578, 0.578	0.290	ga08
-3.310	15.100	2.735, 2.735	0.849	mo07
-3.271	10.520	1.212, 1.212	0.569	ib09
-3.260	9.720	1.137, 1.137	0.521	bo07
-3.175	10.100	0.686, 0.686	0.333	ga08
-3.081	12.230	1.665, 1.665	0.656	bo07
-3.076	11.170	1.710, 1.710	0.604	ib09
-3.019	10.300	0.869, 0.869	0.340	ga08
-3.013	15.600	2.093, 2.093	0.877	mo07
-2.907	11.590	2.113, 2.113	0.621	bo07
-2.880	12.720	2.583, 2.583	0.688	ib09
-2.865	12.600	1.176, 1.176	0.415	ga08
-2.730	20.640	3.814, 3.814	1.107	bo07
-2.714	20.200	3.396, 3.396	1.136	mo07
-2.710	14.500	1.670, 1.670	0.478	ga08
-2.684	16.020	4.161, 4.161	0.866	ib09
-2.554	22.520	5.309, 5.309	1.207	bo07
-2.554	21.500	2.599, 2.599	0.709	ga08
-2.489	24.600	7.371, 7.371	1.330	ib09
-2.413	34.400	7.166, 7.166	1.935	mo07
-2.391	27.700	3.908, 3.908	0.913	ga08
-2.378	34.840	8.908, 8.908	1.868	bo07
-2.293	40.230	13.467, 13.467	2.176	ib09
-2.243	28.200	4.987, 4.987	0.930	ga08
-2.202	44.000	13.478, 13.478	2.359	bo07
-2.114	63.600	15.421, 15.421	3.577	mo07
-2.098	57.920	23.470, 23.470	3.132	ib09
-2.075	43.900	8.425, 8.425	1.447	ga08
-2.026	29.390	14.784, 14.784	1.576	bo07
-1.937	78.600	10.802, 10.802	2.537	ga08
-1.850	80.990	33.354, 33.354	4.343	bo07
-1.802	86.100	14.273, 14.273	2.779	ga08
-1.678	168.000	24.703, 24.703	5.423	ga08
-1.674	148.800	61.272, 61.272	7.978	bo07
-1.664	86.500	26.451, 26.451	4.865	mo07
-1.552	180.000	36.000, 36.000	0.000	ka79
-1.544	198.000	33.613, 33.613	6.392	ga08
-1.498	91.120	64.615, 64.615	4.886	bo07
-1.418	202.000	41.713, 41.713	6.521	ga08
-1.362	306.000	45.000, 45.000	0.000	ka79

*continued on the next page*

Table 4: *continued*

$\log(S[\text{Jy}])$	norm. cts.	+, -	sampl. err.	ref.
-1.322	334.790	168.360, 168.360	17.951	bo07
-1.263	137.000	45.913, 45.914	4.423	ga08
-1.171	360.000	54.000, 54.000	0.000	ka79
-1.166	217.000	65.874, 65.873	7.005	ga08
-1.063	562.000	189.653, 189.653	31.609	mo07
-1.023	133.000	66.838, 66.838	4.293	ga08
-0.981	360.000	63.000, 63.000	0.000	ka79
-0.915	276.000	113.351, 113.351	8.910	ga08
-0.790	495.000	99.000, 99.000	0.000	ka79
-0.757	339.000	170.352, 170.352	10.943	ga08
-0.600	675.000	153.000, 153.000	0.000	ka79
-0.410	684.000	216.000, 216.000	0.000	ka79
-0.220	1314.000	414.000, 414.000	0.000	ka79
0.096	837.000	369.000, 369.000	0.000	ka79

Reference codes. bo07: Bondi et al. (2007); ga08: Garn et al. (2008); ib09: Ibar et al. (2009); ka79: Katgert (1979); mo07: Moss et al. (2007).

Table 5: Euclidean normalized differential source counts at 1.4 GHz.

$\log(S[\text{Jy}])$	norm. cts.	+, -	sampl. err.	ref.
-4.770	6.480	1.510, 1.510	0.011	ow08
-4.668	6.500	0.890, 0.890	0.011	ow08
-4.602	3.210	0.752, 0.752	0.676	ib09
-4.523	6.110	0.580, 0.580	0.010	ow08
-4.467	2.600	1.624, 1.624	0.278	fo06
-4.398	4.140	0.529, 0.529	0.471	ib09
-4.373	4.100	2.048, 2.048	0.439	fo06
-4.347	5.750	0.690, 0.690	0.010	ow08
-4.340	0.980	0.278, 0.278	0.171	se08A
-4.284	2.300	0.688, 0.688	0.314	ri00
-4.272	5.400	2.372, 2.372	0.578	fo06
-4.244	2.490	0.509, 0.509	0.136	ho03
-4.208	5.120	0.511, 0.511	0.446	ib09
-4.206	2.580	0.528, 0.528	0.276	ke08
-4.180	3.287	0.245, 0.245	0.176	bo08
-4.173	5.700	2.476, 2.476	0.610	fo06
-4.155	2.900	0.803, 0.803	0.396	ri00
-4.151	1.110	0.285, 0.285	0.193	se08A
-4.143	3.270	0.447, 0.447	0.179	ho03
-4.114	7.010	0.740, 0.740	0.012	ow08
-4.092	4.454	0.318, 0.318	0.239	bo08
-4.077	7.000	2.706, 2.706	0.750	fo06
-4.066	3.660	0.614, 0.614	0.201	ho03
-4.060	3.100	0.763, 0.763	0.423	ri00
-4.021	2.520	0.466, 0.466	0.270	ke08
-4.009	5.060	0.473, 0.473	0.374	ib09
-4.000	4.434	0.331, 0.331	0.238	bo08
-4.000	3.910	1.255, 1.255	0.110	ho03
-3.971	2.100	0.839, 0.839	0.254	mi85
-3.960	5.200	2.366, 2.366	0.557	fo06
-3.955	2.700	0.727, 0.727	0.368	ri00
-3.927	1.610	0.369, 0.369	0.280	se08A
-3.914	4.250	0.908, 0.908	0.120	ho03

*continued on the next page*

Table 5: *continued*

$\log(S[\text{Jy}])$	norm. cts.	+, -	sampl. err.	ref.
-3.914	4.944	0.371, 0.371	0.265	bo08
-3.903	6.240	1.110, 1.110	0.011	ow08
-3.836	4.440	0.429, 0.429	0.125	ho03
-3.827	2.880	0.546, 0.546	0.308	ke08
-3.824	5.147	0.438, 0.438	0.276	bo08
-3.810	4.300	0.460, 0.460	0.298	ib09
-3.807	2.400	0.698, 0.698	0.327	ri00
-3.784	5.100	2.364, 2.364	0.546	fo06
-3.783	3.500	0.905, 0.905	0.423	mi85
-3.770	3.600	0.404, 0.404	0.105	ci99
-3.764	4.960	0.500, 0.500	0.140	ho03
-3.738	5.014	0.499, 0.499	0.269	bo08
-3.686	4.730	0.412, 0.412	0.133	ho03
-3.669	1.820	0.487, 0.487	0.317	se08A
-3.650	4.020	0.517, 0.517	0.216	bo08
-3.648	4.460	0.940, 0.940	0.008	ow08
-3.629	4.400	1.313, 1.313	0.532	mi85
-3.627	2.900	0.745, 0.745	0.396	ri00
-3.611	3.880	0.549, 0.549	0.266	ib09
-3.597	4.670	0.412, 0.412	0.131	ho03
-3.569	5.300	1.012, 1.012	0.158	gr99
-3.561	5.300	0.691, 0.691	0.284	bo08
-3.543	4.230	0.817, 0.817	0.453	ke08
-3.509	3.800	1.285, 1.285	0.460	mi85
-3.495	4.610	0.365, 0.365	0.134	ci99
-3.487	4.370	0.380, 0.380	0.123	ho03
-3.472	4.490	0.712, 0.712	0.241	bo08
-3.413	5.480	0.902, 0.902	0.376	ib09
-3.384	4.470	0.816, 0.816	0.240	bo08
-3.378	6.200	2.587, 2.587	0.664	fo06
-3.377	2.530	0.777, 0.777	0.441	se08A
-3.350	4.640	0.411, 0.411	0.131	ho03
-3.347	3.500	0.853, 0.853	0.477	ri00
-3.323	6.500	1.519, 1.519	0.786	mi85
-3.319	7.700	0.642, 0.642	0.229	gr99
-3.297	5.140	1.008, 1.008	0.276	bo08
-3.252	4.780	0.414, 0.414	0.139	ci99
-3.215	4.700	1.185, 1.185	0.322	ib09
-3.208	5.970	1.319, 1.319	0.320	bo08
-3.197	6.150	0.548, 0.548	0.173	ho03
-3.120	4.050	1.190, 1.190	0.217	bo08
-3.111	3.930	1.275, 1.081	0.211	bo08
-3.097	5.400	1.821, 1.821	0.653	mi85
-3.070	6.580	1.666, 1.666	0.705	ke08
-3.060	5.700	0.528, 0.528	0.170	gr99
-3.046	4.230	1.260, 1.260	0.007	ow08
-3.032	5.490	1.607, 1.607	0.294	bo08
-3.031	5.483	1.646, 1.508	0.294	bo08
-3.025	7.980	0.697, 0.697	0.225	ho03
-3.017	7.720	2.175, 2.175	0.530	ib09
-3.000	3.550	0.040, 0.040	0.000	wi97
-2.991	6.560	0.611, 0.611	0.191	ci99
-2.951	3.230	0.050, 0.050	0.000	wi97
-2.900	5.190	0.060, 0.060	0.000	wi97
-2.889	11.490	1.705, 2.035	0.616	bo08
-2.851	7.230	0.080, 0.080	0.000	wi97
-2.824	9.600	3.217, 3.217	1.161	mi85

*continued on the next page*

Table 5: *continued*

$\log(S[\text{Jy}])$	norm. cts.	+, -	sampl. err.	ref.
-2.820	12.330	3.922, 3.922	0.846	ib09
-2.804	7.200	0.828, 0.828	0.214	gr99
-2.801	7.640	0.090, 0.090	0.000	wi97
-2.783	11.500	0.994, 0.994	0.324	ho03
-2.750	9.120	0.110, 0.110	0.000	wi97
-2.738	11.680	1.151, 1.151	0.340	ci99
-2.699	10.040	0.120, 0.120	0.000	wi97
-2.684	8.869	2.457, 2.321	0.476	bo08
-2.650	12.270	0.150, 0.150	0.000	wi97
-2.622	10.630	5.677, 5.677	0.729	ib09
-2.600	12.680	0.170, 0.170	0.000	wi97
-2.550	14.160	0.190, 0.190	0.000	wi97
-2.550	10.100	1.432, 1.432	0.300	gr99
-2.500	15.410	0.220, 0.220	0.000	wi97
-2.481	15.860	2.033, 2.033	0.461	ci99
-2.479	14.080	4.228, 4.061	0.755	bo08
-2.450	17.100	0.250, 0.250	0.000	wi97
-2.400	18.990	0.290, 0.290	0.000	wi97
-2.350	20.540	0.330, 0.330	0.000	wi97
-2.309	23.980	2.073, 2.073	0.675	ho03
-2.300	22.890	0.370, 0.370	0.000	wi97
-2.295	20.900	3.260, 3.260	0.622	gr99
-2.284	55.000	14.272, 14.272	5.890	ke08
-2.283	31.190	8.643, 8.987	1.672	bo08
-2.250	25.260	0.430, 0.430	–	wi97
-2.227	31.610	4.436, 4.436	0.919	ci99
-2.200	27.280	0.490, 0.490	–	wi97
-2.194	14.300	3.820, 3.820	1.531	fo06
-2.150	31.380	0.570, 0.570	–	wi97
-2.100	34.540	0.650, 0.650	–	wi97
-2.078	32.370	12.085, 13.899	1.736	bo08
-2.050	37.240	0.740, 0.740	–	wi97
-2.040	30.000	6.066, 6.066	0.892	gr99
-2.000	42.040	0.850, 0.850	–	wi97
-1.971	61.870	9.600, 9.600	1.799	ci99
-1.950	46.010	0.970, 0.970	–	wi97
-1.900	50.670	1.110, 1.110	–	wi97
-1.873	84.690	31.638, 29.689	4.541	bo08
-1.850	54.590	1.260, 1.260	–	wi97
-1.800	59.780	1.430, 1.430	–	wi97
-1.783	52.200	12.398, 12.398	1.553	gr99
-1.750	66.180	1.650, 1.650	–	wi97
-1.716	59.070	14.433, 14.433	1.718	ci99
-1.700	77.710	1.940, 1.940	–	wi97
-1.668	86.270	41.191, 43.000	4.626	bo08
-1.650	85.570	2.220, 2.220	–	wi97
-1.600	80.120	2.350, 2.350	–	wi97
-1.550	100.880	2.870, 2.870	–	wi97
-1.529	105.000	27.279, 27.279	3.123	gr99
-1.500	114.910	3.340, 3.340	–	wi97
-1.478	84.390	11.429, 11.429	2.374	ho03
-1.461	109.100	30.416, 30.416	3.172	ci99
-1.450	102.910	3.450, 3.450	–	wi97
-1.400	134.730	4.300, 4.300	–	wi97
-1.350	119.970	4.420, 4.420	–	wi97
-1.300	138.130	5.170, 5.170	–	wi97
-1.274	84.500	37.883, 37.883	2.514	gr99

*continued on the next page*

Table 5: *continued*

$\log(S/Jy)$	norm. cts.	+, -	sampl. err.	ref.
-1.250	160.170	6.070, 6.070	–	wi97
-1.206	162.100	57.503, 57.504	4.713	ci99
-1.200	179.240	7.000, 7.000	–	wi97
-1.150	172.490	7.490, 7.490	–	wi97
-1.100	208.600	8.980, 8.980	–	wi97
-1.050	230.730	10.290, 10.290	–	wi97
-1.019	122.400	70.794, 70.794	3.641	gr99
-1.000	223.840	11.050, 11.050	–	wi97
-0.950	244.700	109.631, 109.631	7.115	ci99
-0.950	231.560	12.260, 12.260	–	wi97
-0.900	258.500	14.120, 14.120	–	wi97
-0.850	246.720	15.030, 15.030	–	wi97
-0.800	328.630	18.920, 18.920	–	wi97
-0.763	197.100	139.523, 139.523	5.863	gr99
-0.750	260.160	18.350, 18.350	–	wi97
-0.700	308.060	21.770, 21.770	–	wi97
-0.695	236.400	167.241, 167.241	6.874	ci99
-0.650	321.100	24.230, 24.230	–	wi97
-0.600	371.500	28.410, 28.410	–	wi97
-0.550	375.950	31.160, 31.160	–	wi97
-0.500	305.910	30.640, 30.640	–	wi97
-0.450	296.630	32.890, 32.890	–	wi97
-0.400	340.950	38.440, 38.440	–	wi97
-0.350	351.930	42.580, 42.580	–	wi97
-0.300	364.210	47.220, 47.220	–	wi97
-0.250	328.270	48.880, 48.880	–	wi97
-0.200	632.160	73.940, 73.940	–	wi97
-0.150	482.540	70.430, 70.430	–	wi97
-0.100	273.390	57.790, 57.790	–	wi97
-0.050	490.070	84.350, 84.350	–	wi97
0.002	286.500	65.800, 80.300	–	wi97
0.050	339.200	81.900, 92.700	–	wi97
0.100	286.400	75.900, 97.000	–	wi97
0.149	512.800	111.800, 136.700	–	wi97
0.198	317.500	115.400, 107.500	–	wi97
0.246	291.800	133.000, 107.600	–	wi97
0.296	436.900	181.700, 139.400	–	wi97
0.350	318.600	29.375, 31.090	9.191	br72
0.351	283.600	114.100, 161.800	–	wi97
0.449	851.100	276.900, 287.400	–	wi97
0.452	254.925	23.457, 18.821	7.354	br72
0.498	568.200	213.800, 289.700	–	wi97
0.547	488.800	300.500, 246.900	–	wi97
0.548	212.512	32.643, 30.965	6.130	br72
0.596	311.300	295.300, 214.080	–	wi97
0.700	332.400	268.400, 299.410	–	wi97
0.704	206.865	31.751, 32.569	5.967	br72
0.798	557.200	646.800, 362.300	–	wi97
0.891	141.885	23.999, 22.338	4.093	br72
1.359	150.570	27.903, 25.461	4.343	br72

Reference codes. bo08: Bondi et al. (2008); br72: Bridle et al. (1972); ci99: Ciliegi et al. (1999); fo06: Fomalont et al. (2006); gr99: Gruppioni et al. (1999a); ho03: Hopkins et al. (2003); ib09: Ibar et al. (2009); ke08: Kellermann et al. (2008); mi85: Mitchell & Condon (1985); ow08: Owen & Morrison (2008); ri00: Richards (2000); se08A: Seymour et al. (2008); wi97: White et al. (1997).

Table 6: Euclidean normalized differential source counts at 4.8 GHz.

$\log(S[\text{Jy}])$	norm. cts.	+, -	sampl. err.	ref.
-4.750	0.810	0.562, 0.562	0.156	fo91
-4.587	1.080	0.341, 0.341	0.208	fo91
-4.347	1.890	0.453, 0.453	0.364	fo91
-3.928	1.161	0.455, 0.455	0.149	do87
-3.870	0.990	0.331, 0.331	0.191	fo91
-3.862	1.975	1.192, 0.977	0.381	fo84
-3.682	1.503	0.416, 0.416	0.193	do87
-3.483	2.136	0.967, 0.971	0.412	fo84
-3.319	3.807	1.116, 1.116	0.489	do87
-2.919	4.383	2.161, 2.134	0.845	fo84
-2.886	9.027	2.823, 2.823	1.158	do87
-2.857	6.750	3.160, 3.160	1.301	fo91
-2.721	6.210	1.726, 1.726	0.235	wr90
-2.538	8.370	2.987, 2.987	0.317	wr90
-2.352	9.630	3.618, 3.618	0.364	wr90
-2.137	14.850	6.235, 6.235	0.562	wr90
-1.961	29.700	11.037, 11.037	1.124	wr90
-1.921	20.340	6.982, 6.982	0.285	pa80
-1.796	28.080	8.675, 8.675	0.394	pa80
-1.785	34.151	2.586, 2.586	0.243	al86
-1.668	40.000	2.003, 2.003	0.104	gr96
-1.668	44.165	4.130, 4.130	0.314	al86
-1.648	46.350	7.216, 7.216	0.650	pa80
-1.536	40.520	4.083, 4.083	0.288	al86
-1.523	45.000	2.001, 2.001	0.046	gr96
-1.389	60.322	6.204, 6.204	0.429	al86
-1.387	54.270	8.814, 8.814	0.761	pa80
-1.372	55.000	3.001, 3.001	0.057	gr96
-1.222	64.000	3.000, 3.001	0.056	gr96
-1.206	63.551	7.664, 7.664	0.452	al86
-1.071	70.000	4.000, 4.000	0.061	gr96
-1.020	73.650	12.119, 12.119	0.524	al86
-0.903	78.000	4.001, 4.001	0.068	gr96
-0.894	75.960	15.542, 15.542	1.066	pa80
-0.757	81.000	5.000, 5.001	0.070	gr96
-0.602	84.000	5.001, 5.001	0.073	gr96
-0.398	90.000	5.001, 5.001	0.078	gr96
-0.222	84.000	6.000, 6.000	0.073	gr96
-0.071	107.000	9.001, 9.000	0.093	gr96
0.032	103.410	10.710, 8.100	-	ku81
0.097	96.000	9.000, 9.000	0.083	gr96
0.102	92.250	6.210, 7.263	-	ku81
0.173	84.987	5.733, 5.400	-	ku81
0.243	83.000	12.000, 12.000	0.072	gr96
0.278	79.587	9.675, 8.622	-	ku81
0.398	62.000	11.000, 11.000	0.054	gr96
0.412	87.813	9.117, 12.042	-	ku81
0.539	79.587	11.133, 16.317	-	ku81
0.764	62.244	11.088, 12.762	-	ku81

Reference codes. al86: Altschuler (1986); do87: Donnelly et al. (1987); fo84: Fomalont et al. (1984); fo91: Fomalont et al. (1991); gr96: Gregory et al. (1996); ku81: Kuehr et al. (1981); pa80: Pauliny-Toth et al. (1980); wr90: Wrobel & Krause (1990).



Table 7: Euclidean normalized differential source counts at 8.4 GHz.

$\log(S[\text{Jy}])$	norm. cts.	+, -	sampl. err.	ref.
-4.863	0.231	0.050, 0.050	–	fo02
-4.717	0.520	0.385, 0.385	0.106	wi93
-4.611	0.192	0.043, 0.043	–	fo02
-4.480	0.530	0.263, 0.263	0.108	wi93
-4.348	0.288	0.064, 0.064	–	fo02
-4.192	1.320	0.577, 0.577	0.270	wi93
-3.710	0.441	0.096, 0.096	–	fo02
-3.678	0.834	0.352, 0.352	0.089	he05
-3.481	1.190	0.547, 0.547	0.244	wi93
-2.745	2.787	1.125, 1.125	0.296	he05
-2.699	8.716	3.107, 3.107	0.393	he05
-2.474	20.374	11.961, 11.961	2.165	he05
-2.360	10.123	4.550, 4.550	0.457	he05
-2.160	10.809	5.426, 5.426	0.488	he05
-2.034	20.953	9.918, 9.918	2.227	he05
-1.901	18.039	8.108, 8.108	0.814	he05
-1.654	19.820	3.769, 4.360	–	wi93
-1.618	41.222	20.695, 20.695	1.860	he05
-1.457	40.823	8.986, 6.514	–	wi93
-1.348	92.022	65.202, 65.202	4.153	he05
-1.250	55.132	15.549, 13.185	–	wi93
-1.052	31.982	6.081, 5.758	–	wi93
-0.855	43.182	8.211, 9.492	–	wi93
-0.658	62.820	11.945, 11.321	–	wi93
-0.461	62.951	19.796, 17.368	–	wi93
-0.263	82.912	23.387, 19.831	–	wi93
-0.056	61.674	9.908, 2.992	–	wi93
0.122	63.343	6.625, 7.380	–	wi93
0.320	58.911	6.161, 5.566	–	wi93
0.527	43.823	8.309, 7.898	–	wi93
0.726	24.797	10.319, 9.330	–	wi93

Reference codes. fo02: Fomalont et al. (2002); he05: Henkel & Partridge (2005); wi93: Windhorst et al. (1993).

Table 10: Euclidean normalized differential source counts from WMAP maps (Massardi et al. 2009).

$\log(S[\text{Jy}])$	norm. cts.	+, -	$\nu$ (GHz)
0.111	48.993	3.720, 3.721	23
0.333	37.111	4.639, 4.639	23
0.556	32.480	6.371, 6.370	23
0.778	32.297	9.324, 9.323	23
1.000	11.597	7.538, 10.594	23
0.111	75.708	8.316, 8.317	33
0.333	38.878	4.646, 4.647	33
0.556	28.717	5.863, 5.862	33
0.778	28.357	8.550, 8.550	33
1.000	16.662	9.097, 12.730	33
1.222	23.931	15.556, 21.861	33

*continued on the next page*

Table 10: *continued*

$\log(S[\text{Jy}])$	norm. cts.	+, -	$\nu$ (GHz)
0.111	58.115	5.670, 5.670	41
0.333	34.633	4.364, 4.363	41
0.556	28.425	5.802, 5.802	41
0.778	20.413	7.068, 9.138	41
1.000	21.989	10.544, 14.474	41
1.222	23.688	15.397, 21.639	41
1.444	25.516	21.459, 25.516	41
0.333	26.078	3.805, 3.804	61
0.556	21.307	5.022, 5.022	61
0.778	10.201	4.892, 6.715	61
1.000	16.483	9.000, 12.593	61
1.222	23.674	15.388, 21.627	61
1.444	25.502	21.444, 25.502	61

## References

- Afshordi, N., Geshnizjani, G., & Khoury, J. 2008, ArXiv e-prints
- Afshordi, N. & Tolley, A. J. 2008, *PhRvD*, 78, 123507
- Aghanim, N., Balland, C., & Silk, J. 2000, *Astron & Astrophys.*, 357, 1
- Agol, E. 2000, *Astrophys. J. Lett.*, 538, L121
- Aitken, D. K., Greaves, J., Chrysostomou, A., et al. 2000, *Astrophys. J. Lett.*, 534, L173
- Aller, M. F., Aller, H. D., & Hughes, P. A. 2003, in *Astronomical Society of the Pacific Conference Series*, Vol. 300, *Radio Astronomy at the Fringe*, ed. J. A. Zensus, M. H. Cohen, & E. Ros, 159–+
- Altschuler, D. R. 1986, *Astron & Astrophys. Suppl.*, 65, 267
- Antón, S. & Browne, I. W. A. 2005, *Mon. Not. Roy. Astro. Soc.*, 356, 225
- Antonucci, R. & Miller, J. 1985, *ApJ*, 297, 621
- Arnaboldi, M., Neeser, M. J., Parker, L. C., et al. 2007, *The Messenger*, 127, 28
- Auriemma, C., Perola, G. C., Ekers, R. D., et al. 1977, *Astron & Astrophys.*, 57, 41
- Austermann, J. E., Dunlop, J. S., Perera, T. A., et al. 2009, ArXiv e-prints
- Avni, Y. & Bahcall, J. N. 1980, *Astrophys. J.*, 235, 694
- Baganoff, F. K., Maeda, Y., Morris, M., et al. 2003, *Astrophys. J.*, 591, 891
- Barger, A. J., Cowie, L. L., Mushotzky, R. F., et al. 2005, *Astron. J.*, 129, 578
- Barthel, P. 1989, *Scientific American*, 260, 20
- Becker, R. H., White, R. L., & Helfand, D. J. 1995, *Astrophys. J.*, 450, 559
- Begelman, M. C. 1996, *Baby Cygnus A's*, ed. C. L. Carilli & D. E. Harris, 209–+
- Begelman, M. C. 1999, in *The Most Distant Radio Galaxies*, ed. H. J. A. Röttgering, P. N. Best, & M. D. Lehnert, 173–+
- Begelman, M. C., Blandford, R. D., & Rees, M. J. 1984, *Reviews of Modern Physics*, 56, 255
- Benn, C. R., Grueff, G., Vigotti, M., & Wall, J. V. 1982, *Mon. Not. Roy. Astro. Soc.*, 200, 747
- Benn, C. R., Rowan-Robinson, M., McMahon, R. G., Broadhurst, T. J., & Lawrence, A. 1993, *Mon. Not. Roy. Astro. Soc.*, 263, 98
- Bennett, A. S. 1962, *Mon. Not. Roy. Astro. Soc.*, 68, 163
- Bennett, C. L., Halpern, M., Hinshaw, G., et al. 2003, *Astrophys. J. Suppl.*, 148, 1
- Benson, B. A., Church, S. E., Ade, P. A. R., et al. 2004, *Astrophys. J.*, 617, 829
- Best, P. N., Kaiser, C. R., Heckman, T. M., & Kauffmann, G. 2006, *Mon. Not. Roy. Astro. Soc.*, 368, L67
- Best, P. N., Kauffmann, G., Heckman, T. M., & Ivezić, Ž. 2005, *Mon. Not. Roy. Astro. Soc.*, 362, 9
- Bird, J., Martini, P., & Kaiser, C. 2008, *Astrophys. J.*, 676, 147
- Birkinshaw, M. 1999, *Phys. Rep.*, 310, 97
- Blain, A. W. & Longair, M. S. 1993, *Mon. Not. Roy. Astro. Soc.*, 264, 509
- Blain, A. W. & Longair, M. S. 1996, *Mon. Not. Roy. Astro. Soc.*, 279, 847
- Blake, C., Ferreira, P. G., & Borriell, J. 2004a, *Mon. Not. Roy. Astro. Soc.*, 351, 923

**Table 8** Euclidean normalized differential 15.2 GHz source counts from the 9C survey (Waldram et al. 2003, 2009).

$\log(S[Jy])$	norm. cts.	+, -
-2.229	8.680	1.810, 1.810
-2.152	6.597	1.440, 1.440
-2.051	8.054	1.758, 1.758
-1.979	12.287	1.993, 1.993
-1.923	10.112	1.542, 1.542
-1.852	11.647	1.842, 1.842
-1.757	10.083	1.594, 1.594
-1.650	16.120	2.581, 2.581
-1.561	12.667	1.416, 1.416
-1.477	14.355	4.053, 3.640
-1.314	17.579	2.558, 1.136
-1.105	26.424	3.156, 2.269
-0.826	26.424	4.550, 2.819
-0.465	40.551	9.108, 6.666
-0.140	48.529	21.134, 13.935

**Table 9** Euclidean normalized differential 20 GHz source counts for the AT20G Bright Source Sample (Massardi et al. 2008a).

$\log(S[Jy])$	norm. cts.	+, -
-0.108	37.150	2.493, 2.494
0.275	50.314	5.626, 5.625
0.658	35.456	9.155, 9.155
1.042	17.768	12.564, 12.564
1.808	125.487	125.487, 125.487

- Blake, C., Mauch, T., & Sadler, E. M. 2004b, *Mon. Not. Roy. Astro. Soc.*, 347, 787  
 Blake, C. & Wall, J. 2002a, *Mon. Not. Roy. Astro. Soc.*, 329, L37  
 Blake, C. & Wall, J. 2002b, *Mon. Not. Roy. Astro. Soc.*, 337, 993  
 Blandford, R. 1993, in *New York Academy Sciences Annals*, Vol. 688, Texas/PASCOS '92: Relativistic Astrophysics and Particle Cosmology, ed. C. W. Akerlof & M. A. Srednicki, 311–+
- Blandford, R. & Rees, M. 1974, *MNRAS*, 169, 395  
 Blandford, R. D. & Begelman, M. C. 1999, *Mon. Not. Roy. Astro. Soc.*, 303, L1  
 Blandford, R. D. & Begelman, M. C. 2004, *Mon. Not. Roy. Astro. Soc.*, 349, 68  
 Bloom, S. D. & Marscher, A. P. 1993, in *American Institute of Physics Conference Series*, Vol. 280, American Institute of Physics Conference Series, ed. M. Friedlander, N. Gehrels, & D. J. Macomb, 578–582  
 Blundell, K. M., Rawlings, S., & Willott, C. J. 1999, *Astron. J.*, 117, 677  
 Bolton, J. G., Stanley, G. J., & Slee, O. B. 1949, *Nature*, 164, 101  
 Bolton, R. C., Cotter, G., Pooley, G. G., et al. 2004, *Mon. Not. Roy. Astro. Soc.*, 354, 485  
 Bonamente, M., Joy, M., LaRoque, S. J., et al. 2008, *Astrophys. J.*, 675, 106  
 Bonamente, M., Joy, M. K., LaRoque, S. J., et al. 2006, *Astrophys. J.*, 647, 25  
 Bondi, H. 1952, *Mon. Not. Roy. Astro. Soc.*, 112, 195  
 Bondi, H. & Gold, T. 1948, *Mon. Not. Roy. Astro. Soc.*, 108, 252  
 Bondi, M., Ciliegi, P., Schinnerer, E., et al. 2008, *Astrophys. J.*, 681, 1129  
 Bondi, M., Ciliegi, P., Venturi, T., et al. 2007, *Astron & Astrophys.*, 463, 519  
 Bondi, M., Ciliegi, P., Zamorani, G., et al. 2003, *Astron & Astrophys.*, 403, 857  
 Boughn, S. & Crittenden, R. 2004, *Nature*, 427, 45  
 Boughn, S. P. & Crittenden, R. G. 2005, *New Astronomy Review*, 49, 75  
 Bower, R. G., Benson, A. J., Malbon, R., et al. 2006, *Mon. Not. Roy. Astro. Soc.*, 370, 645  
 Bressan, A., Silva, L., & Granato, G. L. 2002, *Astron & Astrophys.*, 392, 377  
 Bridle, A. H. 1967, *Mon. Not. Roy. Astro. Soc.*, 136, 219

- Bridle, A. H., Davis, M. M., Fomalont, E. B., & Lequeux, J. 1972, *Astron. J.*, 77, 405
- Brookes, M. H., Best, P. N., Peacock, J. A., Röttgering, H. J. A., & Dunlop, J. S. 2008, *Mon. Not. Roy. Astro. Soc.*, 385, 1297
- Brown, J. C., Haverkorn, M., Gaensler, B. M., et al. 2007, *Astrophys. J.*, 663, 258
- Burbidge, G. R. 1959, *Astrophys. J.*, 129, 849
- Burke, B. F. & Graham-Smith, F. 1997, *An introduction to radio astronomy* (Cambridge University Press)
- Caccianiga, A. & Marchã, M. J. M. 2004, *Mon. Not. Roy. Astro. Soc.*, 348, 937
- Cara, M. & Lister, M. L. 2008, *Astrophys. J.*, 674, 111
- Carilli, C. L. & Rawlings, S. 2004, *New Astronomy Review*, 48, 1
- Carlstrom, J. E., Ade, P. A. R., Aird, K. A., et al. 2009, *ArXiv e-prints*
- Carlstrom, J. E., Holder, G. P., & Reese, E. D. 2002, *ARA&A*, 40, 643
- Cavaliere, A., Giallongo, E., & Vagnetti, F. 1985, *Astrophys. J.*, 296, 402
- Chamballu, A., Bartlett, J. G., Melin, J. ., & Arnaud, M. 2008, *ArXiv e-prints*
- Chatterjee, S., di Matteo, T., Kosowsky, A., & Pelupessy, I. 2008, *Mon. Not. Roy. Astro. Soc.*, 390, 535
- Chatterjee, S. & Kosowsky, A. 2007, *Astrophys. J. Lett.*, 661, L113
- Choloniewski, J. 1987, *Mon. Not. Roy. Astro. Soc.*, 226, 273
- Ciaramella, A., Bongardo, C., Aller, H. D., et al. 2004, *Astron & Astrophys.*, 419, 485
- Ciardi, B. & Loeb, A. 2000, *Astrophys. J.*, 540, 687
- Cileigi, P., McMahon, R. G., Miley, G., et al. 1999, *Mon. Not. Roy. Astro. Soc.*, 302, 222
- Cileigi, P., Zamorani, G., Hasinger, G., et al. 2003, *Astron & Astrophys.*, 398, 901
- Cirasuolo, M., Magliocchetti, M., & Celotti, A. 2005, *Mon. Not. Roy. Astro. Soc.*, 357, 1267
- Cirasuolo, M., Magliocchetti, M., Gentile, G., et al. 2006, *Mon. Not. Roy. Astro. Soc.*, 371, 695
- Clark, T. A., Brown, L. W., & Alexander, J. K. 1970, *Nature*, 228, 847
- Cleary, K. A., Taylor, A. C., Waldrum, E., et al. 2005, *Mon. Not. Roy. Astro. Soc.*, 360, 340
- Clemens, M. S., Vega, O., Bressan, A., et al. 2008, *Astron & Astrophys.*, 477, 95
- Clewley, L. & Jarvis, M. J. 2004, *Mon. Not. Roy. Astro. Soc.*, 352, 909
- Cohen, A. S., Lane, W. M., Cotton, W. D., et al. 2007, *Astron. J.*, 134, 1245
- Cohen, M. H., Cannon, W., Purcell, G. H., et al. 1971, *Astrophys. J.*, 170, 207
- Colafrancesco, S., Mazzotta, P., Rephaeli, Y., & Vittorio, N. 1997, *Astrophys. J.*, 479, 1
- Condon, J. J. 1984a, *Astrophys. J.*, 287, 461
- Condon, J. J. 1984b, *Astrophys. J.*, 284, 44
- Condon, J. J. 1989, *Astrophys. J.*, 338, 13
- Condon, J. J. 1992, *ARA&A*, 30, 575
- Condon, J. J. 2007, in *Astronomical Society of the Pacific Conference Series*, Vol. 380, *Deepest Astronomical Surveys*, ed. J. Afonso, H. C. Ferguson, B. Mobasher, & R. Norris, 189–+
- Condon, J. J., Anderson, M. L., & Helou, G. 1991, *Astrophys. J.*, 376, 95
- Condon, J. J., Cotton, W. D., & Broderick, J. J. 2002, *Astron. J.*, 124, 675
- Condon, J. J., Cotton, W. D., Greisen, E. W., et al. 1998, *Astron. J.*, 115, 1693
- Condon, J. J. & Mitchell, K. J. 1984, *Astron. J.*, 89, 610
- Cook, M., Lapi, A., & Granato, G. L. 2009, *Mon. Not. Roy. Astro. Soc.*, 397, 534
- Coppin, K., Chapin, E. L., Mortier, A. M. J., et al. 2006, *Mon. Not. Roy. Astro. Soc.*, 372, 1621
- Cotton, W. D., Wittels, J. J., Shapiro, I. I., et al. 1980, *Astrophys. J. Lett.*, 238, L123
- Cowie, L. L., Songaila, A., Hu, E. M., & Cohen, J. G. 1996, *Astron. J.*, 112, 839
- Cress, C. M. & Kamionkowski, M. 1998, *Mon. Not. Roy. Astro. Soc.*, 297, 486
- Crittenden, R. G. & Turok, N. 1996, *Physical Review Letters*, 76, 575
- Croom, S., Boyle, B., Shanks, T., et al. 2004, in *Astronomical Society of the Pacific Conference Series*, Vol. 311, *AGN Physics with the Sloan Digital Sky Survey*, ed. G. T. Richards & P. B. Hall, 457–+
- Croton, D. J., Springel, V., White, S. D. M., et al. 2006, *Mon. Not. Roy. Astro. Soc.*, 365, 11
- Cruz, M. J., Jarvis, M. J., Rawlings, S., & Blundell, K. M. 2007, *Mon. Not. Roy. Astro. Soc.*, 375, 1349
- Dallacasa, D., Stanghellini, C., Centonza, M., & Fanti, R. 2000, *Astron & Astrophys.*, 363, 887
- Dallacasa, D., Stanghellini, C., Centonza, M., & Furnari, G. 2002, *New Astronomy Review*, 46, 299
- Danese, L. & de Zotti, G. 1984, *Astron & Astrophys.*, 131, L1
- Danese, L., Franceschini, A., & de Zotti, G. 1985, *Astron & Astrophys.*, 143, 277
- Danese, L., Franceschini, A., Toffolatti, L., & de Zotti, G. 1987, *Astrophys. J. Lett.*, 318, L15

- de Bruyn, G., Miley, G., Rengelink, R., et al. 2000, *VizieR Online Data Catalog*, 8062, 0
- de Luca, A., Desert, F. X., & Puget, J. L. 1995, *Astron & Astrophys.*, 300, 335
- De Lucia, G. & Blaizot, J. 2007, *Mon. Not. Roy. Astro. Soc.*, 375, 2
- De Zotti, G., Burigana, C., Cavaliere, A., et al. 2004, in *American Institute of Physics Conference Series*, Vol. 703, *Plasmas in the Laboratory and in the Universe: New Insights and New Challenges*, ed. G. Bertin, D. Farina, & R. Pozzoli, 375–384
- De Zotti, G., Granato, G. L., Silva, L., Maino, D., & Danese, L. 2000, *Astron & Astrophys.*, 354, 467
- De Zotti, G., Ricci, R., Mesa, D., et al. 2005, *Astron & Astrophys.*, 431, 893
- De Zotti, G., Toffolatti, L., Argüeso, F., et al. 1999, in *American Institute of Physics Conference Series*, Vol. 476, *3K cosmology*, ed. L. Maiani, F. Melchiorri, & N. Vittorio, 204–+
- Dekel, A. & Birnboim, Y. 2006, *Mon. Not. Roy. Astro. Soc.*, 368, 2
- Di Matteo, T., Carilli, C. L., & Fabian, A. C. 2001, *Astrophys. J.*, 547, 731
- di Matteo, T., Fabian, A. C., Rees, M. J., Carilli, C. L., & Ivison, R. J. 1999, *Mon. Not. Roy. Astro. Soc.*, 305, 492
- Dicke, R. H., Peebles, P. J. E., Roll, P. G., & Wilkinson, D. T. 1965, *Astrophys. J.*, 142, 414
- Dobbs, M., Halverson, N. W., Ade, P. A. R., et al. 2006, *New Astronomy Review*, 50, 960
- Donnelly, R. H., Partridge, R. B., & Windhorst, R. A. 1987, *Astrophys. J.*, 321, 94
- Doroshkevich, A. G., Longair, M. S., & Zeldovich, Y. B. 1970, *Mon. Not. Roy. Astro. Soc.*, 147, 139
- Drinkwater, M. J., Webster, R. L., Francis, P. J., et al. 1997, *Mon. Not. Roy. Astro. Soc.*, 284, 85
- Dunlop, J. S., McLure, R. J., Kukuła, M. J., et al. 2003, *Mon. Not. Roy. Astro. Soc.*, 340, 1095
- Dunlop, J. S. & Peacock, J. A. 1990, *Mon. Not. Roy. Astro. Soc.*, 247, 19
- Eales, S. 1993, *Astrophys. J.*, 404, 51
- Edge, A. C., Pooley, G., Jones, M., Grainge, K., & Saunders, R. 1998, in *Astronomical Society of the Pacific Conference Series*, Vol. 144, *IAU Colloq. 164: Radio Emission from Galactic and Extragalactic Compact Sources*, ed. J. A. Zensus, G. B. Taylor, & J. M. Wrobel, 187–+
- Edge, D. O., Shakeshaft, J. R., McAdam, W. B., Baldwin, J. E., & Archer, S. 1959, *Mon. Not. Roy. Astro. Soc.*, 68, 37
- Fabian, A. C. & Rees, M. J. 1995, *Mon. Not. Roy. Astro. Soc.*, 277, L55
- Fan, X., Hennawi, J. F., Richards, G. T., et al. 2004, *Astron. J.*, 128, 515
- Fanaroff, B. L. & Riley, J. M. 1974, *Mon. Not. Roy. Astro. Soc.*, 167, 31P
- Fanti, C., Fanti, R., Dallacasa, D., et al. 1995, *Astron & Astrophys.*, 302, 317
- Felten, J. E. 1976, *Astrophys. J.*, 207, 700
- Feretti, L. 2008, *Memorie della Societa Astronomica Italiana*, 79, 176
- Ferrarese, L. & Ford, H. 2005, *Space Science Reviews*, 116, 523
- Fixsen, D. J., Kogut, A., Levin, S., et al. 2009, *ArXiv e-prints*
- Fomalont, E. B., Kellermann, K. I., Cowie, L. L., et al. 2006, *Astrophys. J. Suppl.*, 167, 103
- Fomalont, E. B., Kellermann, K. I., Partridge, R. B., Windhorst, R. A., & Richards, E. A. 2002, *Astron. J.*, 123, 2402
- Fomalont, E. B., Kellermann, K. I., Wall, J. V., & Weistrop, D. 1984, *Science*, 225, 23
- Fomalont, E. B., Windhorst, R. A., Kristian, J. A., & Kellerman, K. I. 1991, *Astron. J.*, 102, 1258
- Fossati, G., Maraschi, L., Celotti, A., Comastri, A., & Ghisellini, G. 1998, *Mon. Not. Roy. Astro. Soc.*, 299, 433
- Friedman, R. B. & QUaD Collaboration. 2009, in *American Astronomical Society Meeting Abstracts*, Vol. 213, *American Astronomical Society Meeting Abstracts*, 340.06–+
- Garn, T., Green, D. A., Riley, J. M., & Alexander, P. 2008, *Mon. Not. Roy. Astro. Soc.*, 387, 1037
- Garrett, M. A. 2002, *Astron & Astrophys.*, 384, L19
- Gavazzi, G., Cocito, A., & Vettolani, G. 1986, *Astrophys. J. Lett.*, 305, L15
- Gear, W. K., Stevens, J. A., Hughes, D. H., et al. 1994, *Mon. Not. Roy. Astro. Soc.*, 267, 167
- Geisbüsch, J., Kneissl, R., & Hobson, M. 2005, *Mon. Not. Roy. Astro. Soc.*, 360, 41
- Gendre, M. A. & Wall, J. V. 2008, *Mon. Not. Roy. Astro. Soc.*, 390, 819
- Gervasi, M., Tartari, A., Zannoni, M., Boella, G., & Sironi, G. 2008, *Astrophys. J.*, 682, 223
- Ghisellini, G., Celotti, A., Fossati, G., Maraschi, L., & Comastri, A. 1998, *Mon. Not. Roy. Astro. Soc.*, 301, 451
- Giannantonio, T., Scranton, R., Crittenden, R. G., et al. 2008, *PhRvD*, 77, 123520
- Ginzburg, V. L. 1951, *Dokl. Akad. Nauk. SSSR*, 76, 377

- Giommi, P., Massaro, E., Chiappetti, L., et al. 1999, *Astron & Astrophys.*, 351, 59
- Gower, J. F. R. 1966, *Mon. Not. Roy. Astro. Soc.*, 133, 151
- Granato, G. L., De Zotti, G., Silva, L., Bressan, A., & Danese, L. 2004, *Astrophys. J.*, 600, 580
- Gregory, P. C., Scott, W. K., Douglas, K., & Condon, J. J. 1996, *Astrophys. J. Suppl.*, 103, 427
- Griffith, M. R. & Wright, A. E. 1993, *Astron. J.*, 105, 1666
- Grueff, G. 1988, *Astron & Astrophys.*, 193, 40
- Grueff, G. & Vigotti, M. 1977, *Astron & Astrophys.*, 54, 475
- Gruppioni, C., Ciliegi, P., Rowan-Robinson, M., et al. 1999a, *Mon. Not. Roy. Astro. Soc.*, 305, 297
- Gruppioni, C., Mignoli, M., & Zamorani, G. 1999b, *Mon. Not. Roy. Astro. Soc.*, 304, 199
- Gruppioni, C., Pozzi, F., Zamorani, G., et al. 2003, *Mon. Not. Roy. Astro. Soc.*, 341, L1
- Guo, Q. & White, S. D. M. 2008, *Mon. Not. Roy. Astro. Soc.*, 384, 2
- Hales, S. E. G., Baldwin, J. E., & Warner, P. J. 1988, *Mon. Not. Roy. Astro. Soc.*, 234, 919
- Hales, S. E. G., Baldwin, J. E., & Warner, P. J. 1993, *Mon. Not. Roy. Astro. Soc.*, 263, 25
- Hales, S. E. G., Riley, J. M., Waldram, E. M., Warner, P. J., & Baldwin, J. E. 2007, *Mon. Not. Roy. Astro. Soc.*, 382, 1639
- Hales, S. E. G., Waldram, E. M., Rees, N., & Warner, P. J. 1995, *Mon. Not. Roy. Astro. Soc.*, 274, 447
- Halverson, N. W., Lanting, T., Ade, P. A. R., et al. 2009, *Astrophys. J.*, 701, 42
- Hasinger, G., Miyaji, T., & Schmidt, M. 2005, *Astron & Astrophys.*, 441, 417
- Haslam, C. G. T., Salter, C. J., Stoffel, H., & Wilson, W. E. 1982, *Astron & Astrophys. Suppl.*, 47, 1
- Hazard, C., Mackey, M. B., & Shimmins, A. J. 1963, *Nature*, 197, 1037
- Helou, G., Soifer, B. T., & Rowan-Robinson, M. 1985, *Astrophys. J. Lett.*, 298, L7
- Henkel, B. & Partridge, R. B. 2005, *Astrophys. J.*, 635, 950
- Hinshaw, G. & Naeye, R. 2008, *Sky and Telescope*, 115, 050000
- Hinshaw, G., Nolta, M. R., Bennett, C. L., et al. 2007, *Astrophys. J. Suppl.*, 170, 288
- Ho, S., Hirata, C., Padmanabhan, N., Seljak, U., & Bahcall, N. 2008, *PhRvD*, 78, 043519
- Hodapp, K. W., Siegmund, W. A., Kaiser, N., et al. 2004, in Presented at the Society of Photo-Optical Instrumentation Engineers (SPIE) Conference, Vol. 5489, Society of Photo-Optical Instrumentation Engineers (SPIE) Conference Series, ed. J. M. Oschmann, Jr., 667–678
- Holdaway, M. A., Rupen, M. P., Knapp, G. R., West, S., & Burton, W. B. 1994, in Bulletin of the American Astronomical Society, Vol. 26, Bulletin of the American Astronomical Society, 1328–+
- Hook, I. M., Shaver, P. A., & McMahon, R. G. 1998, in Astronomical Society of the Pacific Conference Series, Vol. 146, The Young Universe: Galaxy Formation and Evolution at Intermediate and High Redshift, ed. S. D’Odorico, A. Fontana, & E. Giallongo, 17–+
- Hopkins, A., Windhorst, R., Cram, L., & Ekers, R. 2000, *Experimental Astronomy*, 10, 419
- Hopkins, A. M., Afonso, J., Chan, B., et al. 2003, *Astron. J.*, 125, 465
- Hopkins, A. M., Mobasher, B., Cram, L., & Rowan-Robinson, M. 1998, *Mon. Not. Roy. Astro. Soc.*, 296, 839
- Hovatta, T., Lehto, H. J., & Tornikoski, M. 2008, *Astron & Astrophys.*, 488, 897
- Hoyle, F. 1948, *Mon. Not. Roy. Astro. Soc.*, 108, 372
- Hoyle, F. & Fowler, W. A. 1963, *Mon. Not. Roy. Astro. Soc.*, 125, 169
- Huynh, M. T., Jackson, C. A., Norris, R. P., & Fernandez-Soto, A. 2008, *Astron. J.*, 135, 2470
- Huynh, M. T., Jackson, C. A., Norris, R. P., & Prandoni, I. 2005, *Astron. J.*, 130, 1373
- Ibar, E., Ivison, R. J., Biggs, A. D., et al. 2009, *Mon. Not. Roy. Astro. Soc.*, 397, 281
- Impey, C. D. & Neugebauer, G. 1988, *Astron. J.*, 95, 307
- Ivison, R. J., Chapman, S. C., Faber, S. M., et al. 2007, *Astrophys. J. Lett.*, 660, L77
- Jackson, C. A. & Wall, J. V. 1999, *Mon. Not. Roy. Astro. Soc.*, 304, 160
- Jackson, C. A. & Wall, J. V. 2001, in Astronomical Society of the Pacific Conference Series, Vol. 227, Blazar Demographics and Physics, ed. P. Padovani & C. M. Urry, 242–+
- Jarvis, M. J. & Rawlings, S. 2000, *Mon. Not. Roy. Astro. Soc.*, 319, 121
- Jarvis, M. J., Rawlings, S., Willott, C. J., et al. 2001, *Mon. Not. Roy. Astro. Soc.*, 327, 907
- Jarvis, M. J., Teimourian, H., Simpson, C., et al. 2009, *ArXiv e-prints*
- Jennison, R. C. & Das Gupta, M. K. 1953, *Nature*, 172, 996
- Johnston, S., Taylor, R., Bailes, M., et al. 2008, *Experimental Astronomy*, 22, 151
- Jones, M. E., Edge, A. C., Grainge, K., et al. 2005, *Mon. Not. Roy. Astro. Soc.*, 357, 518

- Kapahi, V. K. 1981, *Astron & Astrophys. Suppl.*, 43, 381
- Katgert, J. K. 1979, *Astron & Astrophys.*, 73, 107
- Kellermann, K. I. 1964, *Astrophys. J.*, 140, 969
- Kellermann, K. I. 1966, *Astrophys. J.*, 146, 621
- Kellermann, K. I., Fomalont, E. B., Mainieri, V., et al. 2008, *Astrophys. J. Suppl.*, 179, 71
- Kellermann, K. I. & Pauliny-Toth, I. I. K. 1969, *Astrophys. J. Lett.*, 155, L71+
- Kellermann, K. I., Pauliny-Toth, I. I. K., & Williams, P. J. S. 1969, *Astrophys. J.*, 157, 1
- Kellermann, K. I. & Wall, J. V. 1987, in *IAU Symposium*, Vol. 124, *Observational Cosmology*, ed. A. Hewitt, G. Burbidge, & L. Z. Fang, 545–562
- King, A. J. & Rowan-Robinson, M. 2004, *Mon. Not. Roy. Astro. Soc.*, 349, 1353
- Klamer, I. J., Ekers, R. D., Bryant, J. J., et al. 2006, *Mon. Not. Roy. Astro. Soc.*, 371, 852
- Kosowsky, A. 2006, *New Astronomy Review*, 50, 969
- Kovac, J. M., Leitch, E. M., Pryke, C., et al. 2002, *Nature*, 420, 772
- Krolik, J. H. & Chen, W. 1991, *Astron. J.*, 102, 1659
- Kuehr, H., Witzel, A., Pauliny-Toth, I. I. K., & Nauber, U. 1981, *Astron & Astrophys. Suppl.*, 45, 367
- Lacy, M., Hill, G. J., Kaiser, M. E., & Rawlings, S. 1993, *Mon. Not. Roy. Astro. Soc.*, 263, 707
- Lagache, G., Puget, J.-L., & Dole, H. 2005, *ARA&A*, 43, 727
- Laing, R. A. & Peacock, J. A. 1980, *Mon. Not. Roy. Astro. Soc.*, 190, 903
- Laing, R. A., Riley, J. M., & Longair, M. S. 1983, *Mon. Not. Roy. Astro. Soc.*, 204, 151
- Lancaster, K., Birkinshaw, M., Gawroński, M. P., et al. 2007, *Mon. Not. Roy. Astro. Soc.*, 378, 673
- Landt, H., Perlman, E. S., & Padovani, P. 2006, *Astrophys. J.*, 637, 183
- Lapi, A., Cavaliere, A., & De Zotti, G. 2003, *Astrophys. J. Lett.*, 597, L93
- Lapi, A., Shankar, F., Mao, J., et al. 2006, *Astrophys. J.*, 650, 42
- Leahy, J. P., Muxlow, T. W. B., & Stephens, P. W. 1989, *Mon. Not. Roy. Astro. Soc.*, 239, 401
- Ledlow, M. J. & Owen, F. N. 1996, *Astron. J.*, 112, 9
- Limber, D. N. 1953, *Astrophys. J.*, 117, 134
- Lister, M. L. 2008, in *Astronomical Society of the Pacific Conference Series*, Vol. 386, *Extragalactic Jets: Theory and Observation from Radio to Gamma Ray*, ed. T. A. Rector & D. S. De Young, 240–+
- Liu, Y. & Zhang, S. N. 2007, *Astrophys. J.*, 667, 724
- Lo, K. Y., Chiueh, T. H., Martin, R. N., et al. 2001, in *American Institute of Physics Conference Series*, Vol. 586, *20th Texas Symposium on relativistic astrophysics*, ed. J. C. Wheeler & H. Martel, 172–+
- Longair, M. S. 1966, *Mon. Not. Roy. Astro. Soc.*, 133, 421
- Longair, M. S. & Scheuer, P. A. G. 1970, *Mon. Not. Roy. Astro. Soc.*, 151, 45
- López-Cañiego, M., González-Nuevo, J., Herranz, D., et al. 2007, *Astrophys. J. Suppl.*, 170, 108
- Lovell, J. E. J., Jauncey, D. L., Senkbeil, C., et al. 2007, in *Astronomical Society of the Pacific Conference Series*, Vol. 365, *SINS - Small Ionized and Neutral Structures in the Diffuse Interstellar Medium*, ed. M. Haverkorn & W. M. Goss, 279–+
- Lynden-Bell, D. 1969, *Nature*, 223, 690
- Lynden-Bell, D. 1971, *Mon. Not. Roy. Astro. Soc.*, 155, 95
- Machalski, J. & Godłowski, W. 2000, *Astron & Astrophys.*, 360, 463
- Magliocchetti, M., Maddox, S. J., Hawkins, E., et al. 2004, *Mon. Not. Roy. Astro. Soc.*, 350, 1485
- Magliocchetti, M., Maddox, S. J., Jackson, C. A., et al. 2002, *Mon. Not. Roy. Astro. Soc.*, 333, 100
- Magliocchetti, M., Maddox, S. J., Lahav, O., & Wall, J. V. 1998, *Mon. Not. Roy. Astro. Soc.*, 300, 257
- Magliocchetti, M., Maddox, S. J., Lahav, O., & Wall, J. V. 1999, *Mon. Not. Roy. Astro. Soc.*, 306, 943
- Majumdar, S., Nath, B. B., & Chiba, M. 2001, *Mon. Not. Roy. Astro. Soc.*, 324, 537
- Maraschi, L., Ghisellini, G., & Celotti, A. 1992, *Astrophys. J. Lett.*, 397, L5
- Mason, B. S., Pearson, T. J., Readhead, A. C. S., et al. 2003, *Astrophys. J.*, 591, 540
- Mason, B. S., Weintraub, L. C., Sievers, J. L., et al. 2009, *ArXiv e-prints*
- Massardi, M., Ekers, R. D., Murphy, T., et al. 2008a, *Mon. Not. Roy. Astro. Soc.*, 384, 775

- Massardi, M., Lapi, A., de Zotti, G., Ekers, R. D., & Danese, L. 2008b, *Mon. Not. Roy. Astro. Soc.*, 384, 701
- Massardi, M., López-Cañiego, M., González-Nuevo, J., et al. 2009, *Mon. Not. Roy. Astro. Soc.*, 392, 733
- Masson, C. R. & Wall, J. V. 1977, *Mon. Not. Roy. Astro. Soc.*, 180, 193
- Matarrese, S., Coles, P., Lucchin, F., & Moscardini, L. 1997, *Mon. Not. Roy. Astro. Soc.*, 286, 115
- Mather, J. C., Fixsen, D. J., Shafer, R. A., Mosier, C., & Wilkinson, D. T. 1999, *Astrophys. J.*, 512, 511
- Mauch, T., Murphy, T., Buttery, H. J., et al. 2003, *Mon. Not. Roy. Astro. Soc.*, 342, 1117
- Mauch, T. & Sadler, E. M. 2007, *Mon. Not. Roy. Astro. Soc.*, 375, 931
- McEwen, J. D., Vielva, P., Hobson, M. P., Martínez-González, E., & Lasenby, A. N. 2007, *Mon. Not. Roy. Astro. Soc.*, 376, 1211
- McEwen, J. D., Wiaux, Y., Hobson, M. P., Vanderghenst, P., & Lasenby, A. N. 2008, *Mon. Not. Roy. Astro. Soc.*, 384, 1289
- McGilchrist, M. M., Baldwin, J. E., Riley, J. M., et al. 1990, *Mon. Not. Roy. Astro. Soc.*, 246, 110
- McGreer, I. D., Becker, R. H., Helfand, D. J., & White, R. L. 2006, *Astrophys. J.*, 652, 157
- McLure, R. J., Willott, C. J., Jarvis, M. J., et al. 2004, *Mon. Not. Roy. Astro. Soc.*, 351, 347
- Mesa, D., Baccigalupi, C., De Zotti, G., et al. 2002, *Astron & Astrophys.*, 396, 463
- Mészáros, P. 1999, *Astron & Astrophys. Suppl.*, 138, 533
- Miley, G. & De Breuck, C. 2008, *Astron. & Astrophys. Rev.*, 15, 67
- Mills, B. Y., Slee, O. B., & Hill, E. R. 1958, *Australian Journal of Physics*, 11, 360
- Minkowski, R. 1960, *PASP*, 72, 354
- Mitchell, K. J. & Condon, J. J. 1985, *Astron. J.*, 90, 1957
- Moffet, A. T., Gubbay, J., Robertson, D. S., & Legg, A. J. 1972, in *IAU Symposium*, Vol. 44, *External Galaxies and Quasi-Stellar Objects*, ed. D. S. Evans, D. Wills, & B. J. Wills, 228–+
- Moscardini, L., Coles, P., Lucchin, F., & Matarrese, S. 1998, *Mon. Not. Roy. Astro. Soc.*, 299, 95
- Moss, D., Seymour, N., McHardy, I. M., et al. 2007, *Mon. Not. Roy. Astro. Soc.*, 378, 995
- Muchovej, S., Mroczkowski, T., Carlstrom, J. E., et al. 2007, *Astrophys. J.*, 663, 708
- Murphy, T., Mauch, T., Green, A., et al. 2007, *Mon. Not. Roy. Astro. Soc.*, 382, 382
- Muxlow, T. W. B., Richards, A. M. S., Garrington, S. T., et al. 2005, *Mon. Not. Roy. Astro. Soc.*, 358, 1159
- Natarajan, P. & Sigurdsson, S. 1999, *Mon. Not. Roy. Astro. Soc.*, 302, 288
- Negrello, M., Magliocchetti, M., & De Zotti, G. 2006, *Mon. Not. Roy. Astro. Soc.*, 368, 935
- Negrello, M., Perrotta, F., González-Nuevo, J., et al. 2007, *Mon. Not. Roy. Astro. Soc.*, 377, 1557
- Nieppola, E., Tornikoski, M., & Valtaoja, E. 2006, *Astron & Astrophys.*, 445, 441
- Nieppola, E., Valtaoja, E., Tornikoski, M., Hovatta, T., & Kotiranta, M. 2008, *Astron & Astrophys.*, 488, 867
- O’Dea, C. P. 1998, *PASP*, 110, 493
- Oh, S. P. 1999, *Astrophys. J.*, 527, 16
- Oh, S. P., Cooray, A., & Kamionkowski, M. 2003, *Mon. Not. Roy. Astro. Soc.*, 342, L20
- Oort, M. J. A., Steemers, W. J. G., & Windhorst, R. A. 1988, *Astron & Astrophys. Suppl.*, 73, 103
- Orienti, M. & Dallacasa, D. 2008, *Astron & Astrophys.*, 479, 409
- Orienti, M., Dallacasa, D., & Stanghellini, C. 2007, *Astron & Astrophys.*, 475, 813
- Orienti, M., Dallacasa, D., Tinti, S., & Stanghellini, C. 2006, *Astron & Astrophys.*, 450, 959
- Orr, M. J. L. & Browne, I. W. A. 1982, *Mon. Not. Roy. Astro. Soc.*, 200, 1067
- Overzier, R. A., Röttgering, H. J. A., Rengelink, R. B., & Wilman, R. J. 2003, *Astron & Astrophys.*, 405, 53
- Owen, F. N. & Morrison, G. E. 2008, *Astron. J.*, 136, 1889
- Owen, F. N., Morrison, G. E., Klimek, M. D., & Greisen, E. W. 2009, *Astron. J.*, 137, 4846
- Pace, F., Maturi, M., Bartelmann, M., et al. 2008, *Astron & Astrophys.*, 483, 389
- Padovani, P. 2007, *APSS*, 309, 63
- Padovani, P., Giommi, P., Landt, H., & Perlmutter, E. S. 2007a, *Astrophys. J.*, 662, 182
- Padovani, P., Mainieri, V., Tozzi, P., et al. 2007b, in *Astronomical Society of the Pacific Conference Series*, Vol. 380, *Deepest Astronomical Surveys*, ed. J. Afonso, H. C. Ferguson, B. Mobasher, & R. Norris, 205–+



- Padovani, P., Mainieri, V., Tozzi, P., et al. 2009, *Astrophys. J.*, 694, 235
- Padovani, P., Perlman, E. S., Landt, H., Giommi, P., & Perri, M. 2003, *Astrophys. J.*, 588, 128
- Padovani, P. & Urry, C. M. 1992, *Astrophys. J.*, 387, 449
- Pauliny-Toth, I. I. K., Steppe, H., & Witzel, A. 1980, *Astron & Astrophys.*, 85, 329
- Pauliny-Toth, I. I. K., Wade, C. M., & Heeschen, D. S. 1966, *Astrophys. J. Suppl.*, 13, 65
- Peacock, J. A. 1985, *Mon. Not. Roy. Astro. Soc.*, 217, 601
- Peacock, J. A. & Gull, S. F. 1981, *Mon. Not. Roy. Astro. Soc.*, 196, 611
- Peacock, J. A. & Nicholson, D. 1991, *Mon. Not. Roy. Astro. Soc.*, 253, 307
- Peacock, J. A. & Wall, J. V. 1982, *Mon. Not. Roy. Astro. Soc.*, 198, 843
- Peebles, P. J. E. 1980, *The large-scale structure of the universe* (Research supported by the National Science Foundation. Princeton, N.J., Princeton University Press, 1980. 435 p.)
- Peebles, P. J. E., Page, L. A., & Partridge, R. B. 2009, *Finding the Big Bang* (Cambridge University Press)
- Penzias, A. A. & Wilson, R. W. 1965, *Astrophys. J.*, 142, 419+
- Pérez-González, P. G., Rieke, G. H., Villar, V., et al. 2008, *Astrophys. J.*, 675, 234
- Pierpaoli, E. & Perna, R. 2004, *Mon. Not. Roy. Astro. Soc.*, 354, 1005
- Pietrobon, D., Balbi, A., & Marinucci, D. 2006, *PhRvD*, 74, 043524
- Platania, P., Burigana, C., De Zotti, G., Lazzaro, E., & Bersanelli, M. 2002, *Mon. Not. Roy. Astro. Soc.*, 337, 242
- Polatidis, A., Wilkinson, P. N., Xu, W., et al. 1999, *New Astronomy Review*, 43, 657
- Porciani, C., Magliocchetti, M., & Norberg, P. 2004, *Mon. Not. Roy. Astro. Soc.*, 355, 1010
- Prandoni, I., Parma, P., Wieringa, M. H., et al. 2006, *Astron & Astrophys.*, 457, 517
- Press, W. H. & Schechter, P. 1974, *Astrophys. J.*, 187, 425
- Quataert, E. & Narayan, R. 1999, *Astrophys. J.*, 520, 298
- Raccanelli, A., Bonaldi, A., Negrello, M., et al. 2008, *Mon. Not. Roy. Astro. Soc.*, 386, 2161
- Readhead, A. C. S., Taylor, G. B., Pearson, T. J., & Wilkinson, P. N. 1996, *Astrophys. J.*, 460, 634
- Rees, M. J. 1967, *Mon. Not. Roy. Astro. Soc.*, 135, 345
- Rees, M. J., Begelman, M. C., Blandford, R. D., & Phinney, E. S. 1982, *Nature*, 295, 17
- Rees, M. J. & Ostriker, J. P. 1977, *Mon. Not. Roy. Astro. Soc.*, 179, 541
- Rees, N. 1990, *Mon. Not. Roy. Astro. Soc.*, 244, 233
- Rengelink, R. 1999, in *The Most Distant Radio Galaxies*, ed. H. J. A. Röttgering, P. N. Best, & M. D. Lehnert, 399+
- Rengelink, R. B., Tang, Y., de Bruyn, A. G., et al. 1997, *Astron & Astrophys. Suppl.*, 124, 259
- Ricci, R., Sadler, E. M., Ekers, R. D., et al. 2004, *Mon. Not. Roy. Astro. Soc.*, 354, 305
- Richards, E. A. 2000, *Astrophys. J.*, 533, 611
- Rigby, E. E., Best, P. N., & Snellen, I. A. G. 2008, *Mon. Not. Roy. Astro. Soc.*, 385, 310
- Robertson, J. G. 1977, *Australian Journal of Physics*, 30, 241
- Robertson, J. G. 1978, *Mon. Not. Roy. Astro. Soc.*, 182, 617
- Robertson, J. G. 1980, *Mon. Not. Roy. Astro. Soc.*, 190, 143
- Rosa-González, D., Terlevich, R., Terlevich, E., Friaça, A., & Gaztañaga, E. 2004, *Mon. Not. Roy. Astro. Soc.*, 348, 669
- Röttgering, H. J. A., Braun, R., Barthel, P. D., et al. 2006, *ArXiv Astrophysics e-prints*
- Rowan-Robinson, M. 1968, *Mon. Not. Roy. Astro. Soc.*, 138, 445
- Rowan-Robinson, M. 1970, *Mon. Not. Roy. Astro. Soc.*, 149, 365
- Rowan-Robinson, M., Benn, C. R., Lawrence, A., McMahon, R. G., & Broadhurst, T. J. 1993, *Mon. Not. Roy. Astro. Soc.*, 263, 123
- Ryle, M. & Clarke, R. W. 1961, *Mon. Not. Roy. Astro. Soc.*, 122, 349
- Ryle, M. & Scheuer, P. A. G. 1955, *Royal Society of London Proceedings Series A*, 230, 448
- Ryle, M., Smith, F. G., & Elsmore, B. 1950, *Mon. Not. Roy. Astro. Soc.*, 110, 508
- Sadler, E. M., Cannon, R. D., Mauch, T., et al. 2007, *Mon. Not. Roy. Astro. Soc.*, 381, 211
- Sadler, E. M., Jackson, C. A., Cannon, R. D., et al. 2002, *Mon. Not. Roy. Astro. Soc.*, 329, 227
- Sadler, E. M., Ricci, R., Ekers, R. D., et al. 2006, *Mon. Not. Roy. Astro. Soc.*, 371, 898
- Sadler, E. M., Ricci, R., Ekers, R. D., et al. 2008, *Mon. Not. Roy. Astro. Soc.*, 385, 1656
- Saunders, W., Rowan-Robinson, M., Lawrence, A., et al. 1990, *Mon. Not. Roy. Astro. Soc.*, 242, 318
- Scheuer, P. A. G. 1957, in *Proceedings of the Cambridge Philosophical Society*, Vol. 53, *Proceedings of the Cambridge Philosophical Society*, 764–773

- Scheuer, P. A. G. 1974, *Mon. Not. Roy. Astro. Soc.*, 166, 513
- Scheuer, P. A. G. 1987, in *Superluminal Radio Sources*, ed. J. A. Zensus & T. J. Pearson, 104–113
- Scheuer, P. A. G. & Readhead, A. C. S. 1979, *Nature*, 277, 182
- Schmidt, M. 1963, *Nature*, 197, 1040
- Schmidt, M. 1965, *Astrophys. J.*, 141, 1295+
- Schmidt, M. 1968, *Astrophys. J.*, 151, 393
- Schmidt, M. 1976, *Astrophys. J. Lett.*, 209, L55+
- Schmidt, M., Schneider, D. P., & Gunn, J. E. 1995, *Astron. J.*, 110, 68
- Scott, S. E., Dunlop, J. S., & Serjeant, S. 2006, *Mon. Not. Roy. Astro. Soc.*, 370, 1057
- Seaton, D. B. & Partridge, R. B. 2001, *PASP*, 113, 6
- Seldner, M. & Peebles, P. J. E. 1981, *Mon. Not. Roy. Astro. Soc.*, 194, 251
- Seymour, N., Dwelly, T., Moss, D., et al. 2008, *Mon. Not. Roy. Astro. Soc.*, 386, 1695
- Seymour, N., McHardy, I. M., & Gunn, K. F. 2004, *Mon. Not. Roy. Astro. Soc.*, 352, 131
- Shakeshaft, J. R., Ryle, M., Baldwin, J. E., Elsmore, B., & Thomson, J. H. 1955, *Mon. Not. Roy. Astro. Soc.*, 67, 106
- Shaver, P. A., Hook, I. M., Jackson, C. A., Wall, J. V., & Kellermann, K. I. 1999, in *Astronomical Society of the Pacific Conference Series*, Vol. 156, *Highly Redshifted Radio Lines*, ed. C. L. Carilli, S. J. E. Radford, K. M. Menten, & G. I. Langston, 163–+
- Shaver, P. A. & Pierre, M. 1989, *Astron & Astrophys.*, 220, 35
- Shaver, P. A., Wall, J. V., Kellermann, K. I., Jackson, C. A., & Hawkins, M. R. S. 1996, *Nature*, 384, 439
- Sheth, R. K. & Tormen, G. 1999, *Mon. Not. Roy. Astro. Soc.*, 308, 119
- Shklovskii, I. S. 1952, *Astron. Zh.*, 29, 418
- Sikora, M., Begelman, M. C., & Rees, M. J. 1994, *Astrophys. J.*, 421, 153
- Silverman, J. D., Green, P. J., Barkhouse, W. A., et al. 2005, *Astrophys. J.*, 624, 630
- Simpson, C., Martínez-Sansigre, A., Rawlings, S., et al. 2006, *Mon. Not. Roy. Astro. Soc.*, 372, 741
- Smith, F. G. 1952, *Mon. Not. Roy. Astro. Soc.*, 112, 497+
- Smolčić, V., Schinnerer, E., Scodreggio, M., et al. 2008, *Astrophys. J. Suppl.*, 177, 14
- Snellen, I. A. G. 2008, *ArXiv e-prints*
- Snellen, I. A. G. & Best, P. N. 2001, *Mon. Not. Roy. Astro. Soc.*, 328, 897
- Snellen, I. A. G., Schilizzi, R. T., Miley, G. K., et al. 2000, *Mon. Not. Roy. Astro. Soc.*, 319, 445
- Staniszewski, Z., Ade, P. A. R., Aird, K. A., et al. 2009, *Astrophys. J.*, 701, 32
- Steidel, C. C., Giavalisco, M., Dickinson, M., & Adelberger, K. L. 1996, *Astron. J.*, 112, 352
- Stern, D. 2000, *PASP*, 112, 1411
- Subrahmanya, C. R. & Harnett, J. I. 1987, *Mon. Not. Roy. Astro. Soc.*, 225, 297
- Sullivan III, W. 2009, *Cosmic Noise* (Cambridge University Press, in press)
- Sunyaev, R. A. & Zeldovich, Y. B. 1972, *Comments on Astrophysics and Space Physics*, 4, 173
- Takeuchi, T. T., Yoshikawa, K., & Ishii, T. T. 2003, *Astrophys. J. Lett.*, 587, L89
- Taylor, A. C., Grainge, K., Jones, M. E., et al. 2001, *Mon. Not. Roy. Astro. Soc.*, 327, L1
- Taylor, A. R., Stil, J. M., Grant, J. K., et al. 2007, *Astrophys. J.*, 666, 201
- Taylor, G. B., Marr, J. M., Pearson, T. J., & Readhead, A. C. S. 2000, *Astrophys. J.*, 541, 112
- The Planck Collaboration. 2006, *ArXiv Astrophysics e-prints*
- Tinti, S., Dallacasa, D., de Zotti, G., Celotti, A., & Stanghellini, C. 2005, *Astron & Astrophys.*, 432, 31
- Tinti, S. & de Zotti, G. 2006, *Astron & Astrophys.*, 445, 889
- Toffolatti, L., Argüeso Gomez, F., de Zotti, G., et al. 1998, *Mon. Not. Roy. Astro. Soc.*, 297, 117
- Toffolatti, L., De Zotti, G., Argüeso, F., & Burigana, C. 1999, in *Astronomical Society of the Pacific Conference Series*, Vol. 181, *Microwave Foregrounds*, ed. A. de Oliveira-Costa & M. Tegmark, 153–+
- Toffolatti, L., Franceschini, A., Danese, L., & de Zotti, G. 1987, *Astron & Astrophys.*, 184, 7
- Torniainen, I., Tornikoski, M., Teräsanta, H., Aller, M. F., & Aller, H. D. 2005, *Astron & Astrophys.*, 435, 839
- Trushkin, S. A. 2003, *Bull. Special Astrophys. Obs.*, 55, 90
- Trshager, W., Schilizzi, R. T., Röttgering, H. J. A., Snellen, I. A. G., & Miley, G. K. 2000, *Astron & Astrophys.*, 360, 887

- 
- Tucci, M., Martínez-González, E., Toffolatti, L., González-Nuevo, J., & De Zotti, G. 2004, *Mon. Not. Roy. Astro. Soc.*, 349, 1267
- Turtle, A. J., Pugh, J. F., Kenderdine, S., & Pauliny-Toth, I. I. K. 1962, *Mon. Not. Roy. Astro. Soc.*, 124, 297
- Urry, C. M. & Padovani, P. 1995, *PASP*, 107, 803
- Valtonen, M. J., Lehto, H. J., Nilsson, K., et al. 2008, *Nature*, 452, 851
- van Breugel, W., De Breuck, C., Stanford, S. A., et al. 1999, *Astrophys. J. Lett.*, 518, L61
- Verheijen, M. A. W., Oosterloo, T. A., van Cappellen, W. A., et al. 2008, in *American Institute of Physics Conference Series*, Vol. 1035, *The Evolution of Galaxies Through the Neutral Hydrogen Window*, ed. R. Minchin & E. Momjian, 265–271
- Vigotti, M., Carballo, R., Benn, C. R., et al. 2003, *Astrophys. J.*, 591, 43
- Voss, H., Bertoldi, F., Carilli, C., et al. 2006, *Astron & Astrophys.*, 448, 823
- Waddington, I., Dunlop, J. S., Peacock, J. A., & Windhorst, R. A. 2001, *Mon. Not. Roy. Astro. Soc.*, 328, 882
- Waizmann, J.-C. & Bartelmann, M. 2009, *Astron & Astrophys.*, 493, 859
- Waldram, E. M., Bolton, R. C., Pooley, G. G., & Riley, J. M. 2007, *Mon. Not. Roy. Astro. Soc.*, 379, 1442
- Waldram, E. M., Pooley, G. G., Davies, M. L., Grainge, K. J. B., & Scott, P. F. 2009, *ArXiv e-prints*
- Waldram, E. M., Pooley, G. G., Grainge, K. J. B., et al. 2003, *Mon. Not. Roy. Astro. Soc.*, 342, 915
- Waldram, E. M., Yates, J. A., Riley, J. M., & Warner, P. J. 1996, *Mon. Not. Roy. Astro. Soc.*, 282, 779
- Wall, J. V. 1980, *Royal Society of London Philosophical Transactions Series A*, 296, 367
- Wall, J. V. 1994, *Australian Journal of Physics*, 47, 625
- Wall, J. V. & Jackson, C. A. 1997, *Mon. Not. Roy. Astro. Soc.*, 290, L17
- Wall, J. V., Jackson, C. A., Shaver, P. A., Hook, I. M., & Kellermann, K. I. 2005, *Astron & Astrophys.*, 434, 133
- Wall, J. V., Pearson, T. J., & Longair, M. S. 1980, *Mon. Not. Roy. Astro. Soc.*, 193, 683
- Wall, J. V., Pearson, T. J., & Longair, M. S. 1981, *Mon. Not. Roy. Astro. Soc.*, 196, 597
- Wall, J. V., Pope, A., & Scott, D. 2008, *Mon. Not. Roy. Astro. Soc.*, 383, 435
- Waxman, E. 1997, *Astrophys. J. Lett.*, 485, L5+
- Webster, A. 1976, *Mon. Not. Roy. Astro. Soc.*, 175, 61
- White, R. L., Becker, R. H., Helfand, D. J., & Gregg, M. D. 1997, *Astrophys. J.*, 475, 479
- White, S. D. M. & Rees, M. J. 1978, *Mon. Not. Roy. Astro. Soc.*, 183, 341
- Wijers, R. A. M. J. & Galama, T. J. 1999, *Astrophys. J.*, 523, 177
- Willmer, C. N. A. 1997, *Astron. J.*, 114, 898
- Willott, C. J., Rawlings, S., Blundell, K. M., Lacy, M., & Eales, S. A. 2001, *Mon. Not. Roy. Astro. Soc.*, 322, 536
- Wilman, R. J., Miller, L., Jarvis, M. J., et al. 2008, *Mon. Not. Roy. Astro. Soc.*, 388, 1335
- Windhorst, R. A., Fomalont, E. B., Partridge, R. B., & Lowenthal, J. D. 1993, *Astrophys. J.*, 405, 498
- Windhorst, R. A., Hopkins, A., Richards, E. A., & Waddington, I. 1999, in *Astronomical Society of the Pacific Conference Series*, Vol. 193, *The Hy-Redshift Universe: Galaxy Formation and Evolution at High Redshift*, ed. A. J. Bunker & W. J. M. van Breugel, 55–+
- Windhorst, R. A., Miley, G. K., Owen, F. N., Kron, R. G., & Koo, D. C. 1985, *Astrophys. J.*, 289, 494
- Windhorst, R. A., van Heerde, G. M., & Katgert, P. 1984, *Astron & Astrophys. Suppl.*, 58, 1
- Woltjer, L. 1966, *Astrophys. J.*, 146, 597
- Wright, A. & Otrupcek, R. 1990, in *PKS Catalog (1990)*, 0–+
- Wright, E. L., Chen, X., Odegard, N., et al. 2009, *Astrophys. J. Suppl.*, 180, 283
- Wrobel, J. M. & Krause, S. W. 1990, *Astrophys. J.*, 363, 11
- Yamada, M., Sugiyama, N., & Silk, J. 1999, *Astrophys. J.*, 522, 66
- York, D. G., Adelman, J., Anderson, Jr., J. E., et al. 2000, *Astron. J.*, 120, 1579
- Yun, M. S., Reddy, N. A., & Condon, J. J. 2001, *Astrophys. J.*, 554, 803
- Zwart, J. T. L., Barker, R. W., Biddulph, P., et al. 2008, *Mon. Not. Roy. Astro. Soc.*, 391, 1545